1-1-2021

Evaluation Of Heart Rate Variability And Cardiovascular Regulation To In-Flight Workload And Thermal Stress

Bradley Hoffmann

EVALUATION OF HEART RATE VARIABILITY AND CARDIOVASCULAR REGULATION TO IN-FLIGHT WORKLOAD AND THERMAL STRESS

by

Bradley Thomas Hoffmann

Bachelor of Science, Electrical Engineering, North Dakota State University, 2016
Master of Science, Mechanical Engineering, North Dakota State University, 2018

A Dissertation

Submitted to the Graduate Faculty

of the

University of North Dakota

in partial fulfillment of the requirements

for the degree of

Doctor of Philosophy

Grand Forks, North Dakota
December
2021

This dissertation, submitted by Bradley Hoffmann in partial fulfillment of the requirements for the Doctor of Philosophy in Biomedical Engineering from the University of North Dakota, has been read by the Faculty Advisory Committee under whom the work has been done and is hereby approved.

_____
Kouhyar Tavakolian, Chairperson

_____
Annie Tangpong, Committee Member

_____
Andrew Blaber, Committee Member

_____
Nicholas Wilson, Committee Member

_____
Alejandro Garbino, Committee Member

_____
Rashid Ahmed, Committee Member

_____
Hassan Reza, Member at Large

This dissertation is being submitted by the appointed advisory committee as having met all of the requirements of the School of Graduate Studies at the University of North Dakota and is hereby approved.

_____
Dr. Chris Nelson
Associate Dean of the School of Graduate Studies

_____
Date

PERMISSION

Title Evaluation of Heart Rate Variability and Cardiovascular Regulation to In-flight Workload and Thermal Stress

Department Biomedical Engineering

Degree Doctor of Philosophy

In presenting this dissertation in partial fulfillment of the requirements for a graduate degree from the University of North Dakota, I agree that the library of this University shall make it freely available for inspection. I further agree that permission for extensive copying for scholarly purposes may be granted by the professor who supervised my dissertation work or, in his absence, by the Chairperson of the department or the dean of the School of Graduate Studies. It is understood that any copying or publication or other use of this dissertation or part thereof for financial gain shall not be allowed without my written permission. It is also understood that due recognition shall be given to me and to the University of North Dakota in any scholarly use which may be made of any material in my dissertation.

Bradley Hoffmann
November 5th, 2021

ACKNOWLEDGEMENTS

First and foremost, I am thankful to my advisor and mentor Dr. Kouhyar Tavakolian for allowing me the academic freedom to explore interesting and new research topics. He inspires me to pursue multidisciplinary research from his technical knowledge and experience. Thank you for devoting your time to me and my educational growth. I am beyond grateful for the opportunities you have given me and also for encouraging me to pursue my dreams of working with aerospace physiology particularly in spaceflight. Thank you to Dr. Andrew Blaber for providing a collaborative environment of mentorship with the Aerospace Physiology Lab in addition, I am grateful for the opportunities that have allowed me to contribute to the field of aerospace physiology. Thank you to Dr. Nicholas Wilson for his continued guidance in aviation and for allowing me to contribute further to the data collection of pilots in-flight, to which a bulk of this research was crafted.

During my academic pursuits, I was fortunate to work at the NASA Johnson Space Center through a cooperative internship experience. The experience gained during my internship continued to drive my interest in spaceflight physiology. Thank you to Hee Jong Song for his mentorship and enthusiasm. He encouraged me to excel and take on research in human thermal modeling giving me a foundation for reaching my dream of working with spacesuits and life support systems. I am further thankful for the opportunity to work in the H-3PO lab and appreciate the mentorship gained in that lab. This dissertation work would not have been possible without the support of H-3PO and the amazing individuals in that lab. Thank you to Dr. Alejandro Garbino for mentorship within spaceflight and EVA physiology, I appreciate the freedom to explore interconnected datasets in suited operations while also being allowed to take on challenging research responsibilities. Thank you to Dr. Jocelyn Dunn for opening doors of collaborative opportunity with H-3PO and allowing me to take on leading roles of research for human thermal modeling. Without your support and guidance, much of this work would not be possible. Thank you to Dr. Andrew Abercromby for taking on a mentorship role, the discussions about general engineering and career paths have guided me more than is probably known.

Thank you to my committee members Dr. Andrew Blaber, Dr. Rashid Ahmed, Dr. Annie Tangpong, Dr. Alejandro Garbino, Dr. Nicholas Wilson, and Dr. Hassan Reza for their guidance and constructive feedback on my dissertation work. I would also like to thank my friends and colleagues in the Biomedical Engineering Research Complex for their supportive collaboration. Thank you to my colleague Rabie Fadil. The research discussions have always allowed me to think critically about my work and I am fortunate to have such a peer to challenge and support my work. I would also like to thank the ND Space Grant Consortium for giving me fellowship opportunities to guide my research through my doctoral education. Last but not least I would like to thank my wife Kaspari for her constant support, love, and encouragement through my graduate endeavors.

To Kaspari - You are my sunshine

&

In remembrance of my Uncle Kevin

ABSTRACT

Aerospace environments are physically and mentally demanding. Commercial pilots, as well as astronauts during spaceflight, experience an increasing variety of task workloads. Pilots can become fatigued, leading to human error, which is the main factor in airline accidents. Similarly, astronauts during extravehicular activity (EVA) can become fatigued, which could lead to overexertion compiled with other serious injuries. Objective measures such as cardiovascular and thermal metrics have been shown to respond to changes in stress, however, in-flight physiological measures are lacking. Both cardiovascular and thermoregulation measures can help predict early warning signs of stress due to in-flight workloads. Cardiovascular reactions fluctuate during autonomic nervous system (ANS) responses to stress, varying heart rate, and shifting blood pressure through the baroreflex. Additionally, thermoregulatory fluctuations respond to ANS activity via the hypothalamus initiating effector responses such as vasoconstriction or vasodilation.

The objective of this dissertation is to ascertain the interconnection between cardiovascular and thermal responses focused on vasoactivity in stress-induced flight-like environments. First, heart rate variability (HRV) metrics were identified to determine stress responses of pilots' tasks during flight operations. Further to define flight-like physiology responses, cardiovascular timing intervals were identified using Seismocardiography and blood pressure during prolonged head-down tilt bed rest (HDBR). Building on these metrics, historic EVA heart rate, and metabolic rates were analyzed to develop a regression model providing minute-by-minute workload determination. Techniques were further developed as a cardiothermal model in a novel approach

to determine spacesuit workloads using heart rates, metabolic demand, HRV metrics, and thermal inputs.

During in-flight operations, short-term HRV metrics were found to determine low, medium, and high workloads attributed to stress. Further, during prolonged HDBR, cardiovascular timing intervals decreased similar to spaceflight attributed to fluid shifts. The development of regression models showed linearity predicting energy expenditure from heart rates during historic microgravity EVA. The final cardiothermal model predicted metabolic rates, core temperature, and mean skin temperature during simulated Lunar EVA in the NASA Active Response Gravity Offload System in the Mark III spacesuit. Developed objective cardiothermal metrics show implications of identifying crew stress responses and fatigue states through modeling approaches during flight.

TABLE OF CONTENTS

LIST OF FIGURES

LIST OF TABLES

LIST OF ACRONYMS

AC	Aortic Valve Closing
ANS	Autonomic Nervous System
AO	Aortic Valve Opening
ARGOS	Active Response Gravity Offload System
BP	Blood Pressure
BTU	British Thermal Unit
DBP	Diastolic Blood Pressure
DFA	Detrended Fluctuation Analysis
ECG	Electrocardiogram
EMU	Extravehicular Mobility Unit
EVA	Extravehicular Activity
FDA	Functional Data Analysis
FFT	Fast Fourier Transform
HF	High Frequency
HR	Heart Rate
HRV	Heart Rate Variability
ICT	Isovolumic Contraction Time
IRT	Isovolumic Relaxation Time
ISS	International Space Station
LEO	Low Earth Orbit
LCG	Liquid Cooling Garment
LCVG	Liquid Cooling Ventilation Garment
LF	Low Frequency
LVET	Left Ventricle Ejection Time
MAP	Mean Arterial Pressure
MR	Metabolic Rate
NBL	Neutral Buoyancy Laboratory
PEP	Pre-Ejection Period
PLSS	Portable Life Support System
PNS	Parasympathetic Nervous System
PPG	Photoplethysmogram
PTT	Pulse Transit Time
RMSSD	Root Mean Square of Successive Differences
SBP	Systolic Blood Pressure
SCG	Seismocardiogram
SDNN	Standard Deviation of Normal-to-Normal Sinus Beats
SNS	Sympathetic Nervous System
SVR	Systemic Vascular Resistance
STS	Sit-to-Stand
TINN	Triangular Interpolation of Normal-to-Normal Beats
ULF	Ultra-Low Frequency
VLF	Very-Low Frequency

PART I: MONITORING CARDIOVASCULAR AND THERMAL PHYSIOLOGY RESPONSES TO IN-FLIGHT WORKLOADS – Background, Study, and Current Techniques

CHAPTER 1. INTRODUCTION

1.1 Background

Aerospace environments are physically and mentally demanding on in-flight crews. Commercial and high-altitude pilots, as well as astronauts during spaceflight, experience an increasing variety of task workloads. Pilots during these workloads can become fatigued, leading to human error, which is the major factor in airline accidents [1]–[3]. Similarly, astronaut spacewalk, or extravehicular activity (EVA), workloads can cause fatigue but also overexertion, which could lead to overheating and other serious injuries [4]. Post-flight analysis of early Gemini missions showed astronauts became overheated due to metabolic demand during EVA tasks [4]–[6]. The range of aerospace environments can provide insight into physiological responses for workloads and heat strain on Earth.

Heat is the leading cause of injury or death during weather-related events [7]. As temperatures continue to climb in recent years, heat strain on the body remains dangerous for most populations. The thermoregulatory system comprises afferent thermal sensors distributed throughout the body. These afferent sensors provide a stream of signals to the hypothalamus, which acts like a distributed controller [8], [9]. From the hypothalamus, appropriate effector responses occur as vasoconstriction, vasodilation, shivering, or sweating [10]. However, the most important in thermoregulation is that of blood flow between the core and the periphery [11]. The cardiovascular system and thermoregulation are tied together through the autonomic nervous system (ANS). Cardiac homeostatic reactions fluctuate during ANS responses to stress, increasing or decreasing heart rate (HR) and shifting blood pressure through baroreflex responses [12]–[14]. Understanding timed interactions between both cardiovascular and thermoregulation can help predict early warning signs of stress and strain on crew due to in-flight workloads.

1.3 Research Objectives

The objective of this research was to investigate the interaction of cardiovascular regulation to thermal and workload stressors. An intended goal of this research, divided into three parts, was to develop a cardiovascular model to predict in-flight workload strain during environmental and task-induced stress. Objective one centered on the evaluation of cardiovascular workload stress in a flight environment. The goal of objective one was to test the hypothesis that heartbeat inflections responsive to autonomic nervous system activity will occur at increased workloads and can determine stress levels in-flight. Objective two focused on the evaluation of mechanical cardiovascular vibrations and timing intervals during blood vascular redistribution due to a 6° head-down tilt bed rest. Head-down tilt bed rest (HDTB) provides an accurate depiction of physiologic responses to spaceflight and is widely used as a spaceflight analog. The goal attributed to objective two was to test the hypothesis that headward fluid shifts will attenuate vibrations created from heartbeats detected at the chest. Finally, objective three goals concentrated on the development of a cardiovascular predictive model for workload and thermal stressors, testing the hypothesis that heart rate and cardiovascular timing intervals can be used to predict task workload stress and energy expenditure.

1.4 Approach

Three separate studies were completed to investigate the cardiovascular responses to flight and flight-like environments and workloads tied to the above objectives. The central research question was to determine what effect stress and heat have on the vasoactivity of pilots and astronauts performing in-flight tasks? Central to this dissertation, the three studies focus on testing two hypotheses:

A.1 Increasing in-flight workload demand will increase the sympathetic nervous system activity resulting in decreased vagal tone.

A.2 Increases of in-flight workload will lead to increases in thermal loading resulting in decreased vagal tone.

The first study was to investigate pilot in-flight workloads through heartbeat inflections and heart rate variability. Research questions for each study build on the main research question for the dissertation. The first study research question is split into two, asking how do varying flight task difficulties affect heart rate fluctuations of pilots in-flight? Also, at what sensitivity can heart rate variability be used to predict pilot task workload changes? The hypotheses to be tested were to continue to answer the main hypotheses. For study one, the hypotheses were:

B.1 Increasing sympathetic nervous system response will be seen as a result of high workload flight tasks determined by decreased heart rate variability.

B.2 Short-term heart rate variability metrics will show variations resulting from increased sympathetic nervous system activity comparing low-medium-high task difficulties.

The approach for study one was accomplished by evaluating datasets of ECG and individual heart rate (HR) data collected during 1.3 to 1.5 hours of in-flight pilot task loading. Heart rate variability (HRV) metrics were collected and analyzed from R-R intervals across designated low, medium, and high tasks of in-flight pilot workloads. It is expected that short-term HRV metrics will designate higher sympathetic nervous system responses to increased high task loads compared to low task loads.

The second study focused on objective two to investigate cardiovascular control responses due to fluid shifts that occur from the head-down tilt bed rest. The approach centralized around processing cardiovascular vibrations to gather cardiac timing intervals testing the hypotheses:

C.1 Mechanical deconditioning of the heart will occur observed by decreased SCG amplitude morphologies as a result of increased headward fluid shifts during prolonged head down tilt bedrest.

C.2 The cardiovascular timing interval of pulse transition time would decrease resulting from increased arterial stiffness associated with head down tilt bedrest.

This study was accomplished by evaluating electrocardiography (ECG), seismocardiography (SCG), and blood pressure (BP) collected during prolonged 60-day HDTB. During bed rest, SCG features of Aortic Valve Opening (AO) and Aortic Valve Closing (AC) are expected to be reduced due to increased fluid in the chest, causing attenuation of the signal peaks. Pulse transit time (PTT) derived from the SCG AO peak, and the foot of the BP waveform will be reduced similar to that observed in spaceflight [15], [16]. Additionally, seasonal effects were investigated between HDTB campaigns to observe if seasonal changes affect the outcome of PTT and other timing intervals.

In the third study, the approach focused on iterating data collected in studies one and two to build upon predictive models for identifying crew workload and environmental strain. The first attribute of study three was to collect heart and metabolic rate observations from historic EVA data during 5 to 6 hours of EVA in space to draw correlations of cardiovascular regulation and energy expenditure during varying task loads of simulated lunar EVA tasks. EVA data will be analyzed from historic EVA datasets where heart rate was collected every 20 seconds and metabolic rate every two minutes [4]. The secondary attribute of study three is to investigate heart rate, metabolic rate, and thermal regulation during simulated EVA of lunar workloads. Research questions focused on what effect microgravity has on heart rates and metabolic rates during prolonged EVA workloads? Also, what will be the outcome of the core body and skin temperatures when heart and metabolic rates elevate due to increasing simulated EVA workload? Analysis for study three tested the hypotheses:

D.1 Prolonged microgravity EVA workloads, cardiovascular and metabolic drift will not occur due to physical offloading and headward fluid shifts as a result, heart rate, and metabolic rate will be linearly correlated allowing regression predictions of energy expenditure from heart rate inflections.

D.2 The thermal environment of the suit during increasing simulated EVA workloads will result in fewer delta changes in core temperature as well as skin temperatures, allowing regression predictions from heart rate and metabolic rate inputs.

This is accomplished by using metrics identified from study one and historic EVA heart and metabolic rate correlations to develop a predictive simple linear and multiple regression analysis. The model is tested using simulated EVA heart rate, metabolic rate, and thermal data collected during simulated tasks and comparisons to real as well as modeled outputs. Additionally, predicted stress on the cardiovascular system is be determined through short-term HRV metrics in time-domain, frequency-domain and non-linear measurements. Increases in low frequency and decreases in high frequency are expected to occur as main markers for detecting stress.

1.5 Dissertation Outline

The dissertation is structured into eight chapters organized into four parts. Each part is focused on an overarching theme that encapsulates the subsequent chapters. Each part ties back to the dissertation objectives and ultimate goals of developing real-time monitoring techniques of cardiovascular and thermal responses to in-flight workloads.

Part I focuses on monitoring cardiovascular and thermal physiology responses to in-flight workload, including chapters 1 and 2. Chapter 1 centralizes around providing a background to in-flight workloads and the study design. Chapter 2 provides a literature review of aerospace physiology focused on spaceflight and commercial aviation. Within Chapter 2, physiology changes due to microgravity and responses to stress are discussed as well as aerospace case studies of historic spacewalks and commercial flights. These are presented to detail the necessity for real-time physiology monitoring of workload stress.

Part II encapsulates the evaluation of cardiovascular regulation to in-flight and flight-like environments, including chapters 3 and 4. Chapter 3 details study one findings of monitoring

cardiovascular responses to pilot in-flights during a flight plan created to stress workload. Chapter 4 describes study two findings of observed cardiovascular responses to fluid shifts due to 6° head-down tilt bed rest as a flight-like consequence of microgravity environments.

Part III is focused on the assessment of cardiovascular predictors to EVA energy expenditure and thermal regulation, including chapters 5 and 6. The chapters under Part III center around EVA human performance and findings observed by study three in predicting energy expenditure through cardiovascular metrics. Chapter 5 describes findings to draw metrics from historic EVA data to build correlations between heart rate and metabolic rate. Chapter 6 builds on EVA metrics of heart rate and metabolic rate to present model outputs for monitoring thermal regulation during simulated EVA tasks.

Lastly, Part IV pulls concluding remarks to the dissertation and studies encapsulated in each part, including chapter 6. The interpretations are discussed in Chapter 7 as a conclusion to build on continuing work for monitoring real-time workload and thermal strain in aerospace. Future recommendations are then built for applications to use real-time monitoring techniques for pilot in-flight workloads and EVA thermal monitoring.

CHAPTER 2. INCREASED PHYSICAL AND MENTAL WORKLOAD EFFECTS ON CARDIOVASCULAR AND THERMAL CONTROL: LESSONS LEARNED FROM AEROSPACE CASE STUDIES

2.1 Physiology Responses to Spaceflight

In the weightless environment of space, physiological changes occur over both short- and long-term durations causing time and mechanical varying effects to bodily systems [17]. Without the constant pull of 1-g that our bodies have experienced since birth, upward fluid shifts occur, causing a change in gradient pressures. Compounding effects of these fluid shifts simultaneously target the cardiovascular system, vestibular system, and thermal regulation. Similarly, the shifts in each of these systems also drive corollary effects of the others, such as cardiovascular control and thermoregulatory action during exercise in space [18].

Currently, there are still unknowns to the extent of fluid shifts and physiologic responses, however, it is known that these fluid shifts have a causal relationship with changing vasculature in tandem with time-dependent changes. This notion can give insight into blood pressure regulation and vascular responses (i.e., vasoconstriction, vasodilation). This regulatory response of the baroreflex has been shown to lead to loss of postural control of the body describing driving astronaut orthostatic intolerance upon return to 1-g. There are also studies that have viewed changes of ventricular mass loss, increased arterial stiffness, reduced thermal control. These are all experienced in astronauts in both short-term spaceflights (e.g., space shuttle missions) and in long-term spaceflight (6-Months and beyond) aboard the International Space Station (ISS) [19]–[23].

2.1.1 Cardiovascular Control in Microgravity

The amount of time that a person is subjected to microgravity has a large effect on the physiological adaptations that occur [19], [24]. Short-term missions experience rapid stimulus in both 1-g to 0-g and vice versa. Long-term missions that are seen on the ISS that will be seen in longer missions (e.g., Mars) will subject to the body to six months or more of altered gravity.

Normally on Earth, there is a fluid gradient that is distributed unequally through the body. Most of the pressure is seen in the lower half of the body, with the gradient lightening towards the head. When thrown into a microgravity environment, this gradient disappears, and the fluids within the body equalize in pressure (Figure 2.1), causing more fluid to be distributed in the upper part of the body [25]. During a standing state, blood pressure is controlled through afferent stimulus of the mechanically sensitive baroreceptor impulses. The baroreceptor responses in the upper vasculature, localized in the carotid sinus and the aortic arch, lead to the increased heart rate and systemic vascular resistance (SVR) as a result of vagal withdrawal and sympathetic activation [26].

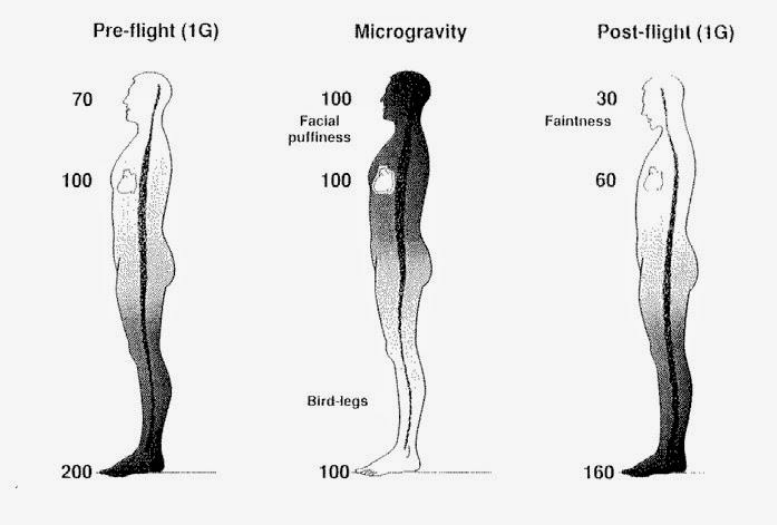

Figure 2.1: Blood fluid shifts within the body from the stimulus of microgravity, Hargens, and Richardson (2009).

The responding effect of blood pressure regulation is called the baroreflex. The change of microgravity, not normally seen by the cardiovascular system, shifts the responses of the Baroreflex to gain back homeostasis by attempting to control the equalizing pressure. The response is relatively quick in adaptation for short-term spaceflight. However, little is still known still of the long-term spaceflight effects. It has been observed that longer stays in microgravity are a detriment to the autonomic control of blood pressure due to changing vasculature [27]. Additionally, altered blood volume, red cell mass, associated changes in vascular wall shear forces, and perfusion pressures in microgravity may alter morphology in the walls of arteries as well as veins of the upper and lower body [28]. These mechanical vascular changes can continue to impair the cardiovascular reflexes distributing blood flow among the various body locations, and especially those reflexes that maintain blood pressure during sudden perturbations in posture or activity [27], [29], [30].

Physical and mechanical changes in blood vasculature and heart muscle mass have direct implications in the blood flow distributions and cardiovascular performance. The fluid shift phenomenon observed in microgravity can be simulated through Head Down Tilt Bed Rest (HDTBR) which has proven analogous to spaceflight changes in physiology [31]–[34]. Westby et al. has shown that there is a remodeling of the left ventricle (LV), causing decreases in LV mass over 60 days of HDTBR [22]. It was also reported that left ventricular volumes had rapidly adapted through bedrest, allowing no change from pre- to post-bedrest of plasma volume levels. However, the mechanical mass loss of the left ventricle did not recover and could continue to be deconditioned for up to two weeks after bedrest or post spaceflight.

The remodeling can continue to alter localized blood flow distributions through changes in blood perfusion through the vasculature and capillary bed responses. Due in part to the baroreflex

response, gravity plays the role of a vasoconstrictor during upright posture due to increased hydrostatic pressure in the lower part of the body [35]. Hughson et al. were the first to report a decrease in systematic vasculature resistance of astronauts after six months of flight utilizing finger pulse pressure [36]. Norsk et al. had shown the effects of weightlessness on the vasorelaxation of microgravity. This relation brings insight to the cardiovascular system and its chronic adaptation mode during continued weightlessness. Mechanically, the research had shown a 9% decrease in systemic vascular resistance, while blood pressure and heart rate remained unchanged [35]. Due to the increased fluid shifts in the upper vasculature, there was an increase in cardiac output and an increase in systemic vasodilation; this dilation is suggested as an attempt to prevent blood pressure from increasing. The observation is inversely related to what is seen on the ground with the vasoconstriction stimulus of gravity.

In a recent review by Norsk, there is an extensive view of the cardiovascular response to microgravity [18]. Going from 1-G to 0-G on the cardiovascular side, there is an increase in both headward fluid shifts and thoracic expansion that drives cardiac distension increases (Figure 2.2). The resultant cardiac distension, mixed with continued headward fluid shifts, cause an inverse relation where vascular constriction decreases and vasodilation increases. Both lead to a decrease in systemic vascular resistance [37]–[39]. In tandem, there is a control loop defined by blood pressure. As blood pressure decreases, there is also a lowering of SVR [36]. The response of the systemic nervous activity (SNA) does not play a large positive or negative role in SVR, potentially due to being secondary to vasodilatory responses. SNA has controlling factors in other facets of the physiologic responses to spaceflight [40]. Coupled with continued decreases in SVR, other recent works in Hughson et al. [16] and Baevsky et al. [15] showed a drastic relationship between spaceflight and increased arterial stiffness that which is shown similarly in ten to twenty years of

aging. These relationships were derived from decreased pulse wave transition time from pre- to post-flight and changes in blood pressure in astronauts aboard the ISS.

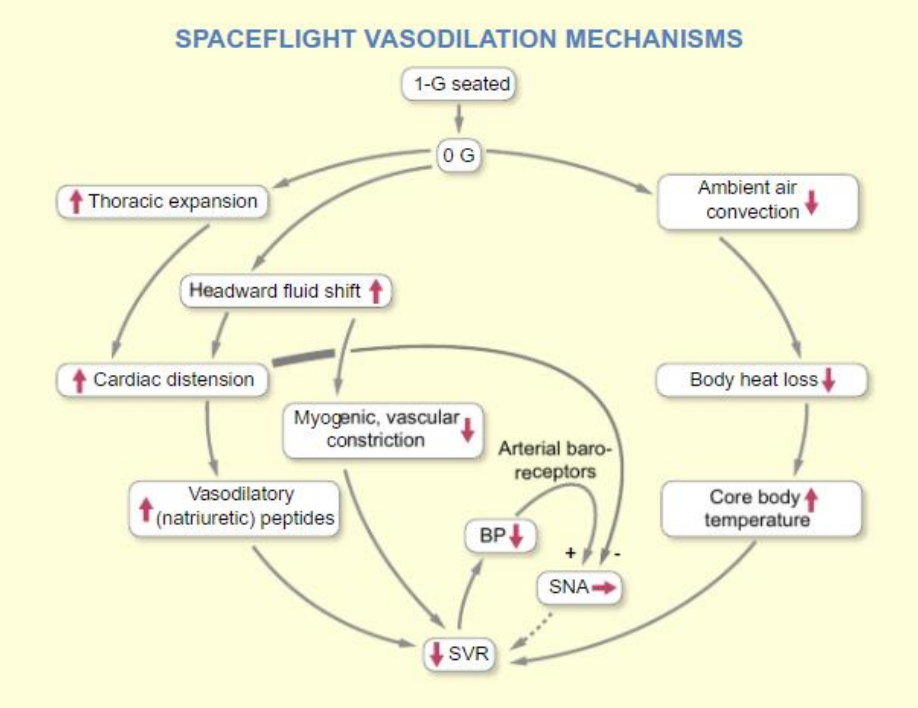

Figure 2.2: A depiction of the Relationship leading to the decrease in systemic vascular resistance (SVR) going from a 1-G to 0-G environment. Headward fluid shifts in tandem with thermoregulatory factors cause decreasing trends of SVR. The decrease in blood pressure (BP) inhibits the arterial baroreceptors that encourage sympathetic nerve activity (SNA), while the fluid shift and thoracic expansion through cardiac distension inhibit it, Norsk 2020.

2.1.2 Human Thermoregulatory Control

Humans can survive across a remarkably wide range of environmental thermal stressors while maintaining a nearly constant core temperature essential for health and wellbeing. It is critically important for core body temperature to be held near the setpoint of 37 °C to maintain personal health, task functionality, and comfort. The sensitivity of the core body temperature is on the order of ± 1°C. Drifting outside of this small thermal window could result in serious consequences such as illness or death [9]. The thermoregulatory system consists of afferent thermal sensors and actuators distributed throughout the body. These afferent sensors provide a constant stream of stimulus signals to the hypothalamus, which acts like a distributed controller by regulating the

functions of blood flow magnitude and blood allocation throughout the body in tandem with metabolic activities, and while keeping control of other essential needs (e.g., sustaining adequate blood pressure levels) [8]. From the hypothalamus, the appropriate effector response is sent, yielding a response of vasoconstriction, vasodilation, shivering, or sweating depending on the environmental conditioning stimulus.

Most important in the thermal regulatory system is blood flow between the core and the rest of the body. Blood provides a large heat capacity and the ability for the cardiovascular system to alter a time-based spatial distribution of heat over large ranges [11]. Flow dynamics of blood circulation provide tremendous efficiency for increasing or decreasing the flow of heat between the core and the surface to meet changing thermoregulatory requirements [10], [41]. Under conditions for which heat removal to the environment is essential, blood flow can be biased to various areas of the skin. This can be at the hands, feet, and face, where vasodilation can aid in cooling. Similarly, when circumstances require the retention of heat, vasoconstriction is attributed to slowing down circulation and the distribution of body heat [42].

In spaceflight and a microgravity environment, the avenues of heat transfer of the body are changed due to the environment. Generally, there are four main categories of heat dissipation of the body (i.e., Radiation, Convection, Evaporation, and Conduction). In microgravity, the convective heat is lessened due to the lack of air movement [43]. Particularly during an EVA inside of a suited environment, astronauts use a liquid cooling garment to provide convective heat transfer from the skin to flowing liquid [44]. In these applications and with small sample sizes of people who have experienced microgravity, developing simulated models of thermal activity is essential for designing human suited and spacecraft systems for long-duration spaceflight. These models break the body apart into multiple related segments such as in the Wissler Model (Figure 2.3).

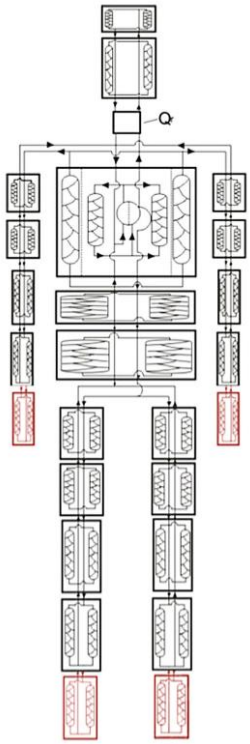

Figure 2.3: The Wissler thermoregulatory model breaks the body into multiple nodes with four main compartments (Skin, Muscle, Bone and Core, Hensley et al. (2013).

This model describes the human body as separate nodes, each with four compartments: core, bone, muscle, and skin. These separate nodes are then connected by a blood flow node. The relationships are designated in heat mass balance equations describing the thermal fluctuation of the body [45], [46].

In normal spaceflight and weightless environments, blood flow distributions may return to normal during a resting, cool environment. However, during normal exercise, peripheral vessels in the skin and muscles dilate, moving blood away from the core to the skin. In this weightless environment, due to physiologic changes, as mentioned earlier, a smaller volume of blood flow will be experienced in the skin and exercising muscle [23], [47]. Continually, the larger residual blood volume may increase vasoconstriction, causing sweat suppression. In addition to this increase in vasoconstriction, also mentioned by Norsk et al., is driven in tandem by the loss of plasma volume impairing heat loss due to lowered vasodilation and sweating. As a result, there is

a higher and quicker rise in body core temperature seen in astronauts during spaceflight [18], [23]. These localized responses in shifting vasorelaxation play a large role in the thermal conduction of the body. With upward fluid shifts and vascular changes that occur due to the weightless environment of microgravity, both cardiac function and thermal regulation play a large role in the performance of the astronaut. Little has been investigated into the relationships of these two systems of an individual inside a spacesuit with only convection of the water from a liquid cooling ventilation garment (LCVG) during extravehicular activity (EVA).

2.1.3 Extravehicular Activity

EVA operations are an essential objective during human spaceflight and exploration missions. During an EVA an astronaut will be within a spacesuit conducting tasks at various workloads for a long period (e.g., 6-8 hours). As a spacesuit is an individualized spacecraft there have been iterative processes in the development of technology to aid the astronaut to conduct the EVA while comfortable, and with vital life support. In the following section, the historic extravehicular activities are discussed to detail operational workloads that lead to human error and overheating. Additionally, technology failures and spacesuit advancements are also discussed.

2.1.3.1 Gemini

During the 1960s the US Gemini missions were conducted as a preliminary to the Apollo moon missions. The critical design elements of Gemini were meant to prove technologically and operationally for Apollo Moon landings. On the cusp of the space race, Gemini IV was launched on June 3rd, 1965. During the Gemini IV mission, Ed White became the first US Astronaut to conduct an EVA utilizing the G4C space suit [48]. In-suit physiology monitoring consisted of a one-lead ECG and respiration measure through impedance pneumogram [4]. During this EVA a multitude of minor operational and technical issues had arisen. During the ingress back into the

Gemini IV spacecraft the outer hatch refused to close, resulting in the overexertion of the astronaut. This increase in energy expenditure was beyond the cooling capacity of his Ventilation Control Module (VCM). This higher energy expenditure was shown in increased heart rate and deemed overexertion during postflight analysis (Figure 2.4) [4], [5]. This caused the astronauts' visor to fog, limiting vision. During ingress, the astronaut accidentally smeared one of the outer windows resulting in minor vision loss outside of the spacecraft [48]. While there were considerable injury risks that could have occurred in the first US EVA, this type of EVA showed the adaptability of human operations during spacewalks.

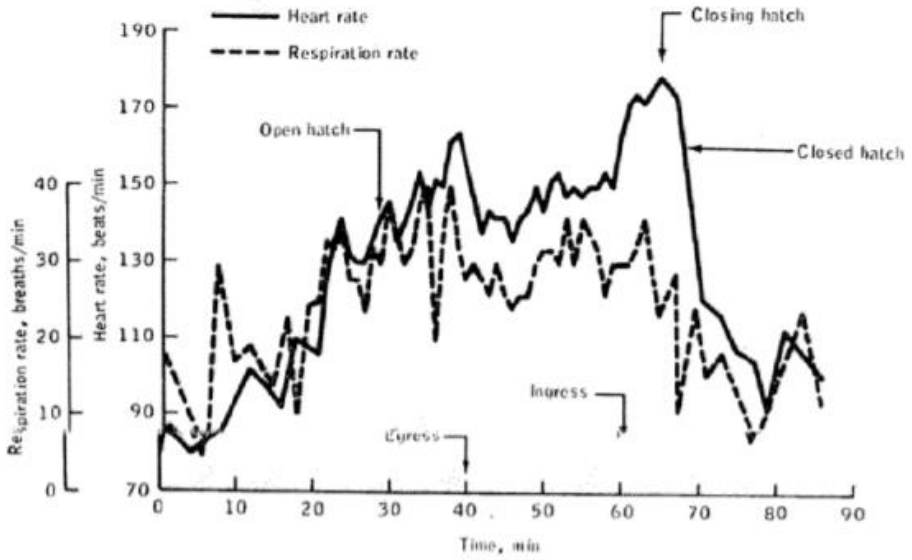

Figure 2.4: Gemini IV umbilical EVA heart rate and respiration rates (Paul, 2012).

The world's 3rd EVA was conducted on the Gemini IX mission that was launched June 5th, 1966. From the success of Gemini IV, this mission of Gemini IX was given more EVA tasks to complete. During the EVA, 50 percent of the astronaut's workload was used just to maintain position resulting in increased physical demand and risk of injury during suit operations [48]. The continuous struggle of motion and accomplishing tasks during this EVA caused the astronaut to accidentally break off an experiment antenna on the Gemini IX spacecraft. This resulted in a tear

in the G4C space suit causing "hot spots" or burns on his back where sunlight had stricken his skin [48]. Additional to this injury, overexertion from higher energy expenditure due to the EVA physical strain was beyond the limits of the life support system fogging the spacesuit helmet resulting in partial blindness [4], [5], [48]. Ultimately, higher than expected heart rates occurred, which caused the termination of the planned EVA (Figure 2.5).

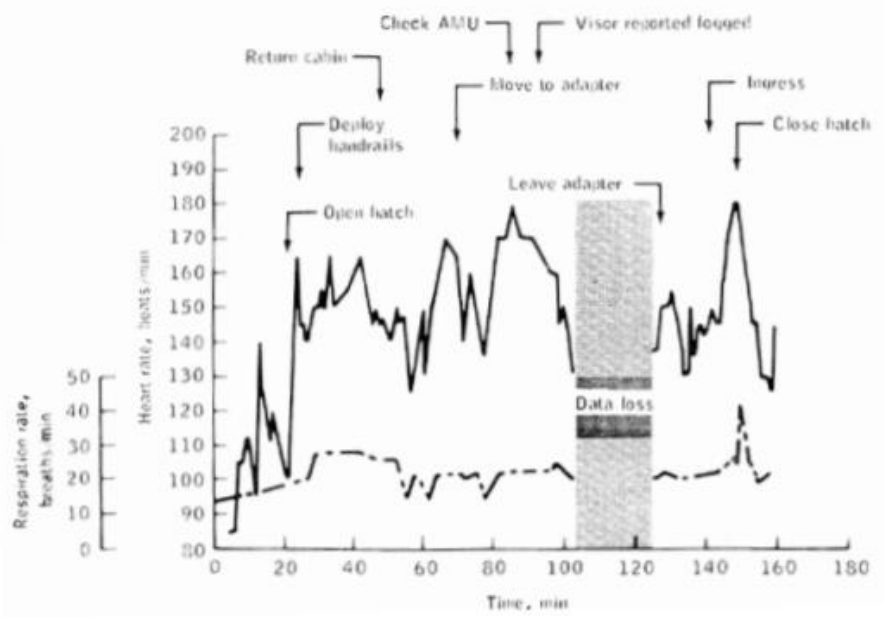

Figure 2.5: Gemini IX EVA heart rate and respiration rates. Overexertion occurred, causing early termination of the planned EVA (Paul, 2012).

The final EVA's of the Gemini missions were conducted with the Gemini X, launched July 10th, 1966 [48]. During this EVA astronauts reported eye irritation while smelling strange odors in their G4C space suits [49]. Upon analysis, it was discovered that lithium hydroxide leaked into their helmets when both suit fans were operated at the same time. This lithium hydroxide was present in the Gemini life support system as a carbon dioxide scrubber. Beyond physical risks, this event points to technical and operational risks that occurred. During the second EVA, heart rates remained low but were elevated, similar to other Gemini EVAs, during hatch closure (Figure 2.6) [4].

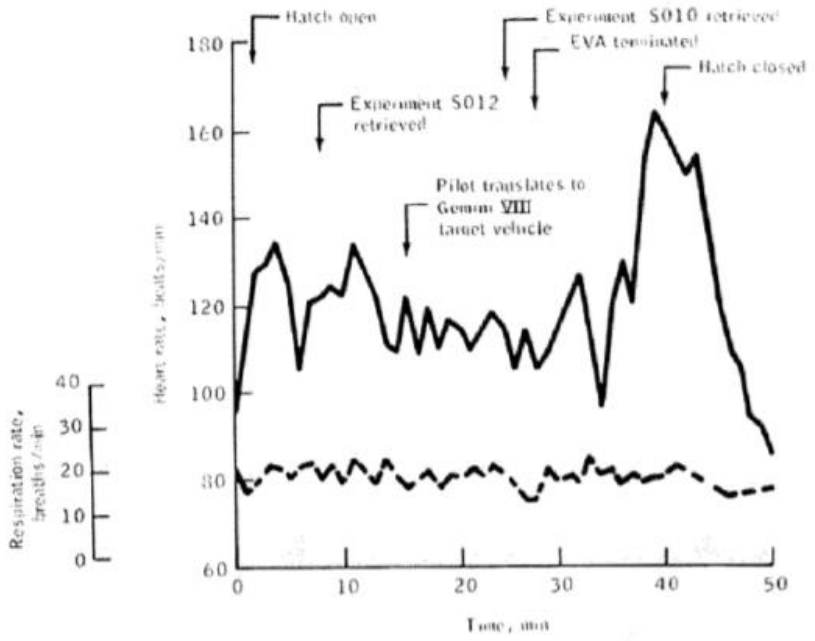

Figure 2.6: Gemini X second EVA heart rate and respiration rates (Paul, 2012).

EVA5 and EVA6 occurred during the Gemini XI launched on September 12th, 1966 [48]. Poor planning of EVA timelines led to early preparation of life support equipment four hours before the scheduled EVAs. This early preparation caused the unnecessary fatigue of the astronaut before his EVA. During the EVA, higher energy expenditures were experienced, causing increased sweat production, which ran down into the eyes [4]. Additionally, higher heart rates occurred during EVA preparation, egressing the spacecraft, and returning into the craft during hatch closure (Figure 2.7). Due to this fatigue, human error played a key factor in near misses, such as missing a tether point causing the astronaut to climb the umbilical as a rope to back to the Gemini XI spacecraft [49]. It was also noted that at this point in early preparation for this mission, the neutral buoyancy simulations were not mandatory for EVA training [48].

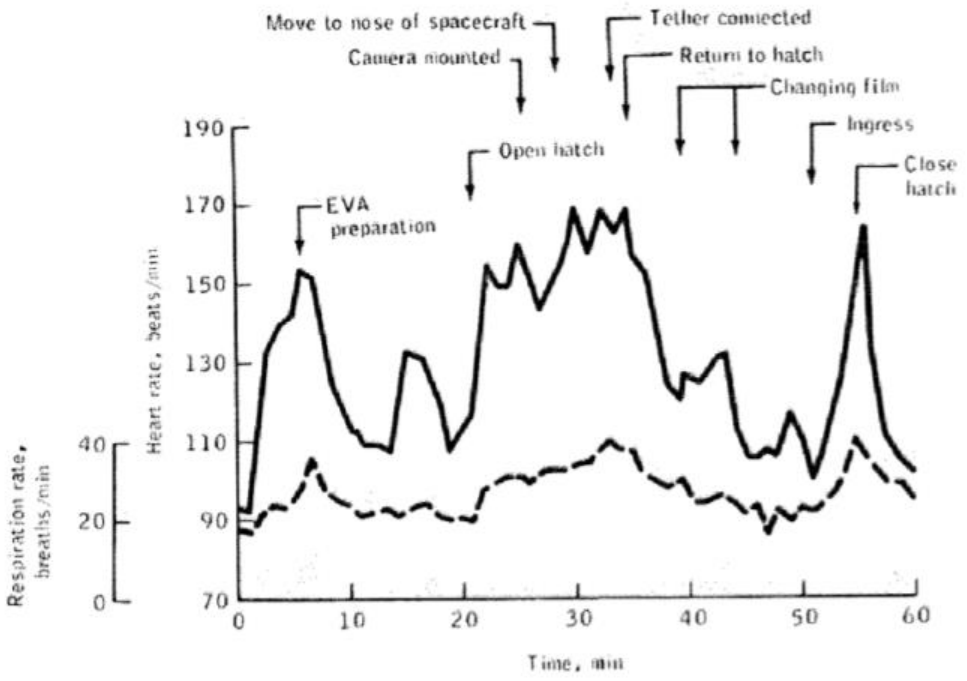

Figure 2.7: Gemini XI heart rate and respiration rates during EVA. Higher heart rates occurred due to fatigue from EVA preparation (Paul, 2012).

The final spacewalks EVA7 and EVA8 were conducted during the Gemini XII. Due to the previous Gemini missions, NASA had taken strict care to train, simulate, and plan for the EVA's [48]. During EVA heart rate was closely monitored, and the crew member was notified if above 140 bpm (Figure 2.8). This was to mitigate any increased workloads and energy expenditure. It was deemed that previous Gemini mission tasks had increased thermal strain when maneuvering the suit attached to the umbilical [4]. Information gathered by the six EVA operations of the Gemini missions paved the way for higher quality training within spacesuits for EVA, as well as technical advancements that led to the Apollo program being a success. Additionally, physiologic monitoring concluded that it was essential to provide real-time metabolic rate monitoring during EVA for workload and energy expenditure during tasks [4], [50].

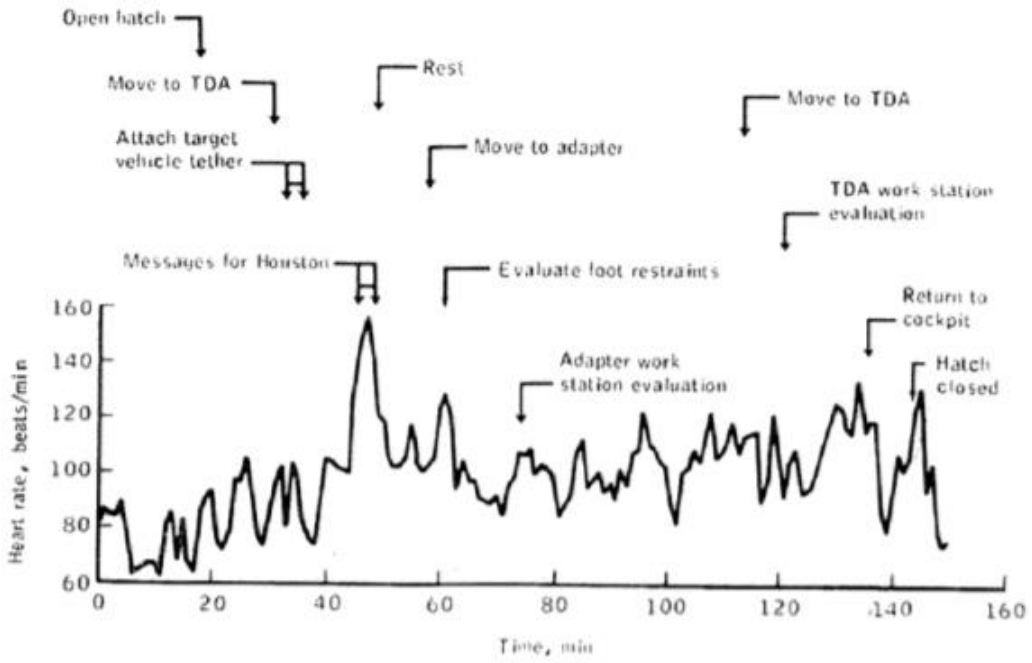

Figure 2.8: Gemini XII heart rate and respiration rates during EVA. Heart rates were monitored more closely than previous Gemini missions to mitigate higher energy expenditure (Paul, 2012).

2.1.3.2 Apollo

Following the Gemini missions, the Apollo program capitalized on the technical and operational advancements of the previous EVA endeavors. The suit A7L Extravehicular Mobility Unit (EMU) consisted of real-time monitoring of heart rate through one lead ECG. Additionally, it was added to use a liquid cooling garment (LCG) due to increased energy expenditure and thermal load experienced during Gemini. The suit also relayed real-time data of the LCG inlet and outlet temperatures in addition to oxygen tank bottle pressure from the portable life support system (PLSS). Metabolic rate was derived from three different relationships of heart rate, differential pressure of oxygen in the PLSS, and LCG heat balance between inlet and outlet temperature [4], [50]. Due to this real-time data and extensive training, metabolic rates describing energy expenditure were minimal during EVA. There were instances of increased energy expenditure

during some EVA tasks but ultimately, due to extensive task planning and lessons learned from Gemini, workload was minimal (Table 2.1) [4], [51].

Apollo 9 launched March 6th, 1969, and demonstrated one EVA testing of the A7L EMU and the PLSS in the Lunar Module (LM) [48]. The EVA did not experience any operational or technical issues other than one astronaut experiencing space motion sickness. With the test of the A7L EMU, the following EVAs for the Apollo missions were conducted on the surface of the moon. The famous Apollo 11 launched July 16th, 1969 and included the first Lunar Surface EVA utilizing the A7L spacesuit. The only technical issue during this EVA was recorded at the beginning of the operation as one astronaut experienced difficulty exiting the LM through the hatch due to his PLSS on is his spacesuit.

Mission	EVA Number	Crew Designation	Metabolic Rate (BTU/Hr)	EVA Duration (hr)
9	Zero-G	Pilot	600	0.98
11	1	Pilot	900	2.42
		Commander	1200	
12	1	Pilot	975	3.90
		Commander	1000	
	2	Pilot	875	3.78
		Commander	1000	
14	1	Pilot	800	4.80
		Commander	930	
	2	Pilot	910	3.58
		Commander	1000	
15	Zero-G	Pilot	940	0.67
		Commander	460	
	1	Pilot	1100	6.53
		Commander	980	
	2	Pilot	1000	7.22
		Commander	810	
	3	Pilot	1030	4.83
		Commander	810	
16	Zero-G	Commander	1998	1.42
	1	Pilot	870	7.18
		Commander	1010	
	2	Pilot	780	7.38
		Commander	830	
	3	Pilot	810	5.67
		Commander	820	
17	Zero-G	Pilot	1200	1.12
		Commander	570	
	1	Pilot	1090	7.2
		Commander	1080	
	2	Pilot	820	7.62
		Commander	830	
	3	Pilot	930	7.25
		Commander	940	

Table 2. 1: Apollo mission average EVA metabolic rates.

Apollo 12 experienced minimal operational issues during EVA which was related to dust accumulation [49]. Upon transit back to Earth, the astronauts had to clean the air filter every two to three hours from the dust accumulation, adding tasks to their mission [48]. Apollo 14 consisted of two EVAs. During EVA2 of Apollo 14 dust and the lunar terrain made it difficult to conduct EVA operations. The dust accumulation covered everything the astronauts worked with including the suits they wore. It was noted that the lunar surface was difficult to maneuver as landmarks seemed closer than they were and the sight was limited to 100-150 yards [48]. One technical issue arose in one of the A7L EMU wrist cables as it became damaged, limiting his hand motion.

The Apollo 15 of five total EVAs. Four of these EVAs were Lunar Surface EVA operations and the world's first deep-space EVA beyond Earth's inner magnetosphere. The astronauts were equipped with an updated spacesuit called the A7LB [48]. This suit allowed for extended EVAs and greater mobility. During this mission, one adapted operation technique that was shifted from the Apollo missions 11, 12, and 14 was the delayed charging of their PLSS backpacks with water. Due to this delay the astronauts were not able to charge their PLSS completely, which resulted in air bubbles causing failure warnings [48]. Other technical issues that arose were dust accumulation, failure in one of the astronaut's drink bag failures limiting water intake, and hand pain/fatigue due to fighting pressure.

During Apollo 16, astronauts conducted four EVA operations. During the EVAs, the usual dust mitigation problem was present however it was reported a close call of one astronaut who fell on the spacesuit PLSS after jumping and slipping on the lunar surface [49]. Additionally, technical issues arose with the Lunar Rover Vehicle (LRV) losing navigation guidance. The final Apollo mission to the moon consisted of Apollo 17. During this mission, a total of four EVA operations were conducted, three of which were Lunar Surface EVAs, and one was a Deep Space EVA.

During the first EVA injury to the hands was reported by astronaut one astronaut during improvisation utilizing tools to extract lunar surface core samples [48]. During the EVA the astronauts' overexerted themselves during core sample collection as the device became stuck. One astronaut's oxygen rose quickly, and with a resultant heart rate elevation to 145 beats per minute. Astronaut Schmitt had to throw his weight into the core sample device, causing him to fall. The Apollo Era led to improved training modalities from lessons of surface and space environment tasks loads experienced by Apollo astronauts. From the testing of real-time metabolic rate measurements, oxygen differential pressure was used for future EVAs.

2.1.3.3 Skylab and Pre-International Space Station

Several applications of human spaceflight were conducted during the time between the Apollo moon landings and the operations of the International Space Station (ISS). These endeavors consisted of the Russian Salyut program, US Skylab space station, Russian Mir space station, and space shuttle. EVA operations of each program added on to lessons learned during spacewalk tasks and close calls that led to minor injuries or could have led to serious injury. Aboard Skylab 4 launched November 16th, 1973 on EVA1 astronauts recorded difficulty in separating the spacesuit umbilical, which could have led to extreme entanglement [48].

The Salyut 6 Principal Expedition (PE) 1 launched December 10th, 1977, experienced similar umbilical and lapses in tether placement that could have led to detachment to the spacecraft. Following the Salyut 6 PE missions, the Salyut 7 PE-1 mission exhibited an EVA that resulted in a minor event that could have led to injury [48]. During one of the EVA tasks, one cosmonaut experienced hand numbness and pain in the Orlan spacesuit due to pressure and hand placement. Additionally, it was noted that difficulty and overexertion occurred when the cosmonauts tried to

exit through the rear suit hatch of the Orlan. Similar hand fatigue and injury were reported on Salyut 7 PE-3 mission EVA6 [48].

During the Russian Salyut and Mir programs, the US conducted flights utilizing the space shuttle. EVAs aboard the space shuttle utilized the extravehicular mobility unit (EMU) and manned maneuvering unit (MMU) for motion. The space shuttle allowed for larger crews to be present for each mission. One space shuttle mission STS-41C aboard the Challenger shuttle, was launched on April 6th, 1984. During this mission, two EVAs were conducted to retrieve and repair the Solar Max Satellite. During the first EVA one astronaut tried to dock to the Solar Max Satellite with the MMU however, the docking failed, which led to a low spin experienced by the satellite. The astronaut attempted to stabilize the satellite however reversed the spin, which caused a two-axis tumble [48]. This is an example of a technical fault event that led to operational improvisation, causing an operational error. Other issues on the second EVA had arisen when astronauts reported EMU helmet fogging and urine contaminant failure. Helmet fogging became an issue in a multitude of EVA operations, including STS-51I aboard the space shuttle Discovery launched August 27th, 1985. During these EVAs astronauts recorded difficulty handling the Leasat 3 satellite due to lack of visual cues and helmet fogging causing a threat of the satellite colliding with the space shuttle [48]. Additionally, it was recorded that there was accidental reuse of lithium hydroxide canisters from the first EVA, which lowered the efficacy to scrub carbon dioxide [49].

In tandem with later space shuttle missions in the late 1980s to mid-1990s, the Mir program conducted multiple EVA operations in the Orlan-DM space suit. On the Mir PE-2 mission, one cosmonaut reported that the Orlan space suit experienced minor pressure drops and was diagnosed with the wrong switch placement. Other Mir missions reported injuries to hands, elbows, and shoulders caused by the pressure of the spacesuits and EVA tasks during operations. During Mir

PE-9 one crew member's space suit heat exchanger failed, which caused helmet fogging and lost visuals. The cosmonaut had to be led back to the Mir station for ingress [48].

Aboard STS-37 on the space shuttle Atlantis one crew member exhibited minor confusion after one of the EMU gloves was punctured by a palm bar [49]. There was also some reported eye irritation. Similar eye irritation was reported on STS-63, STS-97, STS-100, and STS-143. Additionally, on STS-63 during EVA the EMU became unacceptably cold and the EVA was terminated. The temperature fluctuations and overcooling of the EMU have been recorded in multiple space shuttle EVA operations. Leading up to the ISS completion, the EVAs conducted by the space shuttle, Salyut, Mir, and Skylab programs provided continuous microgravity environmental experience for astronaut spacewalk tasks. Task loads and complex EVAs were completed in the repair of satellites and investigations into human performance in microgravity. The primary issues that arose during EVAs resulted in minor injuries to the eyes and hands. Minor operational risks that could have led to major injuries were identified through a common lapse in tether placement and specific tasks trained on the ground.

2.1.3.4 International Space Station

ISS continues operations with a multitude of EVA missions to conduct maintenance of the spacecraft and science equipment. The spacesuits used on the ISS are the extravehicular mobility unit (EMU) and Orlan suit. The EMU utilizes the PLSS with real-time data of heart rate and metabolic rates. The integration from space shuttle EVA operations incorporated a liquid cooling and ventilation garment (LCVG) for thermal control. The PLSS contains ventilation and thermal control to keep the crew member comfortable and provides life support consumables [52].

A few examples of operational and technical issue events are shown with close call incidents. On July 16th, 2013, during an EVA of the International Space Station, one of the crew members reported feeling water on the back of his head midway through EVA [53]. As the crew member continued to work, the water migrated around his head onto his face. The EVA was terminated, and the crew member needed assistance returning for ingress into the ISS. He had to manually feel for his safety tether cables as a pathway to the ISS. During the EVA it was reported that 1 to 1.5 liters of water had entered the crew member's helmet, obstructing his eyes, nose, and ears [53]. This impeded his vision, breathing, and communication with ground control. The resultant operational emergency response was correlated to the technical failure of the EMU ventilation loop. Additionally, dry-out of the EMU in the ISS was completed by use of a vacuum cleaner. The vacuum cleaner unexpectedly pulled oxygen from the EMU secondary high-pressure oxygen tank, causing a dangerous environment with pure oxygen [53]. On U.S. EVA24, during the post-check operations of the EMU, one crew member accidentally actuated the spacesuit's feedwater switch causing water to flood the sublimator [49]. This caused irreparable damage to the EMU and was unfit for use on future EVAs of that mission. During U.S. EVA35 another crew member had mentioned water in the helmet, which caused early termination of the EVA [49].

From the case studies of the EVA operations of early Gemini missions leading up to the current ISS EVAs, technology has greatly improved the knowledge of suited human performance in microgravity. The top factors that can lead to successful EVA operations are focused on human factor error reduction and real-time monitoring of physiologic parameters. Technology in a suited environment is limited and sensors or techniques that can be applied to accomplish multi-process feedback, such as, workload strain and thermal regulation in real-time will be a necessity in long-

duration spaceflight. Long-duration spaceflight will not be able to rely on ground control to give guidance on specific tasks or workload measurements.

2.2 Cardiovascular Responses to Fatigue and Workload a Precursor to Human Error

The cardiovascular system is robust, however, cardiovascular function is profoundly susceptible to stress [54]. Chronic stress has been shown to increase sympathetic nervous system responses, which in turn can elevate arterial blood pressure and cause tachycardia events [55]. Additionally, the effects of stress responses in reaction times to current tasks have associated responses to systolic blood pressure status and heart rate later in life (e.g., 10 to 15 years after reaction tasks) [56]. Workloads and fatigue go hand in hand in normal human operational environments. The focus of this dissertation is primarily on aerospace industries, but any human factor workload increase has a stress component that affects the cardiovascular system and regulation. Increasing task workloads have been shown to shift autonomic nervous system responses that control cardiovascular function leading to an induced stress state [57]–[59]. In many cases, time constraints intensify workload strain increasing situational stress, which can be shown in the following case studies that focus on commercial aviation human error. However, adding in physical or mental fatigue to a set of workload tasks can further alter cardiovascular regulation leading to exhaustion [60].

Measurements of cardiovascular responses, workload, and fatigue can be accomplished through variations of heart rate fluctuations measured through time between heartbeats or R-R intervals. This technique is called heart rate variability (HRV) and is used to measure the effects of the heart in relation to control mechanisms from the autonomic nervous system [12]. Decreases in HRV total power can be attributed to increased stress and fatigue on tasks shown through

increased sympathetic activity metrics. While, increases in HRV total power generally describe rest periods with reduced stress as an increase in parasympathetic activity control [58], [61], [62].

2.2.1 Commercial Aviation Human Error

Human fatigue is a significant concern impacting the welfare and safety of the traveling public in all transportation modes. In this next section discussion of aviation mishaps due to human error is presented. In these case studies, pilot error, fatigue and stress were compounding factors that lead to loss of vehicle and loss of life. Nearly 20 percent of the 182 major National Transportation Safety Board (NTSB) investigations conducted between January 1, 2001, and December 31, 2012, had found fatigue to be the probable cause, finding, or contributing factor to the accident [63]. Human fatigue amplifies an individual's poor judgment, slowed reaction times, and loss of situational awareness. Fatigue also, in these cases, added to workload stress leading ultimately to human error at the time of each accident. Previous research has shown that high levels of task or situational stress are leading causes of pilot error [2], [64], [65]. In tandem with increased task loads, technology advancements meant to reduce human error, however, can add to the complexity of a system having the reverse effect [66] Pilot fatigue and task stress can degrade their ability to safely control the aircraft placing the public unsafe or dangerous circumstances.

2.2.1.1 Colgan Air Flight 3407

On February 12, 2009, at 10:17 eastern standard time, a Cogan Air Bombardier (Q400) flight 3407crashed into a single-family home in Clarence Center, New York, which was 5 nautical miles northeast of the intended airport. The crash occurred when the aircraft was on instrument approach to Buffalo-Niagara International Airport or (BUF). Unfortunately, both pilots, two flight attendants, and 45 passengers aboard the flight were killed, in addition to one person on the ground who was in the single-family residence [67]. The probable cause of the accident was determined

by National Transportation Safety Board (NTSB) to be likely due to the captain's incorrect response to activation of the stick shaker, which in turn led to an aerodynamic stall to which ultimately the aircraft did not recover. Other compounding factors that led to the accident were failure to abide by sterile cockpit procedures, the captain's miss management of the flight, the crew's failure to monitor airspeeds relative to the rising position of the low-speed cue, and Colgan Air's insufficient procedures for appropriate airspeed selection as well as training for managing approaches in icing conditions.

From the accident report, the NTSB concluded that the pilots' flight performance was likely impaired because of fatigue. On the day of the accident, the captain had been working long hours, and his actual sleep amount was unknown. However, he had opportunities to sleep for a 21-hour, 16-minute scheduled rest period. During this period, It was recorded that he did not have adequate resting due to work activities and attempted to sleep in crew quarters [67]. Due to these conditions and the activities of the captain, he would not have had the opportunity to restore sleep loss that had accrued from the previous two scheduled working days [67]. At the time of the accident, the captain would have been awake for more than 15 hours. According to reports, the accident occurred about the same time that the captain's sleep opportunities during the previous days and the time at which he normally went to sleep. The captain had experienced chronic sleep loss, and both he and the first officer had experienced interrupted and poor-quality sleep during the 24 hours before the accident.

The first officer had been awake for almost nine hours at the time of the accident. Leading up to the initial start of flight 3407, however, the first officer made decisions to begin a transcontinental commute 15 hours before her scheduled report time. The first officer did arrive at the initial airport seven hours before her scheduled report time, though this time was reported to

be less than her normal sleep schedule, and evidence had indicated that she was unable to use all of that time for sleep. According to the company guidance, it did not discourage pilots from commuting the same day of a scheduled flight.

Accident investigations and reports have shown negative effects of fatigue on human performance. These effects can reduce alertness, degrade mental state, and decrease physical performance [67]. Some of these can result in vigilance breakdown, reduced and inaccurate reaction times, reduced efficiency in decision-making, lowered risk assessment as well as decreased motivation. Additionally, task prioritization and management be greatly affected by fatigue states. In this flight, the failure of both pilots to detect flight cues compounded by their improper response to the stalled aircraft are consistent fatigue effects. Continually, the pilot's workload management issues and minor errors that occurred during the flight (e.g., delayed responses to altitude alerts) point also to fatigue.

Beyond fatigue, the NTSB also identified that workload management was a large factor attributing to the accident. The captain did not recognize the onset of the stick shaker and the first officer's tasks at the time the low-speed cue occurred would have likely reduced opportunities for her timely recognition of the event [67]. The fact that both pilots failed to recognize these situations had shown a significant lapse in their workload management. According to the accident report of flight 3407, if the captain had properly responded to this nose-down input and stall condition, the impact might have been avoided due to the aircraft might have recovered its flying speed. Adding a compounding factor, both pilots were distracted because they had held non-flight-related conversations which is beyond the flight rules of a sterile cockpit. The flight crewmembers were fatigued, distracted, and under workload strain leading to operational task errors, lapses in monitoring, and decreased situational awareness.

2.2.1.2 UPS Airlines Flight 1354

August 14, 2013, at 04:47 central standard time an Airbus A300-600, operating as a UPS Flight 1354 crashed short of the runway at Birmingham-Shuttlesworth International Airport (BHM), Birmingham, Alabama. The crash occurred during a localizer non-precision approach to BHM runway 18. In this flight, unfortunately, both pilots sustained fatal injuries and were killed [68]. The probable cause of the accident of flight 1354 was determined by the NTSB to be associated with the flight crew's compounding errors centralized around the continuation of an un-stabilized approach and failure to monitor the aircraft's altitude during the approach. These factors ultimately led to descent below the minimum approach altitude and steered the aircraft into surrounding terrain [68]. Six total elements contributing to the accident that was identified by the NTSB were the following: the captain's flight performance lowered by fatigue, confusion, and distraction; the first officer's fatigue state due to critical sleep loss; the captain's failure to communicate actions and intentions to the first officer when the vertical aircraft profile was not captured; the crew's failure to verify proper configuration of the flight system for the profiled approach; the crew's lapse in judgment of cloud visibility at 1,000 ft above ground level as a result of incomplete weather information; the first officer's delay and failure to make minimums callouts [68].

From the accident report leading up to the accident, the captain had stated concerns about increasing demand on flying schedules. The NTSB concluded performance regarding the captain's actions was consistent with fatigue due to circadian factors that were present at the time of the accident. Additionally, the NTSB concluded that the captain's poor performance during the flight was likely due to past insufficiencies in flying non-precision approaches. The building errors that the captain had made were shown from the analysis that he had shown confusion as to why the

flight profile was not engaged. This resulted in his belief that the aircraft altitude was higher than actually recorded [68].

Analysis of the off-duty schedule of the captain had shown he had opportunities to recover any sleep loss. However, as this flight had taken place in the early morning hours, the time is associated with a decline in circadian rhythm leading to a fatigued state. Previous research has shown that well-rested individuals experience decreased operation performance during these times [69]–[71]. Ultimately, it is described that the captain is solely responsible for control and tone of the cockpit for which remains critical during higher workloads attributed approach and landing phases of flight. At the time of the accident, the captain had made poor decisions in continuing the approach when the profile did not engage and by not communicating the approach method changes. Additionally, tasks associated with monitoring the descent rate and altitude were not followed and errors occurred to initiate alternative approach decisions when un-stabilized below 1,000 ft [68].

Aside from the captain's actions, the NTSB also concluded that the first officer was fatigued due to acute sleep loss and circadian rhythm factors. The fatigued state compounded with higher workloads combined with the change in approach created additional time compression resulting in multiple errors made during the time leading up to the accident. Because the accident occurred in the early morning again associated with declined circadian rhythms, the first officer was susceptible to fatigue effects. It was also reported that the first officer had been awake for 13 hours before reporting for duty with 2.5 hours to recover sleep. The first officer's day of duty required an additional 9.5 hours of awake time [68].

Consequently, the type of approach for flight UPS 1354 leads to higher workloads. A non-precision approach can lead to variations in the descent rate of the aircraft and flight path angle of the final approach fix and the runway. This approach analogous to stair-stepping to the runway is

coined “dive and drive” as a technique [68]. In the analysis, it is reported that these step-downs that are flown without constant descent require multiple inputs of thrust, altitude adjustments, and pitch which can greatly increase the pilot workloads leading to potential errors [68]. Finally, the NTSB concluded that the change to a vertical speed by the captain after not capturing the glide path profile was not appropriately associated with known procedures or guidance, which, created increased workload and time constraints for the first officer to the necessary required tasks.

2.2.1.3 American Airlines Flight 1420

American Airlines Flight 1420, operating a McDonnel Douglas DC-9-82 aircraft on June 1, 1999, at 11:30 pm central standard time, crashed after overrunning the end of the runway during landing sequences at Little Rock National Airport in Little Rock, Arkansas. There were eleven fatalities, including the captain and ten passengers. From the accident report, the NTSB determined that the cause of the accident of American Airlines flight 1420 was predominately the flight crew’s failure to discontinue an approach in the presence of a severe thunderstorm in addition to human procedural errors. It was also determined that compounding factors that contributed to this accident were as follows: The crew’s lowered flight performance associated with fatigue and situational stress under the landing circumstances; continued approach to landing when the maximum crosswind created by a severe storm was exceeded acceptable limits; and inappropriate use of reverse thrust greater than 1.3 engine pressure ratio after landing the aircraft [72].

In the analysis report, as the aircraft intercepted the final approach course for the runway, the crew entered into a high workload and event-dependent flight phase [72]. It is defined that normally, during this phase, flight tasks can include maneuvering and controlling the aircraft, configuration of the landing sequence into the aircraft computer, final landing checks, and monitoring but also evaluating the aircraft criteria for landing [72]. Leading up to this accident,

the crew's decision to accept and perform a short approach greatly increased the already high workloads due to creating time constraints to perform required tasks.

Additionally, upon landing, the flight crew utilized manual braking too, which the NTSB detailed at the time, airplane operators can choose not to use automatic braking due to wearing of the brake system, which could occur faster which may require more frequent brake replacement. In the accident report, it was determined that high workload landing situations may require more aggressive use of the rudder pedals, to which the use of the automatic brake system provides pilots with faster and more consistent braking on the runway. From this observation, the NTSB concluded that automatic braking systems ultimately reduce strain on the pilot's workload during wet, slippery, and high crosswind landing conditions [72].

Through investigations of fatigue, it was found that the flight crew had been awake continuously for 16 hours. Previous research of transportation accidents from the NTSB had found that a normal waking day is between 14 and 16 hours and as a corollary, the lapse of vigilance is shown to increase if the waking day is extended [72]. In addition, the NTSB conducted a study in 1994 of flight crew-related major aviation accidents, which found that flight crew made significantly more errors if awake for an average of about 13 hours compared to crews with an average waking time of 5 hours [73]. As a compounding factor, the accident time was approximately two hours after the time both pilots started sleep schedules. Previous studies have shown that an individual's ability to consider alternative options decreases with increased fatigue but alternatively, they become fixated on a predetermined desired outcome [72]. Additionally, it becomes more difficult for an individual who is fatigued to remember if tasks have been completed or not [69]. Particularly at the time of the accident, several factors point to these fatigued states such as no alternative considerations taken regarding delaying or diverting the landing, the first

officer did not validate landing tasks, and the captain did not realize his callout tasks. Further defining these events, fatigue can deteriorate an individual's performance on specific tasks that are time-sensitive and event-dependent sequences. As a result of this analysis, the NTSB had concluded that flight performance of the flight crew had been observed as a known effect of fatigue.

Both pilots made rudimentary errors in flight operations and included basic routine tasks, such as required callouts. Situational stress from the severe weather provided environmental stressors that increased the workload for the two pilots. The NTSB also concluded the flight performance had shown evidence of situational stress by their specific operational errors in addition to their poor decision-making. Stress has been shown to impede the ability to assess alternative options [72]. The fact that the crew had set expedited the landing sequences in the presence of weather events caused distractions that preoccupied their attention from other critical activities leading up to the accident.

2.3 Current Techniques and Limitations of In-flight Monitoring of Workload and Heat Strain

The workload is the representation of the ability or cost of a human operator to accomplish specific task requirements. In a perfect world, a person could complete tasks efficiently, on time, and with little effort, however, generally, this is not the case due to the "cost" such as fatigue or stress. Additionally, the workload can be classified as either physical or mental activities and can be affected by three defining categories, such as the time to complete the task, the type or amount of work being done, and circumstances (e.g., fatigue) related to the performance of an individual [74], [75]. High and low workloads could both reduce an individual's performance dependent on fatigue states. High workloads during fatigue can be classified as active fatigue and could surpass

the mental capacity of an individual due to high mental demands in turn causing distress. Alternatively, low workloads during fatigue can be classified as a passive fatigue state which occurs when a task does not stimulate the individual enough to keep them engaged (e.g., drowsiness) [74], [76]. There are multiple approaches for detecting workload fatigue, to which the two primary categories are either subjective or objective measures.

Subjective measures focus on the individual's self-assessment of workload task efficiency, while objective measures concentrate on performance measurements through monitoring physiological responses [77]. Subjective measures investigate an individual's behavior by helping determine how those individuals perceived responses to task loads or situations. Generally, in the form of surveys or questionnaires, subjective measures can be susceptible to influences, such as, internal and external environmental factors that could lead to unreliable results. Examples of fatigue self-reporting scales include Karolinska Sleepiness Scale, NASA Task Load Index, and Samn-Perelli Fatigue Scale [77]. These scales ask subjective questions regarding sleep frequency, sleep duration, and levels of sleep. However, the NASA Task Load Index (NASA TLX) focuses on six subscales of workload that represent physical, mental, frustration, temporal demands, effort, and performance. The combination of these six subscales represents a total value of workload (Figure 2.9) [78], [79]. Though, subjective measures could yield less reliable results when compared to objective measures. Previous studies had shown lower perceived stress from subjective measurements, whereas objective physiologic measurements had shown these drops in performance [77], [80].

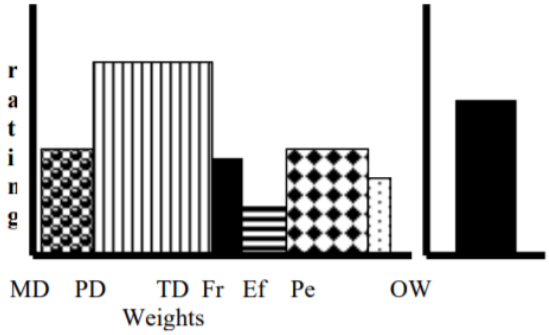

Figure 2.9: Graphical representation of NASA TLX six subscale weights of task loads and total workload.

Objective measurements of workload and fatigue yield unbiased analysis of data free from input from the subject. These measurements used in previous research include eye movements, posture, brain activity through electroencephalogram (EEG), and cardiovascular metrics [77], [81]. Other common objective measures that are used focus on stimulus-response tasks such as psychomotor vigilance tasks (PVT), decision-making, cognitive task loading or mental rotations (e.g., simple math or puzzles), or complex problem-solving tasks or pattern-matching [82]–[84]. Objective measures are robust; however, they can be susceptible to environmental factors and noise.

In aerospace environments, objective and subjective measures are difficult to obtain during actual tasks. Technical hardware can become distracting to pilots that could lead to unwanted noise and disrupt workload. A review by West discusses the inadequacy of collected physiologic data in airborne environments to monitor flight crew, particularly fighter pilots, ground-based data collections [85]. As also mentioned by West, the data collection in a flight environment has susceptibility to vibrations, electromagnetic interference, and ambient noise, which could disrupt important physiologic data [85]. As a corollary, in spaceflight environments, limited space for sensor equipment is an additional factor, specifically in a spacesuit. Drawing correlations between physiologic measurements is key to downsizing monitoring techniques to small, simple sensors. As a corollary, limited numbers of research have investigated pilots and astronauts of objective

physiologic metrics for real-time workload determinations in actual flight environments [81]. This fact also holds for spaceflight, particularly in sample size with the limited individuals who have been to space. Popov et al. discuss a focused goal for spaceflight is to gather physiologic data for real-time prognosis focused on long-duration spaceflight where astronauts do not have access to telemedicine or mission control [86]. Ultimately, due to the aerospace environment, most research focuses on analog or flight-like simulations to attain tasks and workloads [81], [87]–[89].

As aerospace becomes more available to the public, opportunities to develop research and data collection techniques for these environments are increasingly crucial. There are increasingly available options to monitor workload through cardiovascular function by utilizing ECG to determine the ANS state due to stress [12], [90]. HRV has been used as an indicator to identify drowsiness or fatigue among pilots [91], [92]. Further HRV metrics are defined in Chapter 3 for applicability in determining fatigue and stress in pilot's during flight tasks. Another non-invasive technique that has been used to measure fatigue states have been photoplethysmogram (PPG). PPG is an optical technique giving information of beat-to-beat blood volume changes via illumination of skin as a measurement of light absorption [93], [94]. Generally, PPG can be collected from a pulse oximeter at the finger. Building cardiovascular correlations is a non-invasive technique that can aid in understanding the body's response to increased workload and fatigue.

2.3.1 Heat Strain and Workload

The workload is highly associated with the individual's interaction with the environment. The thermal characteristics of the environment can have a compounding result that both increases heat and workload strain on the individual. In aviation, an example of flight would be warm climates where most smaller aircraft ventilation becomes cooler in flight. For high altitude flights, pressure suits and cooling ventilation does not start until a certain altitude [95]. On the ground, thermal

limits can be reached, which can degrade cognitive performance leading to lapses in judgment, potentially leading to mistakes. Whereas in spaceflight, thermal regulation and environmental change are drastically associated with physical and mental challenges. Focused primarily on an enclosed space suit, the environment is designed to aid in cooling of the astronaut but can also impair the human thermoregulatory mechanisms, in turn increasing heat stress [44], [95]–[98]. A technique used in the design of these cooling systems is through human thermal modeling which can yield simulated regulatory responses to harsh environments [99]. There have been many studies that have attempted to investigate physiologic responses to heat stress, however, there are not as well-known [23], [100]–[102].

One researcher suggests an approach consulting three ideologies in attributing thermal heat strain to workload cognitive decline [103]: 1) Performance breakdown will be observed if deep-core body temperature increases away from normothermic comfort levels. 2) Observance of a hyperthermic state with constant, elevated core body temperature. While workload cognitive decline can occur, it is mentioned that potential watchkeeping performance can improve potentially due to elevated cardiovascular demand. 3) Environmental thermal load is intense enough to cause maintained elevation of core body temperature.

Generally, the common techniques to determine thermal strain on an individual are centralized around instrumentation that involve objective measures, such as, heart rate, core body temperature, skin temperature, sweating rate, or water loss [104]. However, none of these measurements alone can accurately depict thermal workload strain [105]. Core body temperatures can indicate thermal strain ranging from 38.5°C to 40.0°C but are dependent on the type of clothing worn, fitness level, and the environment [105]–[108]. Increases in heart rate can be attributed to workload increases or blood flow demand through vasodilation [105]. When combining these measurements, a higher

quality depiction of thermal strain can be developed. Heat strain is a risk for occupations that include high heavy workloads, bulky protective encapsulating clothing, and hot environments. In environments and situations, physiological monitoring is imperative to improve workload efficiency and safety.

PART II: EVALUATION OF CARDIOVASCULAR REGULATION TO FLIGHT-LIKE ENVIRONMENTAL STRESSORS

Chapter 3. PILOT CARDIOVASCULAR RESPONSES TO IN-FLIGHT STRESS: WORKLOAD METRICS DETERMINED BY HEART RATE VARIABILITY

3.1 Summary

During flight operations, pilots perform specific procedural tasks in a range of workload conditions, from low to high. A pilot's fatigue state, driven by physiological conditions, can affect their ability to respond appropriately during periods of high or changing workload. The purpose of this study was to investigate the cardiovascular responses to changes in flight task workloads. A three-lead electrocardiogram (ECG) was collected from 12 subjects during a pre-determined flight sequence with varying levels of flight maneuver complexity. R-R intervals were extracted from ECG and utilized to analyze heart rate variability (HRV).

To cross-validate, the physiological data, survey data of flight maneuver workloads were collected from aviation faculty or airport leadership (N = 24). These survey data consisted of workload classifications of flight maneuvers as "high", "medium" or "low" designated by values in a range from 3 to 1, respectively. Mean heart rate (HR) increased (decreased mean R-R interval) with increasing task load.

Time-domain features of SDNN and RMSSD decreased with increasing workload. Frequency-domain metric LF power increased, and HF power decreased in response to increased task complexity. LF/HF reflected this shift by increasing with increased stress. The nonlinear metric SD1 decreased, while SD2 remained stable in relation to increasing tasks load. Detrended fluctuation analysis (DFA) α1 increased with increasing workload. These results indicated that known decreases in short-term HRV associated with physiologically increased sympathetic nervous system (SNS) activity and increased stress during high task loads in-flight were correlated to subjective expert rankings of aviation task complexity.

3.2 Background

Pilots encounter a variety of in-flight environmental interactions while also expected to perform tasks at a high level of alertness. However, compounding factors beyond in-flight tasks can degrade pilot perception, cognitive functions, memory, attention, and spatial awareness, often as a result of fatigue [109], [110]. Fatigue, in a basic form, is a decreased ability to perform physical or mental work as a function of sleep, disruption to circadian rhythm, or task frequency [3], [111], [112]. Increases in workload, abnormal working hours, long duty intervals, impeded sleep, and complexity of human-technology interface are elements that can lead to operational errors [113]–[115]. Rosekind et al. reported that 71% of 1488 surveyed pilots reported "nodding off" at least once during flight [116]. Workload and fatigue are of particular concern in aviation as human error contributes to 66% of flight crew accidents and 79% of fatal accidents attributed to pilot error [1]. Identifying predictive physiologic metrics for fatigue and stress states would aid in mitigating flight risk improving safety. Previous studies have shown correlations between pilot drowsiness and cardiovascular function during simulated flights [81], [93]. Additionally, based on piloting tasks and situations, cardiovascular metrics can be used as an indication of changes in fatigue and mental workload [117], [118].

Cardiovascular function is regulated by the autonomic nervous system (ANS). ANS is split into two elements: the sympathetic nervous system (SNS) and parasympathetic nervous system (PNS) [57]. SNS and PNS activity shift to preserve a balance of vital function or homeostasis. However, due to internal or external stimuli, this balance can be dominated by either branch. This dynamic control is reflected via fluctuations of the time intervals between successive heartbeats, which is called heart rate variability (HRV) [119]. PNS activity has been shown to decrease heart rate and increase HRV, while SNS activity increases heart rate and decreases HRV [120], [121].

As a corollary, studies of in-flight pilot mean heart rate (HR) have shown increases due to increased task complexity [117], [122]–[124]. HRV is a reliable non-invasive measurement in determining the status of cardiovascular and ANS due to stress and recovery [58], [61], [125].

3.2.1 Overview of HRV

HRV is described in metrics of time-domain, frequency-domain and nonlinear measurements. Time-domain features focus on the variations in time intervals between heartbeats. Two common time-domain features are the standard deviation of normal sinus beats (SDNN), and the root means square of successive differences between normal heartbeats (RMSSD). RMSSD is influenced by PNS activity and reflects beat-to-beat variance in HR [12]. RMSSD is one key metric used to estimate vagal activity reflected in HRV [126], [127]. SDNN corresponds to a total cyclic fluctuation of HRV correlated to SNS and PNS activity [128]. High values of SDNN and RMSSD show resilience to stress [128], [129]. Another less common metric of HRV is the triangular interpolation of the normal-to-normal (NN) interval histogram or TINN. This metric measures the width baseline of the RR interval histogram [12]. Lower values of TINN can indicate decreases in RR intervals, increases in HR, and higher stress [62].

Frequency-domain metrics estimate HR through fluctuations in the relative or absolute power of four main frequency bands. These bands correspond to ultra-low-frequency (ULF), very-low-frequency (VLF), low-frequency (LF), and high-frequency (HF). The LF band (0.04-0.14 Hz) and the HF band (0.15-0.4 Hz) are commonly utilized to view the interaction of PNS and SNS activity, including the LF/HF ratio [12]. LF HRV components can be created from both PNS and SNS; however, increases in LF power can be linked to increased SNS activity during stress [125], [128]. HF components are primarily dominated by PNS activity and linked to the RMSSD time-domain metric. Lower HF power is tied to increased stress, panic, worry, and anxiety [12], [57].

Additionally, the relationship between LF and HF shows that lower LF/HF metrics could reflect PNS dominance, whereas high LF/HF values would reflect SNS dominance [130].

Nonlinear Measurements can be used to view the unpredictability in the HRV time series. The first metrics of SD1 and SD2 are fit from a Poincare plot to which the area of this plot corresponds to LF and HF power, RMSSD, and baroreflex sensitivity [12]. SD1 corresponds to the Poincare plot width and reflects short-term HRV [131]. The RMSSD fluctuations are identical to that of SD1 variations. SD2 is determined as the length of the Poincare plot and measures both short-term and long-term HRV related to LF power [132]. Creating a ratio of SD2 and SD1 gives a window into the unpredictability of the R-R interval time series to monitor ANS balance [133], [134]. Further metrics of detrended fluctuation analysis (DFA) allow for analysis of successive R-R intervals over varying time scales. DFA results in two slopes of $\alpha 1$ (short-term fluctuations) and $\alpha 2$ (long-term fluctuations) [12], [135].

3.2.2 HRV of Pilots

Studies of pilot HRV have been conducted in the past, focused on time-domain features of SDNN and RMSSD or frequency domain features of LF, HF, and the ratio LF/HF. These metrics do provide views into task workload for pilots. However, most pilot flight studies have also been conducted using flight simulators [89], [91], [136]–[142]. Cao et al. and Mansikka et al. reported decreases in both SDNN and RMSDD with increases in LF/HF during higher stress maneuvers during a simulated flight environment [89], [139]. Flight simulators provide a safe and economical platform for pilots to learn instrumentation and flight profiles. In contrast to flight simulators studies, few studies have investigated real in-flight HRV relations to stress [117], [140], [143]–[145]. Most of these studies investigated HRV pre-flight in comparison to post-flight on

cardiovascular measurements. However, Sauvet et al. showed that during multi-leg cross-country flights decreases occurred in SDNN, SD1, and SD2 metrics with increased LF/HF [92].

This study aims to identify cardiovascular metrics of workload strain that can be used as predictive metrics of fatigue in pilots during flight. It was hypothesized that HRV metrics could be used to predict increased task workload demand. As a corollary hypothesis, subjective expert ranking of workload complexity would be expected to match ANS fluctuations measured by HRV.

3.3 Methods

3.3.1 Participant

The study participants consisted of collegiate aviation students who held a Federal Aviation Administration (FAA) commercial pilot certificate in addition to either an FAA Class I or Class II medical certificate (N = 12, Average Flight Hours = 327.67±198.92). Each participant was current in the type of aircraft that was flown (Cessna 172S or Piper Archer) and experienced with the Garmin G1000 avionics system. Informed written consent was provided and obtained from each subject. This study protocol was approved by the University of North Dakota Institutional Review Board.

3.3.2 Procedure

The experimental protocol included three phases of data collection. Phase I consisted of pre-flight baseline recordings while the participant was in a quiet office space. The following two phases consisted of the pre-determined flight sequence directed by the PI as the safety pilot. Phase II flight tasks including 'Taxi', 'Take-Off', 'Climb', 'Level Turns', 'Straight and Level', 'Steep Turns', 'Missed-Approach'. Phase III consisted of a repeat of phase I tasks, including the second 'Missed-Approach' and 'Landing'.

Cardiovascular function (ECG and photoplethysmography) was continually assessed during all phases of this study. ECG was collected via two systems in a Lead-I configuration (ABM B-Alert x-24, CA, USA) and (Bitalino ECG, Portugal). Photoplethysmogram signal was collected behind the ear under the pilot headset, also using Bitalino.

Additionally, to add a second cross-reference of workload, survey data of flight maneuver workload ranking was collected from aviation faculty or airport leadership (N = 24). This survey data consisted of classifications of flight maneuvers as "high", “medium” or “low” workload designated by values in a range from 3 to 1 respectively (Figure 3.1).

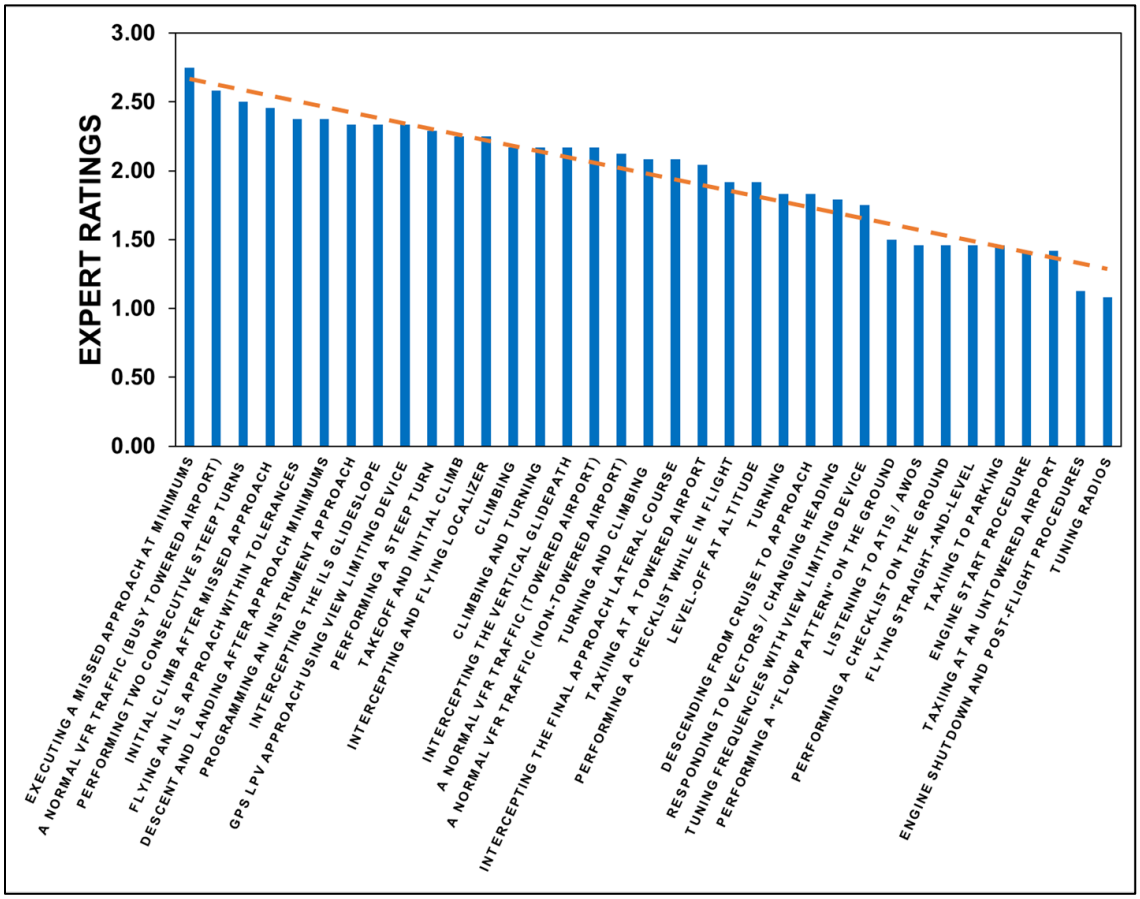

Figure 3. 1: Subjective data from the expert rating of in-flight task loads. Surveyed data scaled task loads from ranges 1 to 3 with values of 1 being low task load and values of 3 being high task load.

3.3.3 Data Analysis

R-R intervals were processed from the ECG waveforms via MATLAB 2019a and exported to Kubios HRV 3.4.3 for further evaluation and artifact removal [146]. Fast Fourier Transformation (FFT) was used with a 256 s window width and 50% overlap. Mean HR and Mean RR were calculated for each subject in addition to Time Domain, Frequency Domain, and Nonlinear HRV metrics. Time-domain HRV metrics included SDNN, RMSSD, pNN50. Frequency Domain metrics consisted of LFnu, HFnu, LF/HF. Nonlinear HRV included the following: Detrended Fluctuation Analysis Alpha-1 and Alpha-2, SD1, SD2, SD2/SD1, and Approximate Entropy.

3.3.4 Statistics

The Shapiro-Wilk test was used to test for Normality at $\alpha = 0.05$. For normally distributed data, a one-way ANOVA was used in comparing HRV metrics for task loads during flight. HRV metrics for tasks of Low to Medium, Low to High, and Low to Medium were compared. For data that were not normally distributed, a non-parametric test was completed using Wilcoxon Rank-Sum Test.

3.4 Results

In-flight tasks show a resultant decrease in HRV total power between low to high workload demand. Additional to traditional HRV metrics, and as expected, increased mean HR and decreased mean RR are present through a comparison of low to high workloads. When comparing low to medium or medium to high workloads, HRV metrics show little to no change.

3.4.1 Time-Domain Metrics

All time-domain HRV metrics had shown differences in the comparison of low to high task loads except pNN50 (Table 3.1). The time-domain feature TINN had shown a decrease from low to medium task loads in addition to the low to high comparison (Table 3.1). SDNN values had shown a decrease comparing low to high task demand, however, the comparison of medium task

loads to low or high demand remained relatively unchanged. SDNN decreased from low to medium with no statistical change and further decreased from medium to high demands. RMSSD also had shown a decrease in comparison to low to high workload (Table 3.1). Similar to SDNN, when comparing medium tasks to low or high tasks, changes were not significant. RMSSD decreased from low to medium and further decreased from medium to high workloads with no statistical change in the intermediate medium stages.

Table 3.1: **Means and standard deviations of HRV metrics for low, medium, and high flight task loads. Task loads were analyzed to determine differences between difficulty low to medium (p_1), medium to high (p_2), and low to high (p_3). Bolded values highlight results of $p < 0.05$.**

	Low Task Load	Medium Task Load	High Task Load	p_1	p_2	p_3
Mean RR (ms)	759 ± 102	734 ± 96	724 ± 106	0.138	0.759	**0.043**
Mean HR (bpm)	80 ± 11	83 ± 10	84 ± 12	0.137	0.655	**0.03**
SDNN (ms)	61 ± 21	59 ± 23	56 ± 23	0.182	0.788	**0.025**
RMSSD (ms)	63 ± 37	61 ± 38	54 ± 35	0.182	0.455	**0.023**
pNN50 (%)	28 ± 15	27 ± 16	24 ± 17	0.649	0.448	0.141
TINN (ms)	311 ± 93	298 ± 107	278 ± 116	**0.025**	0.729	**< 0.01**
LF (n.u.)	59 ± 16	64 ± 16	72 ± 14	0.259	**0.02**	**< 0.001**
HF (n.u.)	40 ± 15	36 ± 16	28 ± 14	0.262	**0.019**	**< 0.001**
LF/HF	1.85 ± 1.1	2.49 ± 1.8	3.62 ± 2.6	0.244	**0.037**	**< 0.001**
DFA Alpha-1	1.14 ± 0.2	1.13 ± 0.3	1.21 ± 0.3	0.759	0.161	**0.048**
DFA Alpha-2	0.88 ± 0.2	0.83 ± 0.2	0.86 ± 0.2	0.586	0.615	0.966
ApEn	1.09 ± 0.1	1.11 ± 0.1	1.09 ± 0.1	0.841	0.154	0.084
SD1 (ms)	45 ± 26	44 ± 27	39 ± 25	0.182	0.448	**0.018**
SD2 (ms)	109 ± 32	104 ± 37	107 ± 43	0.473	0.938	0.463
SD2/SD1	2.9 ± 1.4	2.8 ± 1.3	3.4 ± 1.6	0.427	0.223	**0.029**

3.4.2 Frequency-Domain Metrics

Frequency-domain features of LF, HF, and LF/HF ($p < 0.001$) showed variations in comparison of both low to high and medium to high task loads (Table 3.1). LF showed an increasing trend from low to medium task difficulty and further increases from medium to high task load difficulties (Figure 3.2, A). HF had an opposite change with decreasing values from low

demand to medium demand tasks and a further decrease with the medium to high difficulty task (Figure 3.2, A). The ratio of LF/HF additionally reflected LF and HF shifts of task load through an increasing trend from low to medium and medium to high workload (Figure 3.2, B).

3.4.3 Nonlinear Measurements

Differences in low to high task demands for short-term HRV metrics of DFA α1, SD1, and SD2/SD1 (Table 3.1) were observed in the nonlinear measurements while low to medium and medium to high task comparisons showed little change. DFA α1 had increased significantly between low to high task demand (Figure 3.3). SD1 showed decreasing values from low to high difficulty tasks (Figure 3.3). SD2 showed stable values across the changing task load difficulty. The ratio of SD2 and SD1 reflected SD1 changes through increased values from low to high tasks (Figure 3.2, B) (Table 3.1).

3.5 Discussion

In this study, short-term HRV total power decreased with increasing in-flight pilot workload suggesting increased SNS activity due to stress on task, supporting the first hypothesis that HRV can be used to predict pilot task workload stress. Subject matter expert task ranking of the high, medium, and low task difficulty was correlated to HRV indices reflecting similar workload outcomes, which supports our second hypothesis. Additionally, mean HR increased, mean R-R interval decreased to increased pilot tasks demand confirming results of previous investigators [81], [117], [122]–[124], [145]. This study, to the best of our knowledge, is the first investigation corresponding subjective from expert pilot-rated workload to objective cardiovascular HRV metrics to quantify levels of stress due to increased task demand.

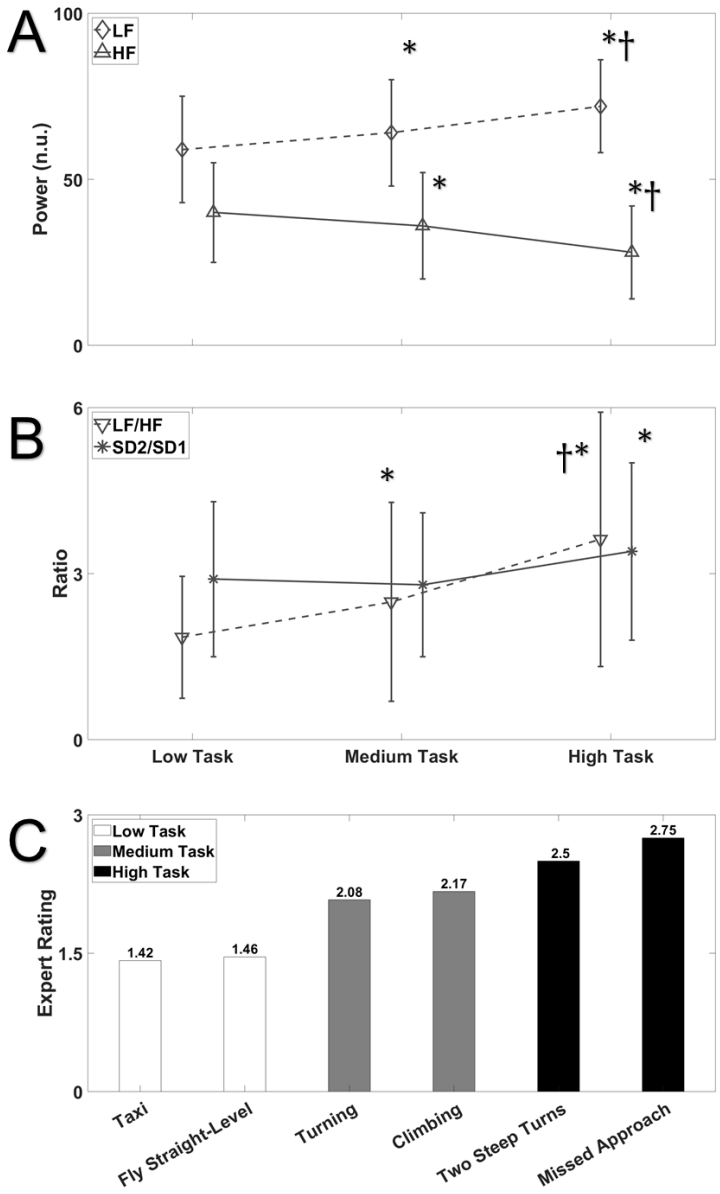

Figure 3.2: Quantitative HRV metrics for low, medium, and high task loads compared with expert subjective ratings. LF power increases through low to medium and medium to high task workload, whereas HF power decreases through increased workload (A). Increases in LF/HF and SD2/SD1 ratios reflect the autonomic balance of increased sympathetic activity during increased workloads (B). Expert subjective ratings were rated on a scale of 1 to 3, with 1 being low task workload and 3 being high task loads (C). Tasks correlated to low, medium, and high workload increase in subjective rating correlated to changes in HRV data. * Denotes significant differences compared to low tasks and † denotes significant differences compared to medium tasks ($p < 0.05$).

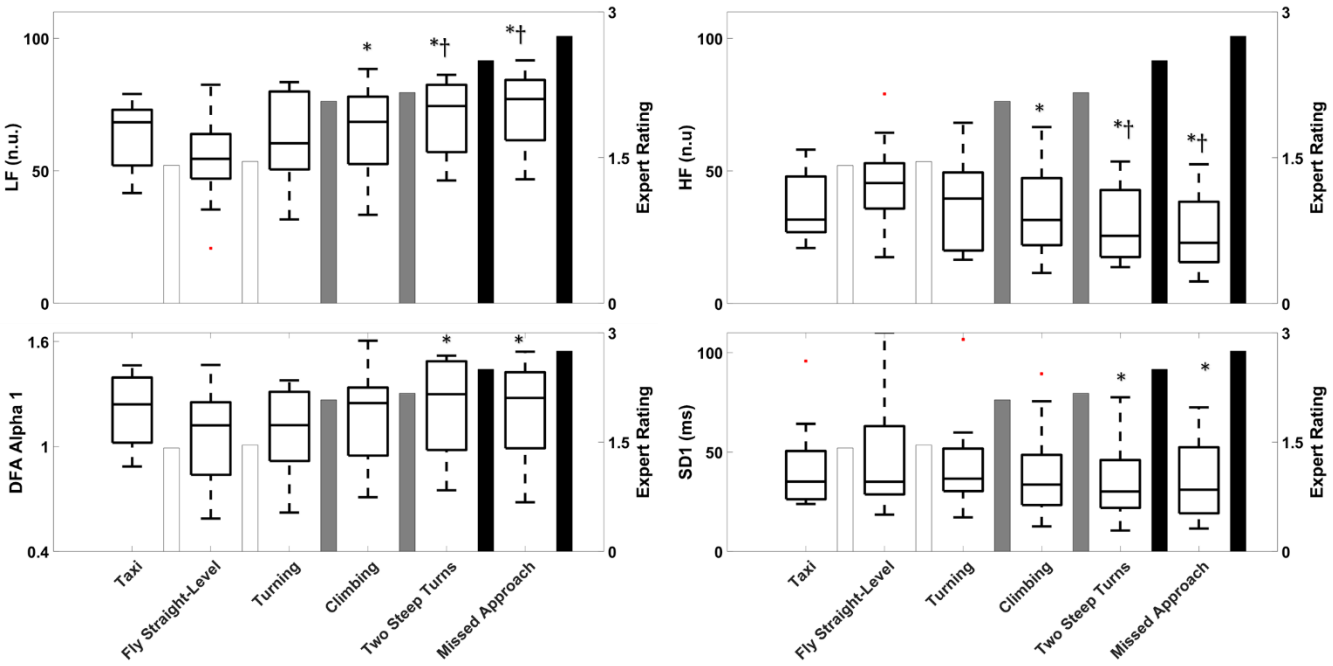

Figure 3.3: Task by task comparison of HRV metrics to expert ratings. Low-frequency power (LF) and detrended fluctuation analysis (DFA) α1 increase with increasing rated task loads. High-frequency power (HF) and Poincare SD1 decrease with increasing task load. The fluctuations of these HRV metrics reflect increased sympathetic responses to short-term stress of increased workload, also providing quantitative physiologic values for expert-rated task load. * Denotes significant differences compared to low tasks and † denotes significant differences compared to medium tasks ($p < 0.05$).

Time-domain features SDNN and RMSSD corresponded to short-term decreases due to increased task loads. Decreases in both SDNN and RMSSD show increases in mental workload demand. This trend is analogous to studies conducted on pilots and in other workload analysis [59], [89], [91], [92], [139], [141]. However, in contrast, Fuentes-Garcia et al, found that HRV metrics did not fluctuate in this regard to comparisons of real flight and simulated flight [145]. The groups' observation is that of high experience resulting in potential higher tolerance of stress workload. Though, in this study SDNN and RMSSD values decrease with higher task loads also in comparison to expert rated task complexity suggesting further trends of increased SNS activity even with higher flight experience. Additionally, TINN had shown decreases from low to medium and low to high task load comparisons. This measurement was the only metric to show a significant decrease from low to medium tasks. As TINN is the baseline width of the R-R interval histogram,

decreases of this metric due to increasing task difficulty could represent a higher sensitivity to corresponding stress. Utilizing TINN in tandem with other metrics, such as frequency-domain measurements, has the potential of providing increased accuracy in stress determinations.

Frequency-domain features showed fluctuations of LF and HF power relationships analogous to standard metrics of workload [12], [57] (Figure 3). The drastic increase of LF/HF from low to high difficulty tasks shows an increase in SNS activity and increased stress. Further, low task LF/HF values of 1.85 correspond to subjective expert ranking values of 1.2 to 1.46, whereas high task LF/HF values of 3.62 correspond to rankings greater than 2.5 (Figure 3.2). Though LF and HF power have been used in previous studies, there is a caveat regarding respiration. Talking during flight, such as talking with air traffic control (ATC), can change respiration rates, ultimately affecting LF and HF values [12], [57], [125]. However, studies have shown that LF and HF components, including respiration rate, still provide an accurate window into stress workload [136], [147]. Significant fluctuations in LF and HF power were seen in a comparison of low to high and medium to high task load difficulty levels in-flight. Further, drastic changes in LF/HF across difficulty levels suggest that LF, HF, and LF/HF metrics can be used to provide highly accurate predictions of stress level to task demand in comparison to other time-domain or nonlinear measurements. However, LF and HF power showed little changes of low to medium task difficulty which could mean that at lower changes of task difficulty, there is lower sensitivity of LF, HF, and LF/HF. Increasing LF and HF accuracy could be improved at lower task difficulty by associating detection with the time-domain metric TINN, potentially allowing for earlier predictive stress in-flight.

LF and HF power are highly sensitive to stress changes, if combined with other heart rate-derived metrics a larger picture into the pilot's reaction to stress could be achieved. The nonlinear

metric of DFA α1 had shown an increase corresponding to increased task demand reflecting complexity and unpredictability in the signal due to stress and increased SNS activity. Additional to subjective expert rating comparisons, this HRV measurement is, to the best of our knowledge, the first investigation using DFA complexity of the cardiovascular time series to correlate stress workloads on pilots in-flight. Task by task breakdown of DFA α1 shows the increasing complexity of the HRV time series corresponds to increased task complexity in comparison to higher expert ratings (Figure 3.3). Alternatively, DFA α2 had shown no change through task difficulty levels pointing to long-term fluctuations in signal complexity were preserved in-flight. As DFA α1 shifts significantly in comparison to DFA α2, short-term fluctuations shower higher dominance of signal complexity for compounding changes in short-term task difficulty. Adding metrics of SD1, SD2, and SD2/SD1 further the observation that task difficulty changes increase short-term stress. SD1 was shown to decrease, whereas SD2 remained steady from low to high task demand. This is reflected in SD2/SD1 increases. The ratio of SD2/SD1 is tied to LF/HF, however not as sensitivity in fluctuations to task difficulty. Incorporating observations of expert task ratings show corresponding increases in task difficulty in subjective data while providing objective data of short-term stress induced by task load (Figure 3.3). By combining short-term HRV metrics from time-domain, frequency-domain and nonlinear measurements objective data backed by the subjective task expert ratings are identified for predictive stress indicators.

3.1 Limitations and Consideration

The physiology data included in this study was furnished through the participation of 12 pilots within a live-flight environment in a single-engine airplane. A larger dataset may improve confidence in study outcomes. Additionally, certain environmental factors such as ambient temperature, wind, turbulence, or other air traffic present in the area may have secondary workload

effects and may influence cardiovascular activity during the data collection period. Finally, data were not collected on the individual subjects' physical fitness, or other psychophysiological characteristics, which could also influence cardiac function, and subsequently the information provided in their physiology data.

This data provides an important addition to the understanding of pilot physiology and cognitive workload using cardiac signals. Cardiac data, such as those provided by PPG or ECG sensors now becoming common in smart electronics, are less invasive than other methods of physiological data collection. As a result of advances in technology, additional research using cardiac signals may become more feasible within the aviation domain. Expanding our understanding of cognitive workload and fatigue within flight operations may yield significant benefits to aviation safety.

3.6 Conclusions

Flight environments provide a wide range of workload interactions. Fatigue can have a compounding effect on a pilot's ability to perform tasks largely influenced by physiologic conditions such as sleep or stress. Pilot in-flight task workload was investigated in this study using observed fluctuations in heart activity. High task loads resulted in increased pilot stress indicated by decreased short-term heart rate variability. HRV provides a window into the ANS balance allowing for quantitative physiological metrics tied to increased pilot task demand. Short-term HRV metrics SDNN, RMSSD, LF, HF, LF/HF, SD1, and DFA $\alpha 1$ can be used in predictive task stress providing a platform for real-time feedback to the pilot for increased performance and safety.

Chapter 4: CARDIOVASCULAR ADAPTATION TO HEAD DOWN TILT BEDREST

4.1 Summary

During head-down tilt bed rest (HDT) the cardiovascular system is subject to headward fluid shifts. The fluid shift phenomenon is analogous to weightlessness experienced during spaceflight microgravity. The purpose of this study was to investigate the effect of prolonged 60-day bed rest on the mechanical performance of the heart using the morphology of seismocardiography (SCG). Three-lead electrocardiogram (ECG), SCG, and blood pressure recordings were collected simultaneously from 20 males in a 60-day HDT study (MEDES, Toulouse, France). The study was divided into two campaigns of ten participants. The first commenced in January, and the second in September. Signals were recorded in the supine position during the baseline data collection (BDC) before bed rest, during 6° HDT bed rest, and during recovery (R), post-bed rest. Using SCG and blood pressure at the finger, the following were determined: Pulse Transit Time (PTT); and left-ventricular ejection time (LVET).

SCG morphology was analyzed using functional data analysis (FDA). The coefficients of the model were estimated over 20 cycles of SCG recordings of BDC12 and HDT52. SCG fiducial points AO (aortic valve opening) and AC (aortic valve closing) amplitudes showed a significant decrease between BDC12 and HDT52 ($p<0.03$). PTT and LVET were also found to decrease through HDT bed rest ($p < 0.01$). Furthermore, PTT and LVET magnitude of response to bed rest was found to be different between campaigns ($p < 0.001$), possibly due to seasonal effects on the cardiovascular system. Correlations between FDA and cardiac timing intervals PTT and LVET using SCG suggest decreases in mechanical strength of the heart and increased arterial stiffness due to fluid shifts associated with the prolonged bed rest.

4.2 Background

The human cardiovascular system has evolved to operate in the presence of gravity [19], [25], [148]. When standing on Earth, hydrostatic gradients reduce arterial pressures located above the heart, while also increasing pressures below the heart, which induces local arterial responses [47], [149]. When introduced to weightlessness, the physical unloading and lack of force pulling blood to the lower extremities causes the phenomenon of upward fluid shift [29]. The once unequal gradient pressures in blood vasculature now equalize, affecting blood pressure regulation and cardiovascular control [36], [150], [151]. Seen in both short and long-term spaceflight, upward fluid shifts have been associated with increased orthostatic intolerance post-flight [30], [152]–[154].

Continuing effects of physical unloading in microgravity can drive cardiovascular remodeling and arterial changes leading to mechanical attenuation of heart function, advanced arterial stiffness [23], [35], [155]. Interventions are being investigated to act as countermeasures to stem the physiological deconditioning of spaceflight (i.e., lower body negative pressure (LBNP) application, exercise activities, short-arm centrifugation, plasma volume replenishment, and nutrient supplementation) [150], [156]–[160]. However, little is known about the effects of extended weightlessness on arterial stiffness and systemic vascular resistance. Hughson et al. showed an increase in arterial stiffness of astronauts after six months aboard the International Space Station similar to that of 10-20 years of aging [16]. The arterial stiffness increase was based on observations of decreased pulse transit time (PTT) and lowered biomarkers, such as insulin [16]. Pulse wave transit time has also been reported to be decreased even after 5 days of spaceflight [15].

A major limiting factor in the interpretation of spaceflight data is the relatively low sample size of individuals who have experienced spaceflight. Therefore, conditions such as 6° head-down tilt bed rest are routinely used as space analogs to simulate the effects of microgravity [18], [161], [162]. Head down tilt bed rest has been shown to mimic the effects of weightlessness on the body including upward fluid shifts [163]. Several studies indicate that vascular remodeling after long-duration bed rest produces a sustained decrease in left ventricular mass during bed rest while causing drastic deconditioning of left ventricular volumes [22], [161], [164]–[169], although a recent study found that ventricular mass loss did not occur [170]. However, in spaceflight, there is a chronic decrease in left ventricular mass of values close to 9-12% loss, while similar observations during HDT studies show 8-16% mass losses [165], [166], [171]. Alternatively, decreases in left ventricular volumes have been attributed to blood plasma loss during bed rest, also seen in spaceflight [163], [170]. In tandem with ventricular remodeling, responses of blood pressure have been shown to lower during head-down tilt bed rest (HDT), analogous to spaceflight [33], [172], [173].

The current study focused on the mechanical performance of the heart during 60-day HDT. With each heartbeat, there are mechanical events that give a windowed look into cardiac performance. Cardio-mechanical techniques such as Seismocardiography (SCG), evaluated via a local accelerometer placement on the chest, can measure cardiac motion, giving information about heart valve opening and closure events [174]. Techniques used to measure cardio-mechanical vibrations have been used to observe deconditioning of the cardiovascular system in spaceflight and early hemorrhage detection [175]–[178].

In the development of a smart garment, Di Rienzo et al. utilized left ventricular ejection time (LVET) and QS2 (electromechanical systole, relation of SCG-AO and ECG Q-wave) as

measurements of heart contractility [176], [179]. Another study by Di Rienzo et al. used SCG techniques for monitoring vital signs during sleep of astronauts on the ISS [180]. In that study, the group used the smart garment with a three-axis SCG on the sternum and a three-axis gyroscope to gather cardiovascular vibrations on the chest and evaluate cardiovascular data during sleep. Initial analysis was done on one astronaut crew member using timing intervals of isovolumic contraction time (ICT), isovolumic relaxation time (IRT), LVET, and pre-ejection period (PEP) over seven sleep intervals [180].

Detection of the effects of early-stage hemorrhage has also been investigated through using SCG. Tavakolian et al., investigated simulated hemorrhage through graded LBNP to quantify correlations between stroke volume via echocardiography and SCG features [177]. Of the features derived by SCG, timing intervals of LVET and PEP were shown to be highly correlated to changes during graded LBNP. This correlation suggested that changes of SCG-derived features (e.g., LVET) in emergency scenarios can be used as warning signs of early hemorrhage [177].

This investigation utilized the HDT space analog together with cardio-mechanical responses of the heart to further the understanding of cardiovascular compliance and resultant arterial stiffness. The cardiovascular vibration technique of SCG was used to provide insight into the mechanical deconditioning of the heart through relationships between blood pressure [181] and cardiovascular timing intervals [177], [182], [183]. It was hypothesized that with increased headward fluid shifts during HDT there would be a decrease in SCG amplitude strength due to mechanical deconditioning of the heart. As a secondary hypothesis, it was predicted that PTT would decrease due to increased arterial stiffness associated with HDT.

4.3 Methodology

4.3.1 Bed rest Protocol

The head-down tilt bed rest study consisted of two campaigns of 10 volunteers, each lasting 60 days. Campaign 1 (height = 1.76 m ± 0.06, weight = 74.86 kg ± 7.81) was started in January 2017 while Campaign 2 (height = 1.76 m ± 0.04, weight = 73.10 kg ± 7.05) was started in September 2017. The clinical trial was registered at ClinicalTrials.gov (Identifier: NCT03594799). An all-male cohort (N = 20) participated in this experiment (ages ranging from 20-45). The experimental group consisted of the nutrient countermeasure group randomly selected (N = 10) and the control group (N=10). This study data collection followed in line with our previous study of cardio-postural effects of prolonged bed rest [172]. The experiments were conducted as an ESA funded study at the Institut de Médecine et de Physiologie Spatiales (MEDES), a Centre National d'Études Spatiales (CNES) facility located in Toulouse, France. This prolonged bed rest study was broken into three phases. Phase one consisted of 14 days of baseline data collection (BDC) before head-down tilt, phase two consisted of 6-degree head-down tilt (HDT) bed rest for 60 days, and phase three was a recovery period (R) 14 days after head-down tilt. Ethical approval was obtained from the Comité de Protection des Personnes / CPP SudOuest Outre-Mer I and the Agence Française de Sécurité Sanitaire des Produits de Santé for each facet of the experimental protocols. Additionally, approval of this study was obtained by the Office of Research Ethics at Simon Fraser University.

Data collection days and times were selected to avoid conflict with the ESA orthostatic tolerance testing. In the previous study protocols, supine to stand (STS) was used to assess the relationship between cardiovascular control and posture [172]. Two of the STS collections were taken during baseline before bed rest (BDC) and post bed rest recovery (R). The data collection

for STS was taken at the same time on BDC12 (12 days before) and BDC2 (2 days before) for a baseline before bed rest. Data collection of STS after bed rest was taken at R8 (8 days after bed rest). STS data collection consisted of 5 minutes of collection in supine and 6 minutes of data collection during standing. In this investigation, only the supine portion of STS testing was investigated for cardiovascular function (ECG, blood pressure, and SCG). During HDT, the cardiovascular function was assessed at 6 degrees head-down for 10 minutes via ECG, blood pressure, and SCG at the same time in the morning on days of HDT 1, 29, and 52 (days during head-down tilt). Plasma volume was measured using CO rebreathe and was made as part of the standard bed rest protocol used by ESA [161].

4.3.2 Signal Acquisition

Continuous blood pressure was collected via non-invasive Portapres (FMS, Amsterdam, The Netherlands). SCG was collected by a unidirectional accelerometer in the dorso-ventral direction positioned on the xiphoid process of each subject. The SCG measured the vibrations of the heart as a resultant beat against the chest wall during each cardiac cycle. Electrocardiogram (ECG) was collected using a three-lead ECG positioned in a Lead II configuration (FD-13, Fukuda Denshi Co. Ltd, Tokyo, Japan). The experimental setup is shown in the HDT schematic (Figure 4.1). A sampling rate of 1,000 Hz was used for data gathering through the National Instruments USB-6218 16-bit data acquisition system and using LabVIEW 2013 software (National Instruments Inc, TX, USA).

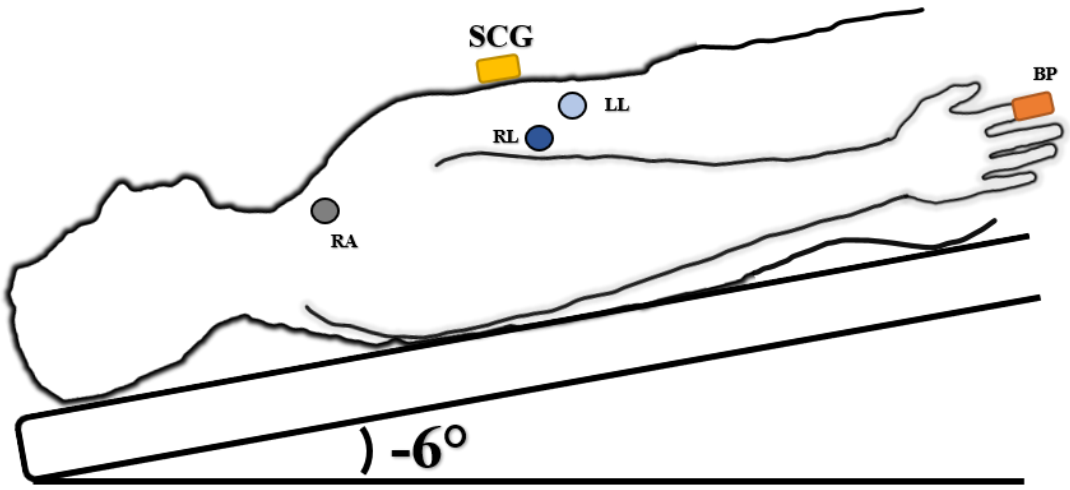

Figure 4.1: HDT schematic of sensor placement. SCG (yellow rectangle) placed on the xiphoid process. Blood pressure measured at the finger (orange rectangle). ECG Lead II shown as RA lead (gray circle) on the right clavicle, RL lead (dark blue circle) on the lower right rib cage, and LL (light blue circle) on the lower left rib cage.

4.3.3 Data analysis

The fiducial points of AO (aortic valve opening) and AC (aortic valve closing) were annotated on SCG [183]–[185]. The cardiovascular timing feature PTT was collected as the timing between the AO peak of SCG and the foot feature of the blood pressure waveform [182] (Figure 4.2). Additionally, the left-ventricular ejection time (LVET) was measured as the time interval between SCG-AO and SCG-AC.

Beyond individual fiducial points, the entire morphology of SCG was analyzed by functional data analysis (FDA) using MATLAB R2019a [186]. Similar techniques have been used in the analysis and interpolation of SCG fiducial points [187]–[189]. In FDA, each SCG cycle was modeled as the linear combination of 23 spline base functions of order 4. The coefficients of the model were estimated and compared over 20 cycles of SCG recordings between BDC12 and HDT52 for the 20 subjects.

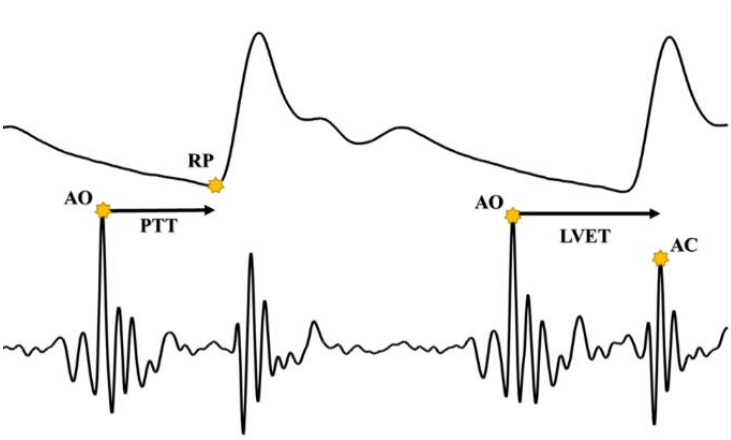

Figure 4.2: Blood pressure and seismocardiogram waveforms with annotations. Pulse Transit Time (PTT) is the time interval between the aortic valve opening (AO) peak of SCG and RP (Foot) of BP. LVET is the time interval between the AO and AC peak of the SCG.

4.3.4 Statistics

Nutrient countermeasure was randomized amongst participants. Statistical analysis of Cocktail countermeasure followed the same technique as outlined in previously reported [172]. If no significance was found between the control and countermeasure groups, then the participants were merged for further analysis. Normality test was conducted using Shapiro-Wilk at $\alpha = 0.05$.

For normally distributed data, two-way ANOVA with replication was completed, followed by a Bonferroni correction comparing cardiovascular changes due to bed rest between BDC12 compared to HDT01, HDT29, HDT52, and R8 in addition to campaign 1 and campaign 2 for seasonal differences. For non-normally-distributed data, a non-parametric test was conducted using the Friedman test. A probability of $\alpha < 0.05$ was considered significant. Additionally, the Wilcoxon Signed Rank test was performed to evaluate the differences between FDA coefficients for BDC12 and HDT52, to determine SCG morphology changes.

4.4 Results

As previously reported by Xu et al., [172], the cocktail countermeasure did not affect the cardiovascular values, and our analyses indicated that this was also the case for the timing intervals in this study (PTT, $F < 0.01$, $p = 0.998$ and LVET, $F = 0.47$ $p = 0.495$).

4.4.1 SCG Morphology and Functional Data Analysis

The heart was analyzed via the vibration peaks caused by the heart hitting the chest wall during each beat. These vibrations AO and AC detected at the xiphoid process by the SCG showed a lowering trend through bed rest (Table 4.1). Through FDA, the coefficients of corresponding spline basis functions describe the SCG waveform in 23 knots. These knots act as windows of the signal dividing it into sections defined by the specific splines shown to represent SCG morphology (Figure 4.3B). The coefficient sets showed wider distributions at the end of bed rest compared to the baseline data collection sets. Spline basis coefficient sets 4, 5, and 6 describe the AO peak complex, while Spline coefficient sets 14, 15, and 16 describe the AC peak complex (Figure 4.3A). The values of AO and AC exhibited mixed behavior, and the Friedman test was conducted.

Averages of 20 cardiac cycles across all 20 subjects showed a decrease in peak morphologies of both AO and AC complexes pre-HDT to day 52 of HDT ($p < 0.03$) (Table 4.1). Furthering the changes in morphology, the peak distribution of AO and AC showed changing allocation of coefficients due to decreasing peak complex amplitudes towards the end of bed rest. Upon entrance into HDT bed rest, the mechanical peak strength of the AO and AC complexes significantly decreased ($p < 0.01$) (Table 4.1). These peak values continued to decrease through the end of bed

rest values. On R8 (8 days post-HDT) there was a slight recovery of the peak strength which was still significantly lower than baseline (BDC12).

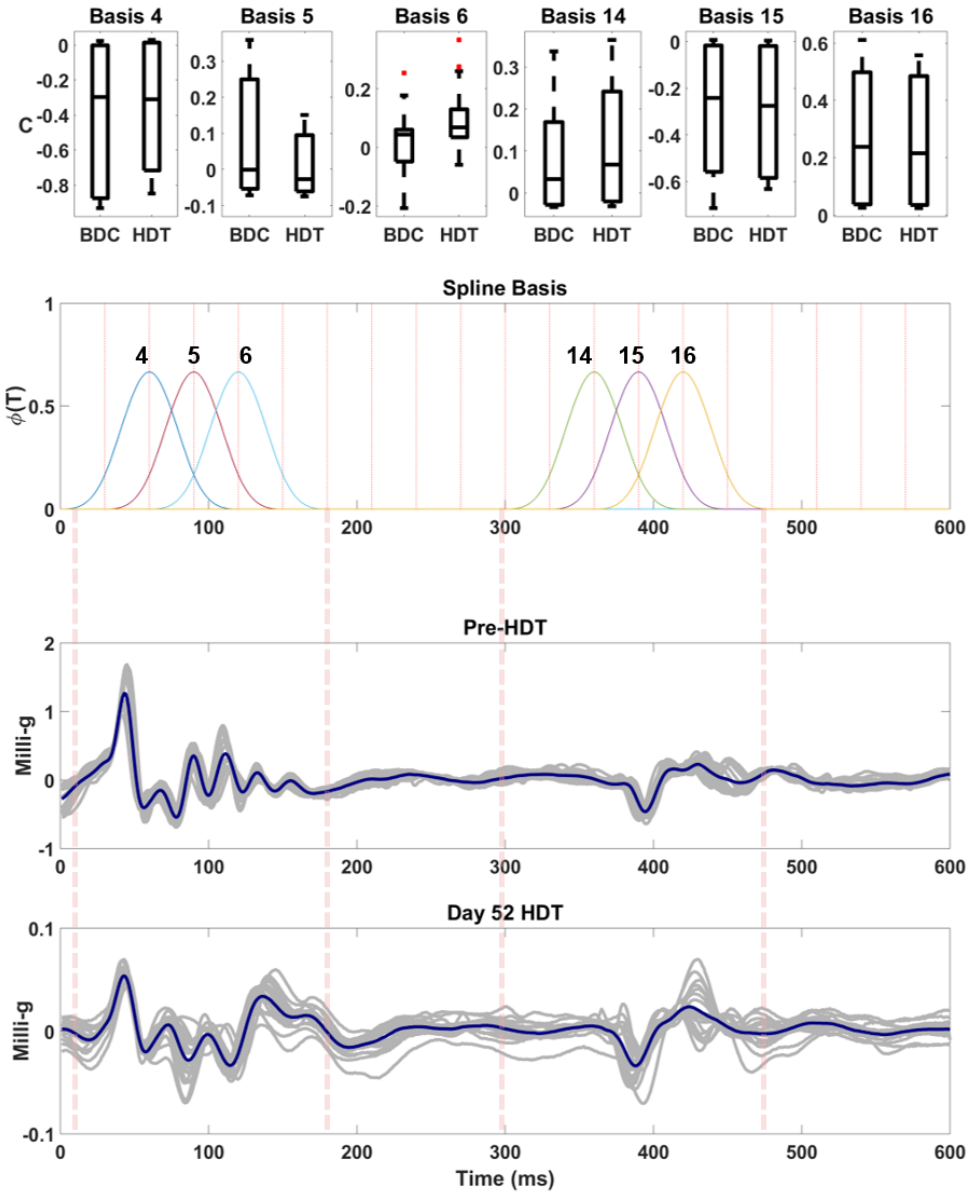

Figure 4.3: FDA analysis of SCG signals containing AO and AC basis function coefficient sets pre-and post-HDT. Average AO and AC peak decrease over 20 cardiac cycles after 52 days head-down tilt bed rest compared to pre-HDT. Morphology spline coefficient sets corresponding to the AO (sets 4, 5, and 6) and AC (sets 14, 15, and 16) peak complexes show distributions from pre-HDT to day 52 HDT furthering the peak changes. Coefficient sets define the spline basis functions shown to describe the SCG signal morphology.

Variable	BDC12		HDT01		HDT 29		HDT52		R8	
	Campaign 1	Campaign 2	Campaign 1	Campaign 2	Campaign 1	Campaign 2	Campaign 1	Campaign 2	Campaign 1	Campaign 2
HR (bpm)	55 ± 4	64 ± 8†	59 ± 11	55 ± 10	61 ± 13*	63 ± 9*	66 ± 15*	67 ± 11*	71 ± 14*	67 ± 7*†
RR (ms)	917 ± 67	1067 ± 133†	983 ± 183	917 ± 167	1017 ± 217*	1050 ± 150*	1100 ± 250*	1117 ± 183*	1183 ± 233*	1117 ± 117*†
SBP (mmHg)	118 ± 13	125 ± 21†	104 ± 11*	120 ± 15*†	123 ± 15	132 ± 18†	113 ± 15	128 ± 19†	116 ± 11	129 ± 21†
DBP (mmHg)	63 ± 8	65 ± 7	54 ± 8*	59 ± 7*	66 ± 9	71 ± 12	64 ± 8	71 ± 12	62 ± 5	70 ± 13
MAP (mmHg)	83 ± 10	85 ± 12	71 ± 9	79 ± 10	85 ± 10	91 ± 13	80 ± 9	90 ± 14	80 ± 7	90 ± 15
PTT (ms)	189 ± 29	209 ± 38†	123 ± 40*	182 ± 60*†	106 ± 29*	208 ± 31†	110 ± 26*	205 ± 36†	113 ± 17*	179 ± 45*†
LVET (ms)	337 ± 28	308 ± 35	344 ± 49*	340 ± 21*	320 ± 38	312 ± 20	308 ± 34*	300 ± 20*	310 ± 23*	313 ± 15*

Table 4. 1: Cardiovascular function and timing intervals through the three phases of bed rest. Campaign groups were paired comparing HDBR phases to baseline BDC12. Further unpaired analysis was done to compare Campaign 1 and Campaign 2. Cardiovascular timing intervals values are split based on phase and further split based on campaign season. Campaign 1 coincides with the first season started in January and Campaign 2 coincides with the second season started in September. * Denotes significant differences compared to BDC12 and † denotes significance between campaigns at each test day (Two-way ANOVA, $p < 0.05$). AO and AC compared via non-parametric Friedman Test ($p < 0.05$).

4.4.2 Pre-bed rest to post-bed rest cardiovascular responses

Cardiovascular timing intervals measured from the SCG peak vibrations were shown to be affected by prolonged bed rest (Table 4.1). Values of HR, DBP, SBP, MAP, PTT, and LVET passed a test of normality ($p > 0.05$). PTT from the AO peak of SCG to the foot of the blood pressure at the finger revealed a drastic decrease immediately into bed rest for both campaigns (Figure 4.4). On HDT day 1, PTT fell dramatically and stabilized significantly faster than baseline towards the end of bed rest on day 52 HDT ($p < 0.01$). The PTT interval did not recover by R8. Additionally, there were significant differences between the campaigns ($p < 0.01$). PTT decreased more drastically between pre- to post-bed rest in Campaign 1 compared to Campaign 2 (Figure 4.4).

LVET had an initial increase on HDT01 with a further decrease from HDT29 to HDT52. The value for LVET showed a slight recovery on R8 but remained significantly lower than on BDC12 ($p < 0.01$). This trend was seen in both campaigns; however, like PTT, there was a significantly greater change of LVET between campaigns 1 and 2 (Figure 4.4).

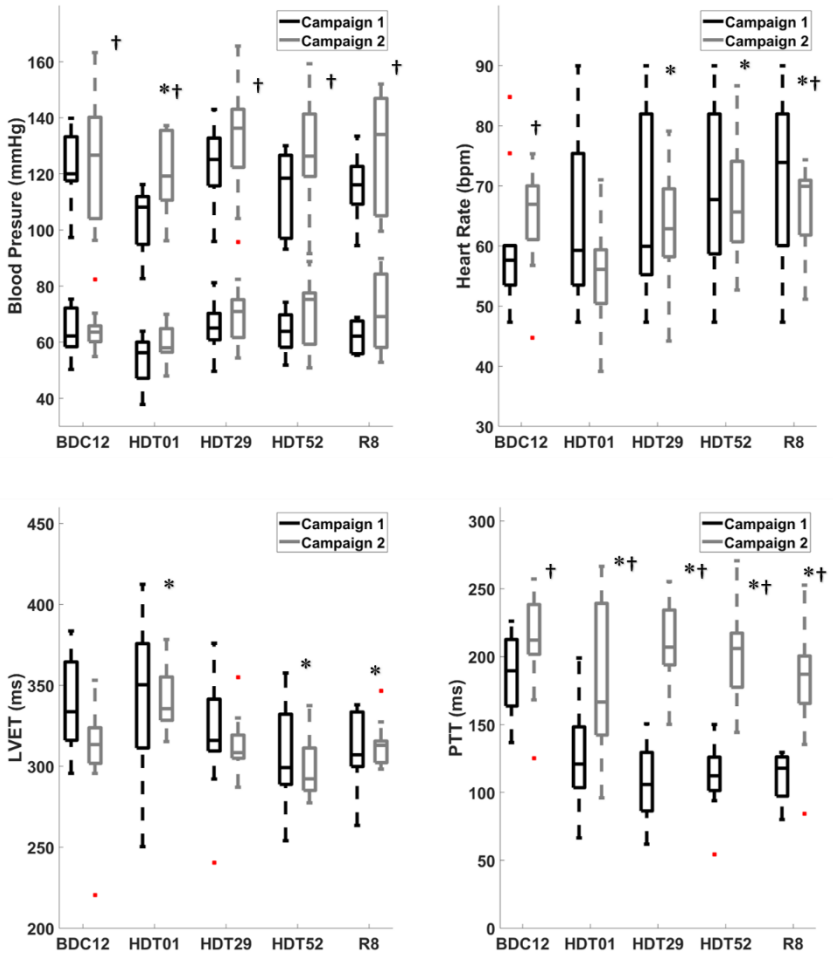

Figure 4.4: Cardiovascular function through the three phases of bed rest. Cardiovascular timing intervals of PTT and LVET were taken from the relationships of SCG and show decreasing trends. PTT has a drastic average decrease that does not recover after 8 days post bed rest. LVET has a variable adjustment to fluid shifts of bed rest but decreases towards the end with a slight recovery. Blood pressure values adjust to fluid shifts with an initial decrease but stabilize towards the end of bed rest. Upper values in the plot represent systolic BP and lower values, diastolic BP. * Denotes significant differences compared to BDC12 and † denotes significance between campaigns at each test day ($p < 0.05$).

Heart rate (HR) had a gradual increase through the entirety of bed rest and 8 days post HDT on R8 ($p < 0.03$) for both campaigns. Campaign 2 had less of an increase in HR compared to

campaign 1, with significant differences at BDC12 and R8. Systolic blood pressure (SBP), diastolic blood pressure (DBP,) and mean arterial pressure (MAP) showed significant changes across bed rest phases ($p < 0.04$). Additionally, there were large significant differences in these changes between campaigns 1 and 2 in blood pressure values. Through bed rest, campaign 1 had lower systolic ($p < 0.001$) and diastolic blood pressures compared to campaign 2 (Figure 4.4). Blood plasma volume decreased an average of 19% from BDC12 (4.10 ± 0.51 L) to the end of HDT (3.31 ± 0.37 L), ($p < 0.03$). No significant change was seen between campaigns ($p=0.45$). Additionally, the fitness levels ($\dot{V}O_2max$) of the participants when they entered the study (BDC 8 baseline) were not different between campaign 1 (39±4 ml/min/kg) and 2 (40±4 ml/min/kg). Fitness decreased by similar amounts in both campaigns to 31±4 ml/min/kg (R1, campaign 1) and 29±2 ml/min/kg (R1, campaign 2).

4.5 Discussion

In this study, the timing interval of pulse transition time decreased analogous to that seen in 6-months of spaceflight [15], [16]. This decrease in PTT of 15-40% without recovery suggests that during 60-days head down tilt, similar mechanics are producing a decrease in vascular compliance leading to increases in arterial stiffness. Likewise, decreases in LVET and attenuation of the SCG peak vibrations compared pre to post-bed rest suggest a decrease in the mechanical performance of the heart due to upward fluid shifts.

Furthermore, differences in blood pressure values and cardiovascular timing intervals between bed rest campaigns suggest a seasonal influence acting on the cardiovascular system. This study, to the best of our knowledge, is the first investigation using mechanical vibration techniques of SCG to derive cardiovascular timing intervals during prolonged HDT. Additionally, this is the first

investigation to bring attention to possible seasonal influences on cardiovascular function during prolonged HDT.

4.5.1 Mechanical Deconditioning of the Heart

The morphology changes observed with SCG during HDT bed rest support our hypothesis of mechanical attenuation of the heart vibrations associated with headward fluid shifts. Additionally, this attenuation of SCG was concurrent with a decrease of PTT, which supports the second hypothesis of increased arterial stiffness through prolonged bed rest. The underlying mechanism that has the highest effect upon the mechanical deconditioning could be related to the vascular changes due to headward fluid shifts in the body. However, headward fluid shifts and changes in hydrostatic pressure together with the lack of compression on the chest, have been shown to increase the geometry of the thoracic cage [18]. Dampened vibrations could also occur due to expansive distension of the thorax as another factor in this vibrational attenuation.

Cardiovascular vibrational assessment techniques have been used in a multitude of previous studies. One such technique parallel to SCG is that of ballistocardiography. Ballistocardiography can record recoil ballistic forces which occur as blood is ejected into the vasculature can be measured through multi-axis sensor placement on the body [190]. One recent study by Rabineau et al. discusses the effects of exercise countermeasure as a mitigation strategy for cardiovascular deconditioning during bed rest [191]. In their finding, ballistocardiography (6-degree of freedom) and apex-SCG were used as monitoring techniques of kinetic energy instead of vibrational peaks and cardiovascular timing. These relationships were used to show the promise of a reactive jump exercise towards the prevention of orthostatic intolerance. However, placement of the SCG beyond the traditional sternum placement creates a signal susceptible to noise artifacts [191], [192].

Vibrational signals are dependent on mass components of the system, defining the equations of motion. In addition to increased upward fluid retention, systemic loss of cardiovascular mass can contribute to the lowered mechanical peak performance. In spaceflight, there is a chronic decrease in left ventricular mass of values close to 9-12% loss while a similar observation during HDT studies shows 8-16% mass losses [165], [169], [171]. Ventricular mass losses have also been observed in previous bed-rest studies [22]. These changes in mass produce hindrances in both left ventricular end-systolic volume and end-diastolic volume. However, vascular changes and pressure regulatory responses to fluid shifts cause relatively quick recovery stabilization of the left ventricular end-diastolic volume [165], [193] while left ventricular end-systolic volume tends to continue to increase during prolonged weightlessness, suggesting a reduction in cardiovascular compliance and functional performance [194].

As shown in the decreased averages and distributions of the FDA spline basis coefficient sets, there are displays of underlying structural changes in SCG peak complexes (Figure 4.3). Upon entrance into HDT01, an instantaneous decrease of the SCG peaks occurs due to the blood displacement towards the head. The spline basis function coefficient distributions define a lowering trend of both AO and AC structures towards the end of bed rest. Structural decreases in these SCG peak vibrations suggest there is a prolonged deconditioning that occurs potentially as seen in ventricular mass loss and increased headward fluid volumes.

4.5.2 Quickening of Cardiovascular Timing Intervals

During spaceflight and prolonged bed rest, regulatory responses of blood pressure occur as the body attempts to retain homeostasis. The shift in blood pressure throughout bed rest is shown in the increase in HR and fluctuational decreases of LVET and PTT. The observation resulting in an instantaneous increase in LVET upon commencement of HDT is in a correlation with this initial

regulation of the increased upward blood volume. Initial increases of central blood volumes seen in head-down tilt bed rest, as well as weightlessness of microgravity cause, increased stroke volume, and increased cardiac output [35], [36]. Resultant increases in LVET at HDT01 seen in our study are defined by these decreases in blood pressure which could be a response to increased stroke volume (Figure 4.4). However, as HR remains continually higher the resultant mechanical deconditioning of the left ventricle causes the continual decrease of LVET. As bed rest confinement continues, offloaded conditions and headward fluid shifts had a prolonged effect on LVET values that showed significant decreases at the end of HDT. The relationship between potential stabilizing left ventricular end-diastolic volume with increased left ventricular end-systolic volume in conjunction with lowered offloaded conditions of bed rest could be a major contributing factor for the decrease of LVET. As seen in previous literature, left ventricular end-diastolic volume and end-systolic volume begin to recover quickly after weightlessness and HDT bed rest [32]. The quick recovery in these parameters could be a driving factor leading to the gradual recovery of LVET 8 days post bed rest seen in an increased value on R8. However, as there were small losses in amplitude peak strength of AO and AC, LVET recovery was relatively small.

The decrease of the pulse transit wave defined by PTT to the finger is analogous to during 6-months of space flight seen by both Hughson et al and Baevsky et al., suggesting the presence of resultant stiffening arteries during bed rest [15], [16]. Upon commencement of HDT01, the PTT values show a decrease of 15-35%. Plasma volume had shown to decrease as well between baseline at BDC compared to the end HDT similar to that found by Pavy-le Traon et al., of blood plasma volume decreases of 10-15% in both spaceflight and head-down tilt bed rest. The viscosity changes of the blood due to this decrease could have potential factors affecting PTT shifts and SCG

attenuation [163]. However, there were no significant differences in blood plasma volume between campaigns still suggesting seasonal changes affect PTT during bed rest. As PTT decreased at HDT01, there was an initial decrease in SBP and DBP while HR increased that point to potential relaxation precursors of vaso-controlled responses of the vasculature. Acute weightlessness and upward fluid shifts seen by Norsk et al. reduce vascular resistance if 24% while chronic weightlessness decreases vascular resistance by 14%, suggesting a presence of vasorelaxation [35]. Prolonged bed rest towards HDT52 and 8 days post of recovery both show decreased PTT values of 15-40% without recovering, hinting at altered vascular compliance. The altered vascular compliance could be in response to continued relaxation of blood vasculature to accommodate blood flow due to headward fluid shifts.

As vascular adaptation occurs, the drop in hydrostatic pressure causes activation of regulatory responses of the baroreflex. The lowered force acting on the blood due to lack of gravity causes lowered shear stress between the blood and vasculature [161]. Vascular distension that occurs due to increased upward localized blood volumes causes increased arterial elasticity, a reduction in arterial compliance, and stiffer arteries also seen in previous bed-rest studies [161], [167]. Rapidly increased headward blood volumes inhibit the ability of vasculature to expand quickly to allow absorbing vibrational effects of traveling blood, resulting in the quickening of PTT to the finger (Figure 4.5). Reductions in arterial compliance along with a reduction in systemic vascular resistance (SVR) are compounding effects that continue to drive the decrease in the mechanical performance of the heart that is observed in both SCG peak complexes and cardiovascular timing intervals (i.e., LVET and PTT). Bed rest and fluid shifts have a significant impact on vasculature changes, of these impacts are increased arterial stiffness as seen in the dramatic decreases of cardiovascular timing intervals such as PTT.

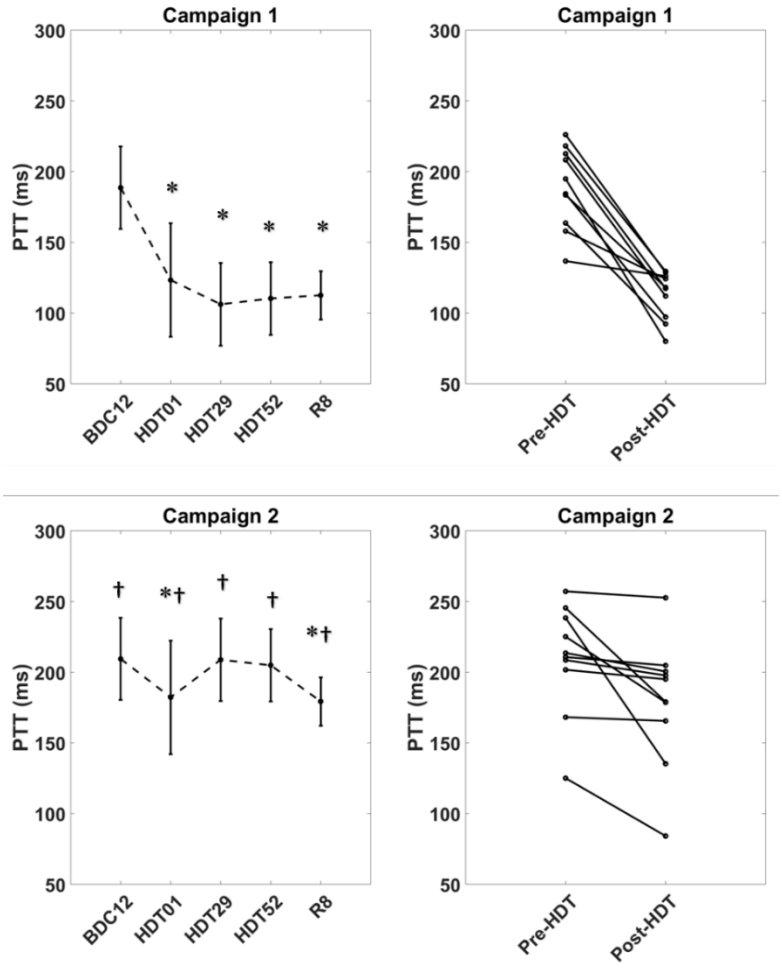

Figure 4.5: PTT comparison through bed rest phases and campaign differences. Rapidly quickening of PTT to the finger upon entrance into HDT through the end of bed rest suggests increased arterial stiffness due to responses of fluid shifts. The value does not recover 8 days post bed rest. Due to the seasonal temperature changes campaign, 1 had shown a more drastic decrease in pulse transit time due potentially to vascular vaso-controlled responses. * Denotes significant differences compared to BDC12 and † denotes significance between campaigns at each test day ($p < 0.05$).

4.5.3 Seasonal Influences

Though both campaigns showed similar trends in cardiovascular relationships and timing intervals, there was a significant difference in the changes between the values over bed rest between campaigns. In campaign 1 as compared to campaign 2, blood pressure (SBP and DBP) values showed lower trends. These changes could potentially be attributed to the seasonal differences (that can influence vaso-control of vasculature) in the two campaigns. As campaign 1 was started in January, SBP in this season is expected to be higher due to constriction of

vasculature for thermal regulatory responses [195], [196]. Upon entering the bed rest study, the individuals would be in a higher indoor temperature environment compared to outdoor ambient temperatures, allowing for more dilation of the vasculature to continue this thermal regulation. Previous literature has shown that by increasing both indoor and outdoor temperatures by 1°C resultant blood pressure reduction occurs [195], [197], [198]. In campaign 2, which was begun in September, the differences in outdoor and indoor temperatures were not as drastic, leading to a lessened vascular response (Figure 4.4). The changes in blood pressure and vascular constriction or dilation further influence the heart rate. This was observed between the two campaigns: in campaign 1 there is a large increase in HR pre- to post- bed rest, while in campaign 2, there is a smaller increase in HR during pre- and post- bed rest periods. These differences in heart rate between the two campaigns could have contributed to the differences in PTT. Throughout bed rest, PTT shows more drastic decreases in campaign 1 due to fluid shifts (and perhaps thermal responses) wherein campaign 2 PTT shows lesser decreases (Figure 4.5). Between the two campaigns, fitness levels ($\dot{V}O_2max$) were not significantly different between baselines and recovery stages. Average values of campaign 1 and campaign 2 differed by only 1 ml/min/kg (campaign 1 BDC8 = 39±4 ml/min/kg, campaign 2 BDC8 = 40±4 ml/min/kg. Similarly, $\dot{V}O_2max$ values for recovery (R) differed only by 2 ml/min/kg (campaign 1 R1 = 31±4 ml/min/kg, campaign 2 R1 = 29±2 ml/min/kg. The small variation of fitness level suggests that the differences in BDC HR were most likely related to seasonal influences rather than cardiorespiratory fitness.

Due to the influences of thermal regulatory responses, potential effects of seasonal changes should be considered in future bed rest studies. During prolonged spaceflight, Stahn et al. investigated that core body temperature increases 1℃, which can affect task performance [199]. Norsk et al. point to both cardiovascular shifts and thermal regulatory responses to decrease

systemic vascular resistance in prolonged spaceflight [18]. Our results from prolonged bed rest confinement suggest that the training temperature of the astronaut and the environmental temperature during spaceflight could potentially influence the changes in cardiovascular function and/or cardiovascular responses. In addition, such temperature changes could further influence the impacts associated with upward fluid shifts and vascular remodeling during prolonged bed rest.

4.5.5 Limitations and considerations

In this study, the participants involved were all males. It has, however, been shown that cardiovascular responses are influenced by sex [158], [200], [201]. Future studies should, therefore, include both males and females. Plasma volume loss was not directly studied in the scope of this investigation as a correlation to seasonal changes and cardiovascular timing. Future studies should investigate blood volume as a potential metric of cardiovascular and thermal strain. Another limitation of this study is that temperature was not controlled. As our results show, temperature changes could potentially affect several parameters. Future bed rest studies should take into account the effects of seasonal changes on cardiovascular and other responses.

4.6 Conclusions

During spaceflight, the cardiovascular system alone experiences rapid deconditioning due to vascular changes occurring during upward fluid shifts. Prolonged head-down tilt bed rest has shown to be analogous to the impacts seen in microgravity. This study has shown the loss of mechanical strength of the heart due to prolonged head-down tilt bed rest. Our results support the hypothesis of continued attenuation of heart vibrations resulting from HDT. The physical-mechanical strength loss seen from the peak inflections of SCG in tandem with blood pressure responses suggests that prolonged fluid shifts result in the quickening of cardiovascular timing intervals corresponding to vascular changes. The rapid drop in PTT had shown that immediately

experiencing fluid shifts cause faster blood distribution transition times to the finger, resulting in the potential for increased arterial stiffness and lowered arterial compliance. Quickening LVET appears to be correlated to the decreases in mechanical strength of the left ventricle, which could arise due to changes in blood volume and ventricular mass loss associated with the HDT.

Our results show that seismocardiography can provide higher fidelity information about the mechanical performance of the cardiovascular system during prolonged HDT bed rest. As the heart beats, there are critical time elements that correspond to resultant vibrations. Traditional techniques that are utilized to gather cardiovascular data overlook this mechanical stimulus and require complex instrumentation. Complex equipment can make monitoring difficult in both operational spaceflight tasks (e.g., extravehicular activity) and during routine medical checkups. Single sensor placement of the SCG can yield crucial cardiac information with less instrumentation and opens monitoring techniques to wearable technologies (e.g., shirt or bands) for spaceflight applications as well as home care monitoring. The insight gained from this study can be further used to gain an understanding of how the vasculature and heart adapt mechanically to sedentary bed rest or prolonged simulated weightlessness.

Finally, The results of this study can give insight into the continuing cardiovascular changes due to aging as well as the consequences of bed rest confinement during hospitalization [173], [202]. Not only can the use of analogs such as HDT build upon our understanding of spaceflight physiology, but they can also aid in terrestrial medical applications.

Part III: ASSESSMENT OF CARDIOVASCULAR PREDICTORS TO EVA ENERGY EXPENDITURE AND THERMAL REGULATION

Chapter 5. EXTRAVEHICULAR ACTIVITY METABOLIC RATE MODEL: METABOLIC RATE ESTIMATED FROM HEART RATE

5.1 Summary

In-flight monitoring of crew metabolic rates during extravehicular activity (EVA) provides crucial information in mitigating injury. The purpose of this study was to investigate the relationship of crewmember heart rate (HR) and metabolic rate (MR) during EVA operations to develop a predictive linear model. HR and MR data were collected from 132 EVAs from Shuttle and International Space Station (ISS) missions. MR determined by O2 consumption was collected every 2-min from portable life support system delta oxygen decay, while HR was collected every 20-sec via electrocardiogram. HR was downsampled to every 2-min to match MR during EVA for evaluation. Two models were developed to predict metabolic rates. The first model predicted MR from HR over the entire duration of EVA through a calculated conversion factor. Further, a new metric was observed from direct relations between MR with HR over EVA time (MR/HR) measured as a BTU/beat. The second model, MR was predicted based on HR values during EVA via a simple linear regression equation using eight percent testing and a twenty percent training paradigm. The model was adapted to find single EVA predictions via a fifty-fifty testing-training paradigm of individual EVA signals. Both HR and MR values were observed to decrease through the duration of all EVAs. The model predicted from MR/HR (BTU/beat) predicted MR for the individual EVAs with root mean square error less than 200 BTU/Hr. A significant regression equation was found using the grouped EVA dataset drawing relations between HR and MR ($F(2923.84)$ and $P<0.0001$) with an R^2 value of 0.402. Individualized crew EVA via single EVA signal regressions improved prediction and R^2 (0.75 ± 0.08). Two models are presented to determine metabolic rate from heart rate during EVA. Results draw comparisons for heart rate and metabolic

rate fluctuations during EVA for individualized crew predictions during future operations. The linear models correlate to Apollo prediction data during historic EVAs.

5.2 Background

Monitoring crew health during spaceflight missions is vital to the mitigation of injury risk during exploration operations such as extravehicular activity (EVA). Spaceflight brings with it a host of unforgiving environments. An element of these environments is altered gravitational forces. Prolonged exposure to microgravity produces an array of deconditioned physiologic systems. Among those systems most affected is the cardiovascular system. Gravity greatly impacts cardiovascular regulation during daily activities. Tasks such as running/walking or lifting objects are known to increase heart rate relative to metabolic energy expenditure [203], [204].

During prolonged weightlessness, metabolic demands of everyday physical activity dramatically change in parallel to the relief of gravitational loading on the cardiovascular system. Baroreflex responses adjust to maintain blood pressure due to headward fluid shifts [25], [172]. Throughout long-term spaceflight, heart rate (HR) has been shown to remain relatively unchanged due to a shift in cardiovascular regulation [15], [148]. One study of the cardiovascular effects of acute weightlessness by Norsk et al. observed that HR remained unchanged with increasing cardiovascular output while increased vasodilation, despite increases in the venous return/cardiac output, leads to decreases in systemic vascular resistance due to headward fluid shifts. All likely responses to mitigate increased blood pressure [148]. Additionally, Fraser et al. have shown that daily HR was not changed compared to ground data during prolonged stays on the ISS, including observations during sleeping and exercise [205].

Tied to cardiovascular activity is metabolic demand. During EVA, the extended high and prolonged workload can lead to physiologic strain and risks of injury. Real-time monitoring of

metabolic rate is an important factor during EVA for tracking life support consumables, crew member safety, and planning task operations. Ultimately, accurate estimations of metabolic rates in real-time can help determine if a crew member is achieving maximum work rates during short maximum efforts, which could cause injury. Further, metabolic rates can give a picture into the physiologic state of the crew member, such as metabolic heat generation. Metabolic heat generated by normal activity can be tracked through oxygen consumption. Measuring oxygen consumption is a widely accepted research methodology to determine energy expenditure [206].

Metabolic rates were not directly measured in real-time during early Gemini missions where it was determined that crew members exhibited higher than expected energy expenditure which stressed the cooling capability of the portable life support system, ultimately indicating evident overheating during EVA [4]. Metabolic rates during these missions were not directly measured, but energy expenditure was determined based on workload correlations post-flight through HR and respirations rate analysis. During Apollo, three techniques were attempted to monitor real-time metabolic rates through oxygen consumption, liquid cooling garment (LCG) heat balance, and HR estimations [4]–[6].

The oxygen consumption method was estimated through differential pressure decay of the oxygen bottle pressure of the portable life support system. This method experienced noise and included suit leakage, which induced error from the oxygen that was not consumed by the crew member. Due to this noise heat balance of the LCG was used through a relation of heat removal and LCG inlet temperature. Similarly, utilizing the current liquid cooling and ventilation garment (LCVG) flow rates, a method comparable to direct calorimetry was shown to be unreliable when used on its own to predict metabolic rates [4].

HR comparisons to the metabolic rate during Apollo were determined for each crew member via pre-flight exercise testing and through linear regressions used in-flight. This technique was subject to noise due to psychophysical responses causing short-term elevated heart rate. However, HR methodology allows for estimations of metabolic cost and energy expenditure per task during minute-by-minute observations [6], [50]. Because of the uncertainty of these methods, all three of them were used simultaneously during Apollo [207]. Current EVA operations use pressure decay of the portable life support system oxygen supply to estimate crew member metabolic rates, however, it is understood that these measurements can induce large errors [4], [208].

Terrestrially, HR and cardiovascular function are highly correlated to energy expenditure. Buresh et al. show that heat production is directly correlated to body size, composition, and HR fluctuations during high-intensity running [209]. Body size and cardiovascular drift seen during exercise have a profound effect on energy expenditure, ultimately affecting heat storage. Increased heat storage can further lead to degradation of physical workload leading to serious injury. Further, predictions of thermal regulation have been investigated by some studies involving soldier and firefighter workloads utilizing HR [210]. Linear regressions have been shown to have high confidence in predicting core temperature and thermal regulatory processes as well as metabolic rates [210], [211].

In this paper, comparisons of heart rates and metabolic rate are drawn and presented from EVAs during Shuttle and International Space Station (ISS) missions. Metrics of a relationship between metabolic rate and HR over time are presented to include conversion factors at various energy expenditure ranges. Further, a linear regression model was developed to predict metabolic rates from heart rates during EVA.

5.3 Methodology

5.3.1 EVA Dataset

The dataset consisted of 140 individual sets of HR and metabolic rate data collected during Shuttle and ISS EVA collected from 2006 to 2015. Metabolic rate was collected every two minutes as a delta decay of oxygen tank pressure of the suit. HR was collected every twenty seconds via electrocardiogram. Data were removed from analysis if the length of EVA was less than five hours and if the signal had more than twenty-five percent of loss of signal (LOS) noise. The final number of signals analyzed in this study was 132 individual EVA heart rate and metabolic rate signals (6.5 Hours ± 0.7).

5.3.2 Heart Rate and Metabolic Rate Calculations

HR and metabolic rate (MR) were investigated to identify if there was cardiovascular or metabolic drift across the EVA time. First, HR was downsampled to every two minutes to correspond to MR sampling. A 10-point moving average was used on both HR and MR values to smooth short-term fluctuation noise [50]. Then HR and MR values were extracted from the EVA signal at various times, Start, 1Hr, 2Hr, 3Hr, 4Hr, and End. Values at each time step were used to determine the difference between the starting value of HR and MR to view if there was a drift occurring.

Additionally, a new metric technique was conducted from direct relations between metabolic rate with HR over EVA time (MR/HR). This metric was defined as a BTU/beat and was used to develop scales of energy expenditure across ranges of metabolic rate activity per heartbeat. Further, MR values were separated into bins of metabolic ranges (BTU/hr) <600, 600-800, 800-1000, 1000-1200, and >1200. EVA tasks were not consistent between each EVA within the dataset. This is due to the EVAs being conducted over multiple different missions and by different

individual crew members. Corresponding HR values were separated into each bin and compared to each other metabolic range to view HR changes due to increased energy expenditure. HR was predicted using sorted and non-sorted MR/HR values as the generated conversion scale. Additionally, MR was predicted from the MR/HR values to compare with outputs to linear regression relations.

5.3.3 Model Evaluation

A simple linear regression model was fit utilizing the EVA dataset developed to observe the response of metabolic rate from corresponding heart rate values. First, a simple linear regression was fit on a subset of the total number of EVA HR and corresponding MR values as a training set. Then the model was tested against the subsequent testing set of EVA HR and MR data. The training-testing paradigm was split eighty percent as training and twenty percent as testing. As EVA tasks were not constant between all the EVAs in the historical dataset, individual crewmember-specific regressions were developed as well. To improve predictions, a separate simple linear regression was also calculated using single EVAs for individual responses, training-testing paradigm was split fifty percent of the signal for training and the remaining fifty percent for testing. A subsection of individual EVA was used as a training set, and the remaining portion of the EVA was the testing set. Root mean square error (RMSE) < 200 BTU/hr has deemed a success from previous Apollo HR data [207].

5.3.4 Statistics

Normality was determined using the Shapiro-Wilk test at $\alpha = 0.05$. For normally distributed data, a one-way ANOVA was used followed by Bonferroni correction to compare HR and MR values at 1Hr, 2Hr, 3Hr, 4Hr, and End compared with values at the start of EVA to determine if cardiovascular drift occurred. Similarly, a one-way ANOVA was used to compare HR values in

different metabolic ranges to determine fluctuations in increasing energy expenditure. MATLAB 2019a (Mathworks Inc., Natick, MA, USA) was used for statistical calculations.

Linear regression modeling was fit using MATLAB *fitlm()* function to fit the regression model. The predicted variable of interest was MR, with the independent value being HR. A one-way ANOVA of the model components was conducted to determine fit regression equation significance and F-statistics. Additionally, RMSE was used to determine acceptance of the linear regression model and conversions scale MR/HR metabolic rate predictions [207].

5.4 Results

Both HR and MR values for all EVAs passed the test for normality. General significant decreases of both HR and MR values were observed as the EVA durations progressed. HR compared to the starting values at one-hour increments: 1Hr ($p = 0.0013$), 2Hr ($p < 0.0001$), 3Hr ($p < 0.0001$), 4Hr ($p < 0.0001$), End of EVA ($p < 0.0001$) (Table 5.1, Figure 5.1). MR compared to starting values at one-hour increments: 1Hr ($p < 0.0001$), 2Hr ($p < 0.0001$), 3Hr ($p < 0.0001$), 4Hr ($p < 0.0001$), End of EVA ($p <0.0001$) (Table 5.1, Figure 5.1). MR/HR metrics were generated to quantify a BTU per beat as a relationship over time. Across EVA, MR/HR metrics did not show trends of cardiovascular or metabolic drift (Table 5.1). Metabolic rate values and predicted metabolic rate values from MR/HR did not show significant differences ($p>0.23$) (Table 5.1).

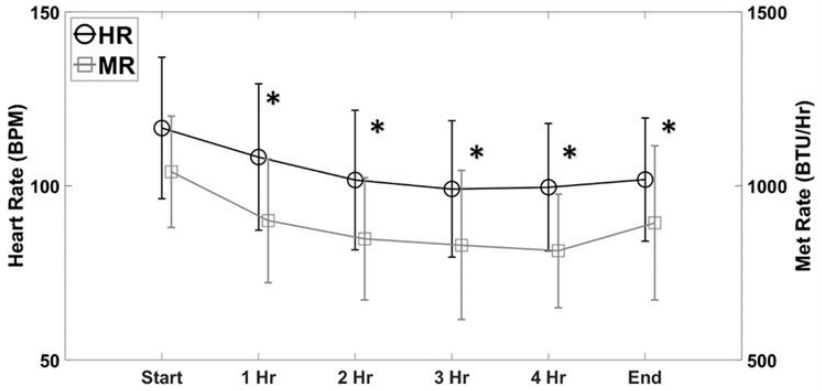

Figure 5.1: Heart rate (HR) and metabolic rate (MR) observations across five hours of operations of 132 EVAs. Both HR and MR values show decreasing trends across the EVA duration suggesting a lack of cardiovascular and energy expenditure drift, however, showed increased linear relations (* designates p<0.05 compared to the starting values).

Table 5.1: EVA observations, predictions including linear regression model F-Test and Coefficient Tests. (* denotes p<0.01 compared to EVA starting values)

EVA INCREMENT TOTALS							
Variable, Unit	**START**	**HOUR 1**	**HOUR 2**	**HOUR 3**	**HOUR 4**	**END**	**ALL**
Metabolic Rate (BTU/hr)	1040.3 ± 159	899.9 * ± 177	847.9 * ± 176	830.0 * ± 214	813.3 * ± 163	893.1 * ± 221	862.9 ± 125
Heart Rate (BPM)	117 ± 20	108 * ± 21	102 * ± 20	99 * ± 19	100 * ± 18	101 * ± 18	103 ± 17
MR/HR (BTU/Beat)	0.153 ± 0.03	0.141 ± 0.02	0.142 ± 0.03	0.142 ± 0.03	0.139 ± 0.03	0.149 ± 0.04	0.142 ± 0.03
Total Generated Heat (BTU)	3111 ± 675	28830 ± 3932	108706 ± 14571	238319 ± 33242	416875 ± 60803	831401 ± 126547	-
MR Predicted From MR/HR (BTU/hr)	1065.9 ± 185	911.3 * ± 177	861.1 * ± 170	834.5 * ± 165	815.3 * ± 150	818.6 * ± 142	873.8 ± 151
Predicted Generated Heat (BTU)	3252 ± 561	29545 ± 5170	110894 ± 19384	242283 ± 42515	422607 ± 73674	783483 ± 138069	-

SIMPLE REGRESSION FROM HEART RATE						
F-TEST						
VARIABLE, UNIT	**numDF**	**denDF**			**F-VALUE**	**P-VALUE**
Metabolic Rate (BTU/hr)	1	15595			2923.84	<0.0001
COEFFICIENT TESTS						
VARIABLE, UNIT	**TEST**	**COEFFICIENT**	**SE**	**DF**	**T-VALUE**	**P-VALUE**
Metabolic Rate (BTU/hr)	Intercept	284.55	10.94	15595	26.02	<0.0001
	Slope	5.984	0.111	15595	54.07	<0.0001

MR/HR metrics did not show decreasing or increasing inflections allowing for averaged values for conversion between heart rate and metabolic rate across EVA (Figure 5.2A). MR was predicted directly from the averaged MR/HR conversion metric, which showed higher RMSE values across EVAs (176.37 ± 84.48 BTU/hr). Prediction accuracy increased slightly, however, not significantly when MR was predicted directly from the sorted MR/HR metric values determined by decreased RMSE compared to non-sorted MR/HR metrics (173.59 ± 80.68 BTU/hr). HR was also predicted from the MR/HR conversion metric and showed higher RMSE values across EVAs (Figure 5.2B). However, the intensity of the general EVA workload could be seen when arranging MR values into bins of increasing values. MR/HR metrics showed an increasing trend in addition to increasing trends of HR when placed in bins of corresponding increasing MR ranges (Figure 5.2C). Predicted HR using the sorted MR/HR metric values during EVA showed decreased RMSE at higher MR ranges compared to non-sorted MR/HR metrics (Figure 5.2D).

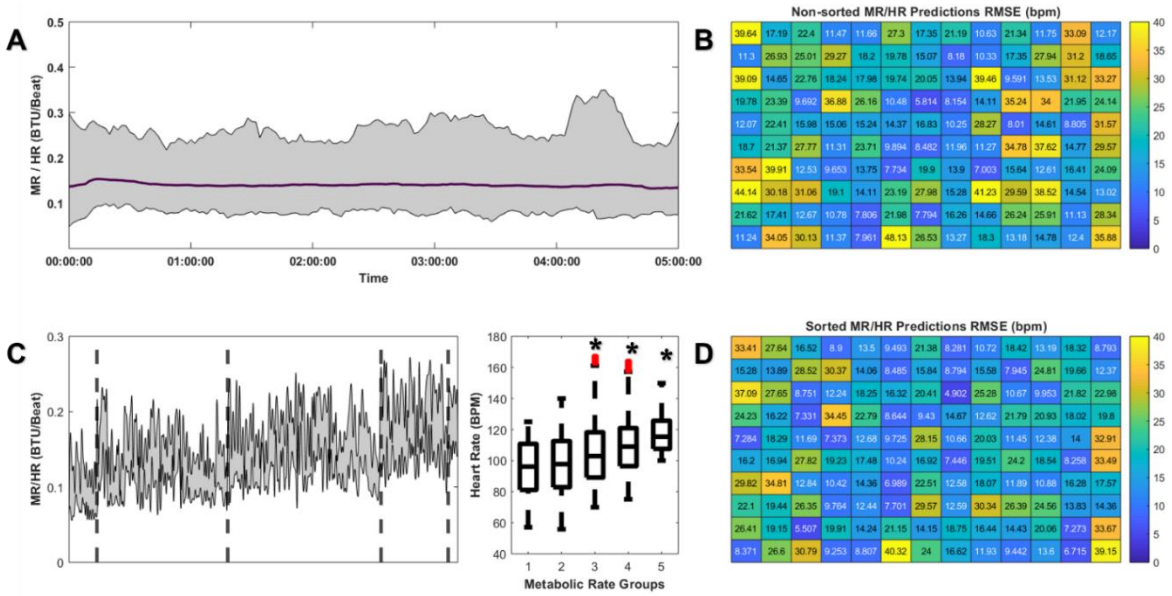

Figure 5. 2: BTU/Beat values were calculated in a new metric of MR/HR to draw correlations between heart rate and metabolic rate during EVA as a conversion scale A. Prediction RMSE of HR from the generated MR/HR scale are presented for individual EVAs B. Metabolic rates were sorted into increasing bins with corresponding sorted MR/HR values and heart rates showing increasing trends (* designates p<0.05 compared to the lowest MR values) C. Predicted RMSE of HR was shown to decrease across EVAs when using the sorted MR/HR scale D.

Further, MR was predicted based on HR values during EVA via a calculated simple linear regression. A regression equation was found drawing relations between HR and MR (F (2923.84) and P<0.0001) with an R^2 value of 0.402 (Table 5.1). As tasks were not common between all EVAs a single simple linear regression was made for each EVA for individual predictions increasing R^2 (0.75±0.08). Predicted and original values of metabolic rate showed agreement with individual responses during EVA (Figure 5.3A, 5.3D, 5.3E). MR/HR conversion metrics showed larger RMSE error (177.22 ± 84.36 BTU/hr) as a comparison to regression outputs (Figure 5.3C). Individual responses, however, showed predicted RMSE decreased ($p < 0.0001$) when using individual crew regressions (89.66 ± 44.24 BTU/hr) compared to MR/HR generated conversion scale (173.59 ± 80.68 BTU/hr) (Figure 5.3F).

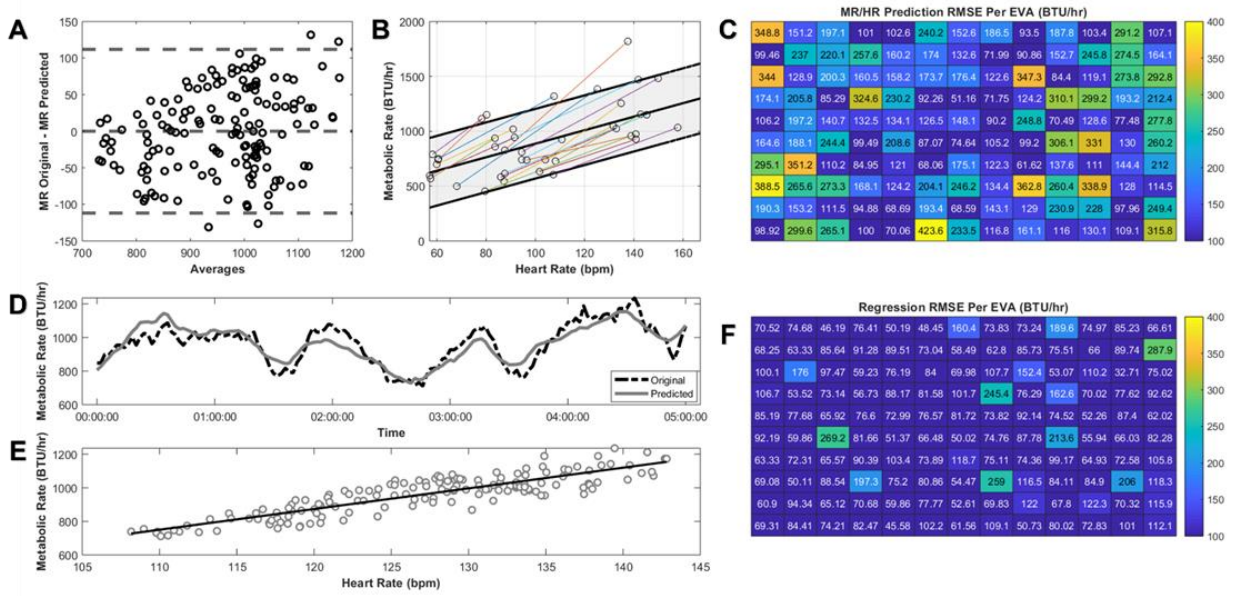

Figure 5.3: Individual crew regression responses show agreement between predicted and original metabolic rate observations A. Individual responses show predictions are within the confidence interval of the larger EVA regression model B. As a comparison metabolic rate predictions were completed using MR/HR which show RMSE values for individual EVAs represented as a heat map for each single EVA C. Prediction of single EVA observations of original and predicted metabolic rates using the individual regression model and corresponding linear trend D and E, RMSE = 56.73 BTU/hr. Individualized regressions for single EVAs show the increased quality of metabolic rate predictions with drastically reduced values of RMSE shown in the heat map of every single EVA compared to MR/HR predictions F.

5.5 Discussion

In this study, metabolic rate was predicted from corresponding heart rate through a new metric of BTU/beat calculation and simple linear regressions. Using the heart rate method and MR/HR metrics provides a minute-by-minute technique for use in future real-time monitoring. MR/HR metrics provided a BTU/beat observation that was used to predict observations between heart rate and metabolic rate. This metric showed reduced error of prediction of HR utilizing a conversion factor of BTU/beat in correspondence to binned metabolic rate averages from the 132 sets of EVA data. HR and MR did not seem to exhibit drift throughout EVA. However, decreases in HR and MR slopes from the start of EVA compared to the end of EVA suggest fatigue responses to increased workload, potentially due to dehydration or workload strain and operational task decisions [212].

Heart rate was observed to decrease across the duration of EVA for all 132 EVA sets. Similarly, this observation was seen in metabolic rate for the duration of EVA. Comparison between the EVA start workloads to one-hour increments to the end of EVA showed decreasing trends. The prolonged workload of EVA was expected to have an increasing drift of these values. However, normally in 1-G, hydrostatic forces create a gradient distribution of fluid pressure in the body. During a standing state, blood pressure is controlled through afferent stimulus of the mechanically sensitive baroreceptor impulses. The baroreceptor responses in the upper vasculature, localized in the carotid sinus and the aortic arch, lead to increased HR and systemic vascular resistance (SVR) as a result of vagal withdrawal and sympathetic activation [26]. During weightlessness, the phenomenon of headward fluid shifts occurs due to the lack of force pulling the blood towards the legs [155]. The change of microgravity, not normally seen by the cardiovascular system, shifts the responses of the Baroreflex to gain back homeostasis by attempting to control the equalizing

pressure. Due to this headward fluid shift, the cardiovascular system may be at a predisposition to have increased cardiac output and increased stroke volume. Whereas heart rate drift is discussed as an increase in heart rate due to constant cardiac output and decreased stroke volume [209]. During microgravity, this cardiovascular response of increased cardiac output and increased stroke volume could account for the decrease in HR and corresponding MR during increased workload (Figure 5.1, Table 5.1) [148], [213]. Additionally, the relationship of HR and MR could be driven by working activity type (e.g., upper body versus lower body). In microgravity EVA the workload is primarily upper body muscle activation versus full body such as lunar EVA during Apollo. As the results show comparable predictive accuracy to that seen during Apollo missions, the use of HR to predict MR provides a metric for minute-to-minute and should be revisited for future applications of microgravity and partial gravity EVA.

It has been thought that these longer stays in microgravity can have a detriment to the autonomic control of blood pressure due to changing vasculature. Hughson et al. were the first to report a decrease in systematic vasculature resistance and increased arterial stiffness of astronauts after six months of flight utilizing pulse width transition time [36]. While Norsk et al. had shown the effects of weightlessness on vasorelaxation and had shown a 9% decrease in systemic vascular resistance, while blood pressure and HR were unchanged [35]. Due to the increased fluid shifts in the upper vasculature, Norsk et al. observed an increase in systemic vasodilation; this dilation is suggested to be the body's attempt to prevent blood pressure from increasing. This decrease in systemic vascular resistance and increase in vasodilatory responses also affect increased core body temperature [199]. While some investigations point to headward fluid shifts as a detriment to the cardiovascular system, it could cause more efficient cardiovascular responses to workload through increased cardiac output and stroke volume [18], [148].

Heat production and energy expenditure are directly correlated to HR and associated drift [209]. MR was found to decrease linearly with decreases in HR. This correlated linear response of both HR and MR during EVA allowed for predictions through simple linear regressions (Figure 5.3D, 5.3E). Direct comparisons between EVA values could not be conducted as EVAs were completed across different missions and with different tasks, however, the grouped trained linear regression was completed with a reduced RMSE output for prediction. This R^2 was lower due to the task variation and subject variability yet, still encapsulated individual responses within the regression confidence levels (Figure 5.3B). The prediction output was improved with R^2 values being reduced when taking individualized crew regressions for partial EVA and predicting subsequent events of EVA metabolic rate. These predictions correspond to results seen in Apollo-based predictions of HR using RMSE as another metric of evaluation. During Apollo, it was determined that RMSE below 200 BTU/hr was deemed an appropriate amount of error in the prediction [207]. Similarly, MR can be used to predict HR with an RMSE below 10 bpm. The prediction of individual crew responses allowed for an increased R^2 and drastic reductions in RMSE when only taking HR and MR observations (Figure 5.3F). The developed model technique will allow for redundant and accurate prediction of suited energy expenditure and cardiovascular response to task loads during long EVAs.

5.5.1 Limitations and Considerations

While including a large set of EVA data, the data only focused on observations of metabolic rate and heart rate. Drawing improved correlations could increase the predictive element of the developed models through direct task analysis during EVA. As this dataset was collected from different Shuttle and ISS missions, the inclusion of additional metrics could improve the model through a multi-factor regression increased from a simple linear regression as presented. Similarly,

the metric of the MR/HR values determines a BTU/beat by incorporating increased task load evaluation of this BTU/beat metric can be improved. As a corollary, having repeat crew members or subjects could also draw correlations in the development of individualized models for future use on exploration missions.

5.6 Conclusions

Monitoring crew health during spaceflight missions is important to mitigate injury during EVA. Microgravity and spaceflight are unforgiving environments. Prolonged exposure to microgravity produces an array of deconditioned physiologic systems. Among those systems, the most affected is the cardiovascular system. Tied to the cardiovascular system, metabolic energy expenditure changes with altered gravity and workload. In this study, comparisons between heart rate and metabolic rate during long durations of EVA were drawn to determine if there is an element that can be used to predict fatigue or cardiovascular drift. A new metric was determined as MR/HR measured in BTU/beat that can be used as a conversion scale to predict metabolic rates from heart rates. Further, in this study, a simple linear regression model was developed for further predictions of metabolic rate from heart rate determined during EVA. These techniques provide a foundation for further improvement on the model to evaluate crew member state during exploration EVA on future spaceflight missions.

CHAPTER 6. EVALUATION OF CARDIOTHERMAL MODEL PREDICTION OF SIMULATED LUNAR EXTRAVEHICULAR ACTIVITY

6.1 Summary

Fewer than 20 extravehicular activities were completed during the Apollo program. The lunar environment has consistent unknowns to address, particularly that of suited performance in partial gravity. The moon has altered gravity that is $1/6^{th}$ that of Earth's. This study is focused on investigating the validation of the regression techniques identified in subsequent chapters and looks to improve predictive outcomes during simulated lunar EVA tasks. Heart rate predictions of metabolic energy expenditure are investigated from Chapter 5 to predict workload throughout simulated lunar EVA conducted in the active response gravity offload system (ARGOS) within the NASA Mark III spacesuit. Heart rate variability metrics developed from Chapter 3 are utilized to identify periods of high workload. Continually, the lunar offload capacity is further characterized to aid in improving the cardiothermal prediction models, including predictions of core temperature, skin temperature, and heat storage using heart rate, metabolic rates, and suit thermal data during the simulated EVA. The outcome of this model provides an application for future use in contingency predictions of energy expenditure during Lunar EVAs and provides a suite of instrumentation to predict workload during training scenarios.

6.2 Background

Spaceflight is a limited environment with less than 600 people who have currently been to space, and of those, only 12 people have walked on the moon. Due to this limited availability, many analogs have been developed to test capabilities for exploration. Most of these analogs focus on low Earth orbit (LEO) for training and suited operations in microgravity [87], [88], [171], [214], [215]. However, as NASA and other space agencies prepare for exploration missions beyond LEO

(e.g., the moon and Mars), there are immediate needs to establish ground-based high-fidelity facilities to support simulated partial-gravity operations. While there is no replacement for the partial gravity effects of spaceflight, NASA has developed several simulation environments, such as the Partial-Gravity Simulator (POGO), Neutral Buoyancy Laboratory (NBL), parabolic flights, and the active response gravity offload system (ARGOS) [216], [217]. Each of these simulation environments has limitations such as work volume, a method to reduce gravity offloading, and degrees of freedom. The POGO directly impacted participant task performance by only allowing (DOF) in the Y and Z axis while also creating significant overhead inertia and passive horizontal translation [218]. A parabolic flight environment allows for more DOF while providing offloading, though the work volume and duration are limitations (30 seconds per parabola) [219]. The NBL provides a large working volume incorporating International Space Station (ISS) mockup training while allowing full DOF. However, water drag is presently affecting the participant during translation and movements [220].

Lastly, the ARGOS provides translational DOF in the horizontal X, Y-axis, and vertical Z-axis (Figure 6.1). In addition to the full DOF, the ARGOS also provides active robotic control of offloading, while also providing active control of translational axes movements removing the inertial effects of the system. The ARGOS uses a gimbal design to attach to the human or suit. Specifically, the active robotic components provide three translational DOF, and the passive gimble designs provide three rotational DOF. Two different gimbal designs have been used, both can attach to the NASA Mark III (MK III) waist-ring interface and have customized adjustable center of gravity alignments for the operator [221], [222]. NASA's JSC Human Performance, Physiology, Protection, and Operations (H-3PO) laboratory have used ARGOS to conduct a

characterization of EVA metabolic rates simulating planetary exploration-class operations using spacesuit prototypes such as the MK III. [216]

The MK III is a planetary spacesuit assembly used to further assess EVA planetary exploration operations, such as simulated lunar gravity (Figure 6.1). Historically, Lunar EVA exploration capabilities were tested at Apollo A7L. The bioinformatics and portable life support systems (PLSS) for the A7L were designed from previous observations learned from earlier Gemini missions. Specifically, metabolic rates were collected using three different techniques, such as differential pressure of the PLSS oxygen, heart rate estimations, and heat balance of the liquid cooling garment (LCG). The Apollo missions were a huge success but there is room for improvement for future exploration suited operations.

Figure 6.1: NASA MK III within the ARGOS simulated EVA environment.

The MK III has been developed and utilized to evaluate technologies that can further extend planetary EVA capabilities beyond that of the A7L. One large change of the MK III prototype spacesuit compared to other spacesuits is the rear-entry donning/doffing capability. The MK III is also designed utilizing both hard and soft components. The main elements of the MK III prototype consist of a hard upper torso (HUT), rolling convolute shoulder design, brief and hip translation components, hip and waste abduction/adduction joints, and bearings incorporated in the upper arm, shoulder, hip, ankle, and waist [223]–[225]. Also, the MK III neck ring allows for the coupling of a circular removable 13-inch helmet. The suit operates at a nominal 4.3 PSIG pressure allowing for gas flow rates of 6 ACFM. Breathing gas enters at the rear of the suit helmet via an inlet vent then the gas flows over the top of the head and the front of the face for CO2 washout. Then the gas flows throughout the body and exits out the suit through an outlet at the lower backplate of the MK III. The main cooling of the suit operator is through a liquid cooling garment (LCG).

While, the MK III and ARGOS provide an environment to test partial-gravity EVA operations, there are still unknown as to how this simulated gravity offloading affects energy expenditure, cardiovascular workload, and thermal strain within the suit. One of the limitations to monitoring these objective measures is biomedical informatics and instrumentation. The first limitation is focused on the spacesuit, the limited space within the spacesuit and around the ARGOS gimble attachment leads to limited availability for space of instrumentation. This study identifies instrumentation to measure thermal loading of space suit operators within the MK III, and ARGOS simulated EVAs, then drawing upon previous chapters, correlated cardiovascular metrics and metabolic activity metrics are identified to help in predicting accurate physiologic responses to increasing workload. The correlations and predictive models aid in helping reduce the amount of

instrumentation needed during training environments increasing fidelity during spaceflight EVA training.

6.3 Methodology

6.3.1 Simulated Gravity Environment and MK III Spacesuit

The Active Response Gravity Offload System (ARGOS) was used to simulate the effects of offloading during data collection of a Lunar Metabolic Rate Characterization study. Within the simulated environment suit, operators donned the rear-entry MK III space suit and were offloaded $1/6^{th}$ G offloading. Metabolic rate during the study was collected through CO2 calculated using a sensor (Vaisala GMP252) in the exhaust stream of the MK III suit [216], [221]. The heart rate for the study is collected from an H-10 Polar heart rate monitor. These measurements were collected every one second recorded via Raspberry PI 3B+. The above-mentioned Lunar Metabolic Rate Characterization study was approved by the NASA Johnson Space Center IRB office as not human subject research as part of Human Health and Performance in Spacesuits During Exploration Task Simulations. Two suit operators (S1 and S2) performed two separate ARGOS simulations called Run 1 (R1) and Run 2 (R2), lasting three to five hours performing various metabolically demanding tasks. These tasks included EVA walk back to simulate walking to and from a lunar crater site. This walk back consisted of different walking grades on a treadmill to simulate going up and down lunar crater terrain. Tasks also included geology sampling, cognitive task loads, and object relocation.

6.3.2 Suited Thermal Sensor Suite

A suited thermal sensor suite was developed to collect suited performance and human thermal regulation metrics during ARGOS MK-III testing. The thermal sensors were chosen to measure physiologic data of core temperature and skin temperature. Additionally, sensors were selected to

measure suited thermal data, including liquid cooling garment inlet and outlet temperature, in-suit gas inlet, and outlet temperature as well as in-suit inlet and outlet humidity. Further below is a description of each sensor selected and the location during ARGOS MK-III testing. The controller for data storage and collection was a Raspberry PI model 3B+ and the code that was written for data collection was Python.

6.3.2.1 Skin Temperature

Sensors to measure skin temperature were selected for minimizing space within the MK III. These sensors consisted of iButton DS1923 Hygrochron Temperature and Humidity Sensor. The hygrochron iButton sensor sampling rate was at one-minute intervals to conserve battery life. Each of the sensors collected localized temperature and humidity and were positioned directly on the skin underneath the LCG on the lower forearm, upper bicep, leg quadriceps, leg calf, mid-chest, and upper back secured with medical tape (Figure 6.2). From the six locations across the body, mean skin temperature was calculated from weighted average using the Ramanathan method (Eq 6.1) [226], [227]. The mean skin temperature calculation was used in comparisons of the cardiothermal regression model and METMAN thermal outputs.

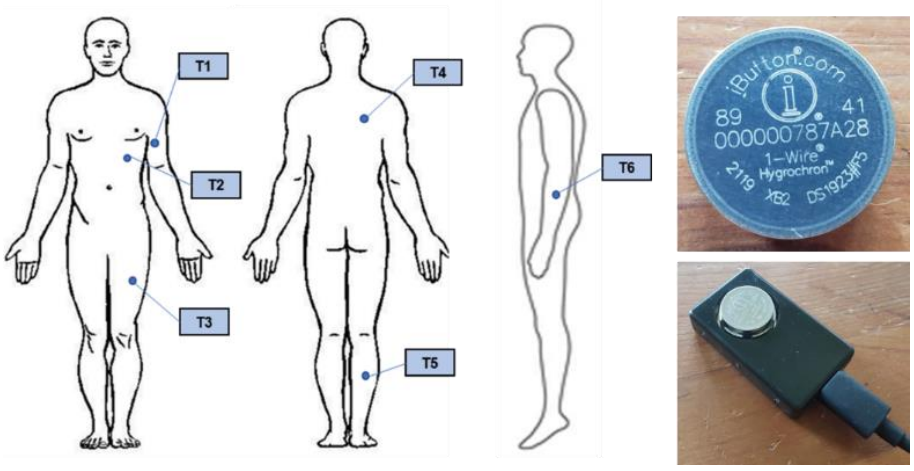

Figure 6.2: Local skin temperature measurements were taken via iButton DS1923 Hygrohron at six locations on the body. Measurements are used to calculate weighted mean skin temperature.

$$Ts = 0.3 * (T1 + T2) + 0.2 * (T3 + T5) \quad \text{Eq. 6.1}$$

6.3.2.2 Core Temperature

Core temperature was collected via the BodyCap eCelsius Performance ingestible pill (Figure 6.3). The pill was ingested three to four hours before the participant donned the MK-III suit and started the EVA. The eCelsius Performance pill transmits in real-time to the eCelsius Viewer by RF transmission (433-434 Hz) and can also store data locally on the pill if the connection is lost. The data that is stored is then offloaded onto the eCelsius Viewer upon re-established wireless connection. In this study, it was chosen to store the data locally and offload the data after the EVA. The sampling rate was set to 30 seconds to allow for the total amount of data to be stored during the duration of the simulated EVA.

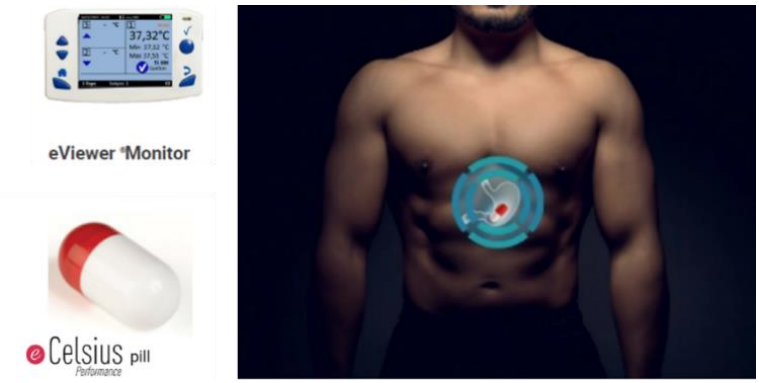

Figure 6.3: Core temperature during the simulated EVA was collected via an ingestible pill three to four hours before the test started to ensure the correct location was reached for accurate measurements.

6.3.2.3 Suit LCG Inlet and Outlet Temperatures

LCG inlet temperature provides an input to the human thermal model METMAN for accurate suit thermal regulation. In this study, both inlet and outlet temperature were collected to not only provide input into the human thermal model but also to the cardiothermal regression to improve the prediction accuracy of metabolic rate, core temperature, and skin temperature. LCG inlet and outlet temperatures were collected via 100 Ohm resistive temperature detectors (RTDs) that were

inset into NPT pipe fittings. The RTD was connected to resistance to digital converter MAX31865 breakout board for input to the Raspberry Pi. A pipe fitting tree was designed to couple between the ARGOS coolant supply and the MK-III LCG inlet/outlet ports (Figure 6.4). This pipe fitting tree was also designed for the quick disconnect to allow removal quickly in case of emergencies. The LCG temperature was sampled every one second and stored on the Raspberry Pi.

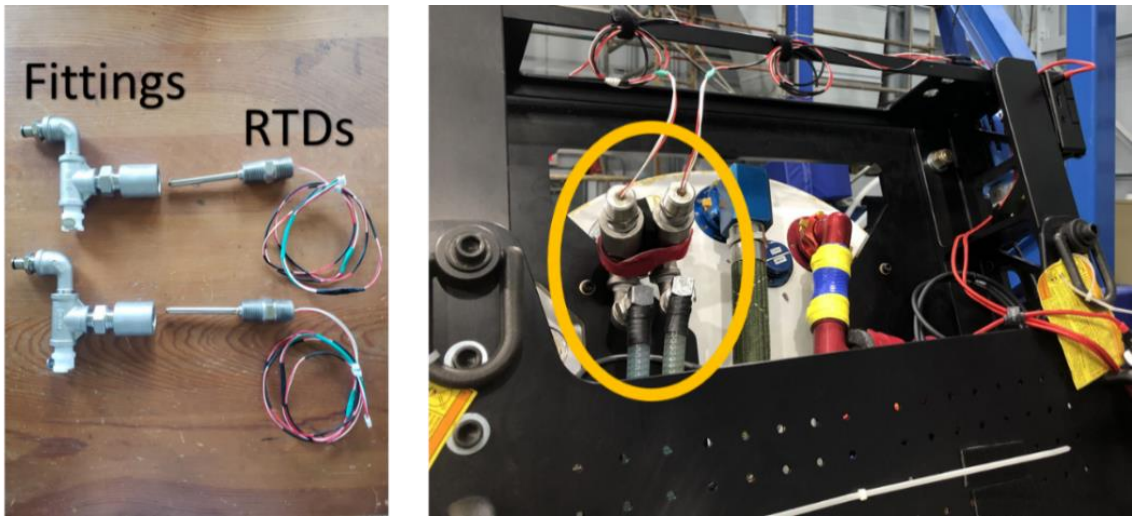

Figure 6.4: Liquid cooling garment inlet and outlet temperatures were gathered via two resistive temperature detectors located in a fittings tree coupled to the back of the MK III.

6.3.2.4 Suit Gas Temperature and Humidity

Similar to LCG inlet temperature, suit gas inlet humidity and temperature are expected inputs to the human thermal model METMAN for accurate thermal regulation characteristics of the suit. In this study, the gas inlet and outlet temperatures and humidity are collected for the METMAN model but also to continue to improve the cardiothermal regression model correlations. The inlet suit gas temperature and humidity were collected using the iButton DS1923 Hygrochron Temperature and Humidity sensor located on the inside of the helmet (Figure 6.5). This was chosen due to its small size and location directly in line with the gas flow stream into the helmet for accurate readings. This inlet sensor was collected every one minute to conserve the battery life of the iButton Hygrochron. The outlet temperature and humidity were collected via a Vaisala HMP7

Temperature and Humidity sensor located downstream of the suit exhaust. This sensor location is coupled to the exhaust a Vaisala GMP252 CO2 sensor used to calculate the metabolic rate for the study (Figure 6.6). This exact location was chosen to not interfere with the CO2 sensor as the main part of the

Figure 6.5: Suit gas inlet temperature and humidity collected via an iButton Hygrochron positioned at the inlet of the helmet of the MK III.

Lunar Metabolic Rate Characterization study by H-3PO. The Vaisala HMP7 connects to the Raspberry PI via an M12 to RS485 USB and collects by Modbus serial communication. The outlet temperature and humidity are collected every one second with the LCG inlet and outlet temperatures.

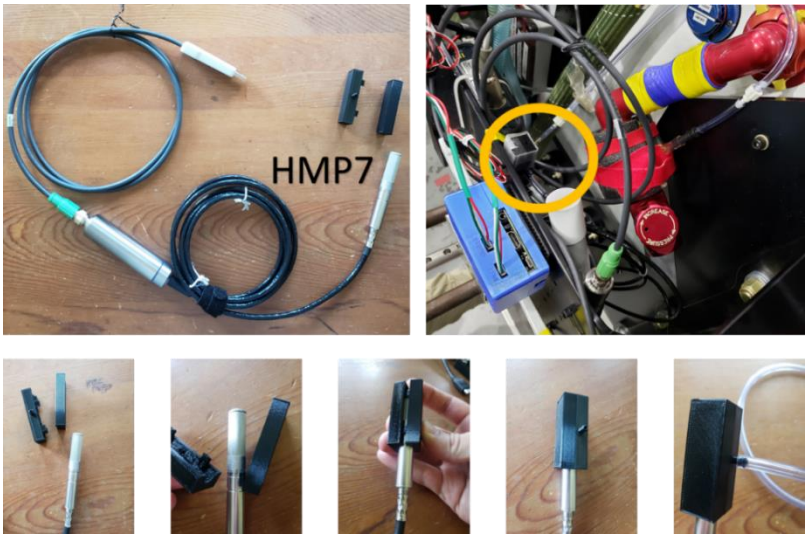

Figure 6.6: Suit gas outlet temperature and humidity are collected using a Vaisala HMP7 temperature and humidity probe located downstream of the exhaust gas of the MK III suit.

6.3.3 Cardiothermal Correlations and Model Evaluation

The first cardiovascular and energy expenditure model tested was utilizing the technique developed from EVA datasets in Chapter 5. Linear regression modeling was fit using Python *statsmodels* regression linear model. An individualized linear regression was built from each subject R1 using metabolic Rate (BTU/hr) as the dependent variable of interest and heart rate as the independent variable. The regression model was then tested in each subject R2 using root mean square error as the determining factor of success from previous Apollo data [207]. Further, the simple metabolic regression model was improved by adding in corresponding MK III suit independent thermal terms creating a multiple regression including LCG inlet temperature, LCG outlet temperature, delta LCG temperature, inlet suit gas temperature, outlet suit gas temperature, delta suit gas temperature, inlet suit humidity, outlet suit humidity, and finally delta suit humidity. Single variable and multivariable models were compared to determine the most linear fit for predicting metabolic rate.

As a continuation, a similar technique was used to determine a cardiothermal regression model to predict both core temperature and mean skin temperature during the subject R1 ARGOS simulations. First, a simple regression was built for both core temperature and mean skin temperature as the dependent variables, and independent terms of heart rate and metabolic rate were used. The regression model was then tested in each subject R2 utilizing root mean square error as the factor for success. The model for core temperature and mean skin temperature regressions were improved for multiple regressions using the same MK III suit terms of LCG temperature, suit gas temperature, and suit humidity. The simple and multiple regression models were compared to determine the most linear fit for predicting core temperature and mean skin

temperature. Further, the regression models were compared with outputs from a commonly used human thermal model METMAN.

HRV metrics were collected from the same techniques utilized in Chapter 3 using r-r intervals collected from the polar H-10 and computed using Kubios HRV 3.4.3 for further evaluation and artifact removal. Fast Fourier Transformation (FFT) was used with a 256 s window width and 50% overlap. Time-domain features of the standard deviation of normal-to-normal sinus beats (SDNN) and root mean square of successive difference (RMSSD) were compiled across R1 and R2 tasks for each suited operator. The low-frequency power (LFnu) and high-frequency power (HFnu) were calculated from the low-frequency band (0.04-0.14 Hz) and the HF band (0.15-0.4 Hz), respectively. The LF/HF ratio was determined from the corresponding values. Additionally, HRV workload status outputs were manually investigated to observe whether high HRV determined workloads corresponded to high metabolic workload and thermal strain (i.e., increased core temperature, modeled heat storage).

6.3.3 Human Thermal Modeling

Considerable work has been conducted by engineers and physiologists to develop and simulate extreme thermal environments through mathematical models. The limited availability and access to these thermal environments (e.g., suited EVA and spaceflight) necessitate the continual advancement of simulated human thermal regulation. Particularly with the increased movement for planetary exploration operations and long-duration spaceflight, human thermal regulation during these scenarios will be close to impossible to conduct human-based analog testing. Therefore, human thermal models such as METMAN (Metabolic Man), Wissler Model, TAITherm, and Fiala allow simulated physiologic responses to develop equipment requirements to encapsulate extreme contingency scenarios [46], [228]–[232].

Particularly, METMAN and Wissler models incorporate environmental thermal parameters associated with suited thermal dynamics. Used in this study is the 41-node transient metabolic man (METMAN). The model separates the body into ten segments consisting of a head, arms, legs, hands, feet, and torso. Each segment is further separated into four corresponding inner compartments or nodes consisting of skin, fat, muscle, and core (Figure 6.7 A). The last node corresponds to a central blood node. Each compartment is described by mathematical representations of heat transfer between each node with the central blood node representing heat convection through the body segments (Figure 6.7 B).

In this study subject suited MK III thermal data was input into the METMAN model, including LCG inlet temperature, in suit gas temperature, in suit gas humidity, external ARGOS

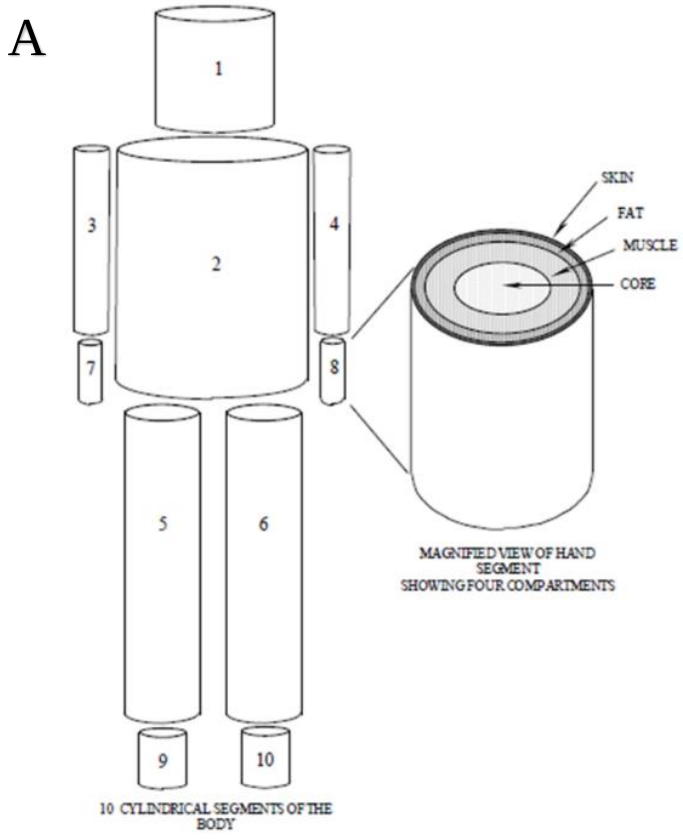

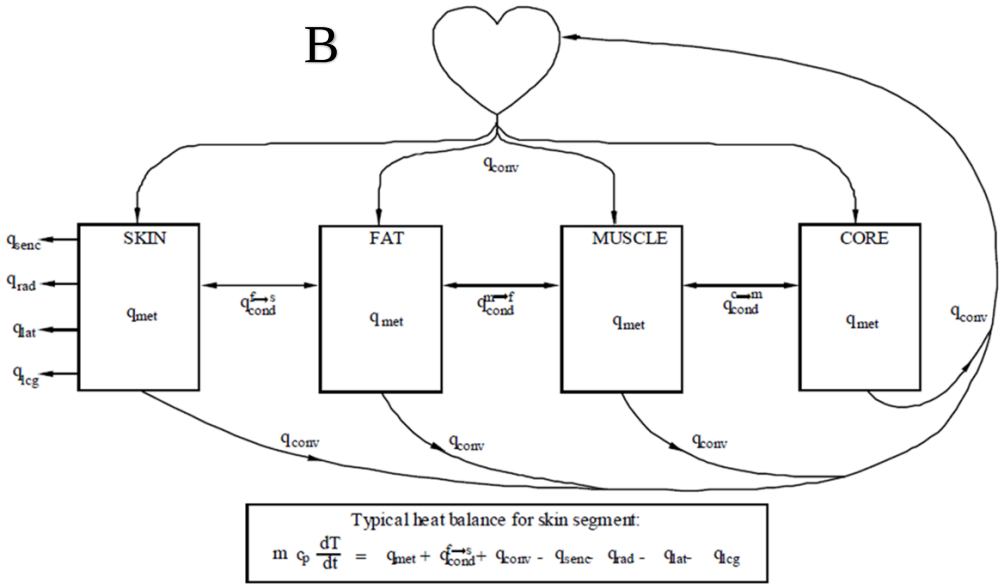

Figure 6.7: Adapted from Bue et al., 41-Node METMAN represented as 10 segments separating head, arms, legs, hands feet, and torso further separated into skin, fat, muscle, core (A). Heat balance relation showing heat transfer between segment nodes of skin, fat, muscle, and core including convective heat transfer due to blood flow (B).

ambient air temperature and humidity. The inputs are used in the model to build the simulated mathematical representations of the suited environment. Outputs of the model include heat transfer metrics of the suit, such as LCG heat transfer, suit heat transfer, evaporative, respiration, and diffusion heat transfer values. Further, heat storage rate, heat storage total, core temperature, mean skin temperature, heat transfer due to shivering, sweat run-off rates, latent heat, and evaporative heat transfer are outputs that are used in correlation with collected ARGOS thermal data.

6.4 Results

Metabolic rate predicted from heart rate provided minute by minute evaluation of energy expenditure during simulated EVA. The predicted metabolic rate during the ARGOS simulated lunar EVA was less than the 200 BTU/hr RMSE threshold corresponding to the accuracy of the model technique from Chapter 5 and values determined during Apollo Lunar EVA. The accuracy of the metabolic linear model was improved lowering the RMSE values < 132 BTU/hr and increasing linearity R^2 (> 0.72). This was done by increasing the input of independent terms

through multiple regressions including MK III suit thermal data not previously collected during simulated training. The suited operator values core temperature, heart rate, and metabolic rate for each ARGOS simulation can be shown in Table 6.1. Values for core temperature, heart rate, and metabolic rates are less during R1 as higher metabolic tasks were planned in R2. Similarly, MK III suited thermal environment values can be found in Table 6.2 for the subsequent ARGOS simulations.

Table 6. 1: Suited Operator Thermal and Cardiovascular Outputs

Operator	Mean Skin Temp (°C)	Core Temp (°C)	Heart Rate (bpm)	Metabolic Rate (BTU/hr)
S1 R1	28.1 ± 1.19	36.7 ± 0.6	56 ± 8	597.4 ± 156.7
S1 R2	27.2 ± 0.69	37.4 ± 0.5	84 ± 17	883.9 ± 364.0
S2 R1	28.5 ± 0.55	37.4 ± 0.3	138 ± 18	859.3 ± 239.5
S2 R2	29.4 ± 1.83	37.6 ± 0.3	143 ± 19	923.46 ± 305.2

Table 6.2: MK III Thermal Environment Outputs

Operator	LCG Inlet Temp (°C)	LCG Outlet Temp (°C)	Suit Inlet Temp (°C)	Suit Outlet Temp (°C)	Suit Inlet Humidity (%)	Suit Outlet Humidity (%)
S1 R1	-	16.8 ± 2.20	23.0 ± 0.62	23.1 ± 0.25	22.5 ± 13.05	21.3 ± 4.48
S1 R2	14.8 ± 0.92	16.9 ± 0.90	22.1 ± 0.30	22.7 ± 0.19	11.1 ± 4.70	24.1 ± 10.50
S2 R1	14.5 ± 0.06	16.4 ± 0.21	22.2 ± 0.20	22.5 ± 0.12	22.7 ± 7.98	28.1 ± 6.52
S2 R2	15.2 ± 1.30	17.2 ± 1.15	22.2 ± 1.18	22.7 ± 0.27	9.9 ± 2.34	28.6 ± 9.65

Significant regression equations were found to predict metabolic rate first with the similar techniques identified in Chapter 5 (Table 6.3). Relationships between metabolic rate from heart rate showed linear trends during R1 with regression responses less than 200 BTU/hr shown in (Figure 6.8A & B). Subsequent significant multiple regressions were found to improve the predictive characteristics of the model. The highest accuracy for S1 consisted of heart rate, LCG, and suit outlet humidity (RH). LCG parameters for S1 had shown to be less likely to be correlated

with metabolic rates, while heart rate and outlet humidity showed increased correlations. The model with the highest accuracy found for S2, allowed inputs of heart rate, LCG inlet temperature, delta LCG temperature, and suit outlet RH (Table 6.3). In comparison to S1, S2 LCG components showed higher correlations to metabolic rates in the regression model. As a corollary, predicted metabolic rate signals for both S1 and S2 ARGOS simulation during R2 using the multiple regressions showed improved response accuracy, RMSE 175.37 BTU/hr, and 177.16 BTU/hr, respectively (Figure 6.9A & B).

Table 6.3: Metabolic Rate Regression Model Predictors and Coefficients

PREDICTOR	TEST	COEFFICIENTS	SE	numDf	denDf	T-STAT	PVALUE
S1							
HR^2	Intercept	344.0590	5056	1	10042	67.931	<0.0001
	Slope	0.0756	0.002			44.791	
HR^2+LCG	Intercept	335.9230	10.876	2	10042	30.887	<0.0001
	X1	0.0761	0.002			42.317	<0.0001
	X2	0.3932	0.465			0.845	0.398
HR^2+LCG+RH	Intercept	284.4705	11.466	3	10042	24.809	<0.0001
	X1	0.0748	0.002			41.874	<0.0001
	X2	0.0888	0.462			0.192	0.847
	X3	2.8352	0.215			13.199	<0.0001
S2							
HR^2	Intercept	42.3454	6.674	1	7147	6.344	<0.0001
	Slope	0.0415	< 0.001			128.585	
HR^2+LCG	Intercept	12270	511.797	2	7147	23.971	<0.0001
	X1	0.0452	< 0.001			130.250	
	X2	-849.3019	35.550			-23.891	
HR^2+LCG+ΔLCG	Intecept	18490	674.452	3	7147	27.417	<0.0001
	X1	0.0455	< 0.001			132.652	
	X2	-1215.8689	43.863			-27.720	
	X3	-526.7327	37.837			-13.921	
HR+LCG+ΔLCG+RH	Intercept	16440	755.483	4	7147	21.766	<0.0001
	X1	0.0452	< 0.001			130.706	
	X2	-1070.2644	50.115			-21.356	
	X3	-475.4377	38.715			-12.281	
	X4	-6.2176	1.043			-5.960	

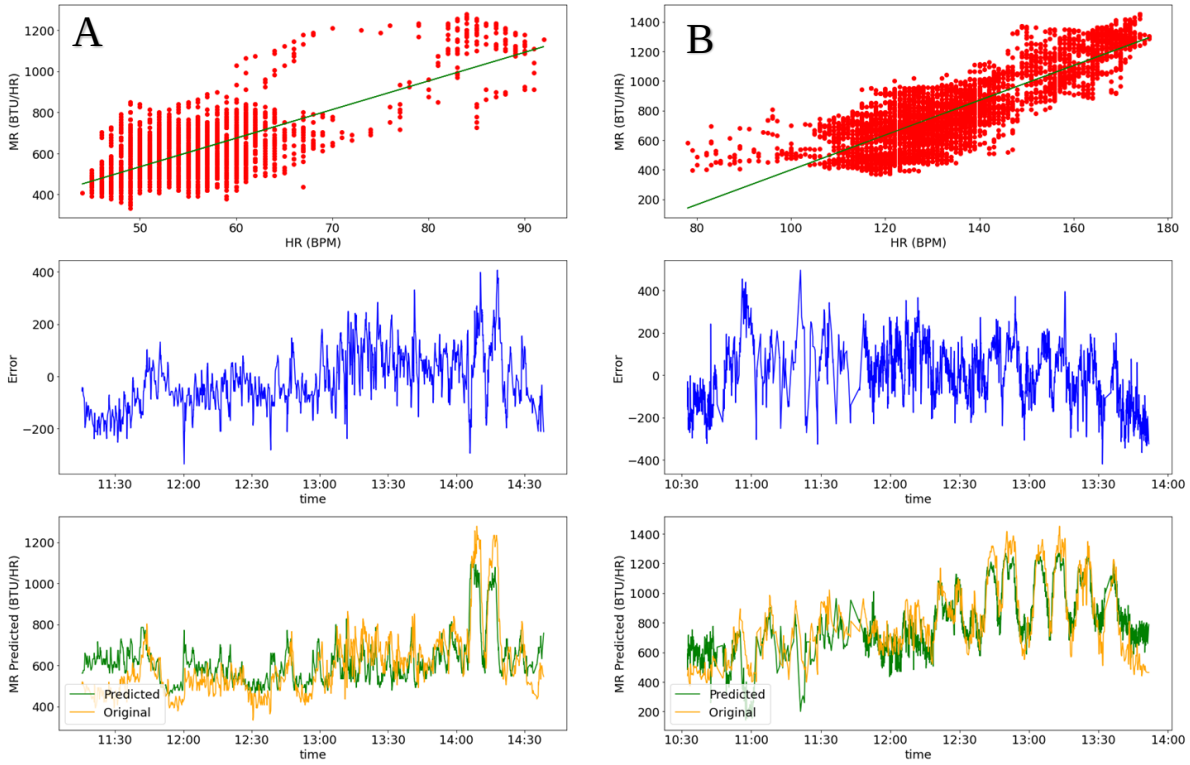

Figure 6.8: Predicted regression responses of the first run for both suited operators. Suited operator one R1 metabolic rate regression built from only heart rate inputs column (A). Suited operator two R1 metabolic regression built from only heart rate inputs column (B). Both responses yield RMSE < 150 BTU/hr.

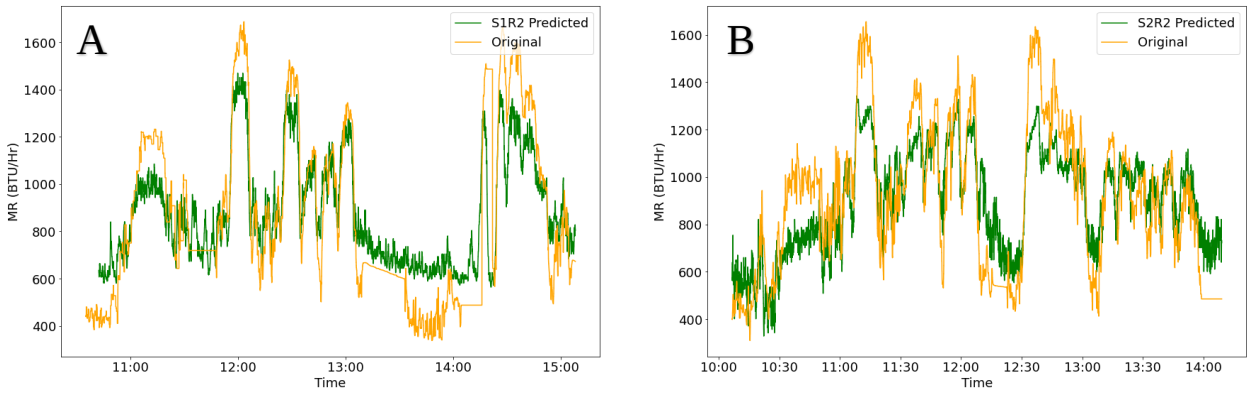

Figure 6.9: ARGOS R2 lunar EVA simulations predicted metabolic rate outputs from regression model for both suit operator S1 (A) and suit operator S2 (B) ARGOS R2 simulations. Both RMSE < 200 BTU/hr.

Predicting core temperature and mean skin temperature was found utilizing the same linear regression observations that were used to determine metabolic rate. It was found that for simple single linear regressions, a significant regression equation was found for both heart rate and metabolic rate as the independent predictors for core temperature and mean skin temperature

(Table 6.4, Table 6.5). Additionally, the metric developed in chapter 5 of MR/HR as a BTU/beat showed correlations through a significant regression equation with core temperature. Additionally, delta LCG temperature and suit outlet RH also showed significant regression equations in predicting core temperature. However, LCG inlet temperature alone did not have a high correlation in the predictions of core temperature regressions. While these regression equations were significant, the accuracy and linearity of the model were lower for the single input models. The core temperature and mean skin temperature linear models were improved by adding multiple regression terms using the highest correlated single terms such as MK III thermal suited metrics of delta LCG inlet temperature, suit gas outlet RH values, metabolic rate, and MR/HR values (Table 6.4, Table 6.5). For S1 the core temperature model with the most accuracy consisted of the terms metabolic rate (MR), MR/HR and outlet RH, RMSE 0.46 C. While for S2 the most accuracy was attained using MR, MR/HR, Δ LCG, and suit outlet RH, RMSE 0.12 C. In comparison, the thermal model METMAN outputs of core temperature showed similar correlations to the regression models. The METMAN output of core temperature for S1 R2 resulted in higher accuracy with RMSE 0.29 C (Figure 6.10 A, Figure 6.11 A). While the S2 core temperature regression model outperformed the METMAN output, RMSE 0.12 and 0.23 C respectively (Table 6.6). Conversely to core temperature, mean skin temperature had shown more reactive responses to changes in LCG while lowest responses were attributed to HR, MR, and RH values. The highest mean skin temperature regression consisted of values of MR/HR and LCG inlet for S1 RMSE 0.67 C and MR/HR, LCG and Δ LCG for S2, RMSE 0.74 C. The regression model for mean skin temperature outperformed the METMAN predicted mean skin temperature (Table 6.6). Values in comparison for mean skin temperature were S1 (0.67 C) and S2 (0.74 C) compared to METMAN mean skin temp RMSE 1.02 C and 1.12 C, respectively (Figure 6.10 B, Figure 6.11 B).

Table 6. 4: Core Temp Regression Model Predictors and Coefficients

PREDICTOR	TEST	COEFFICIENTS	SE	numDf	denDf	T-Stat	PVALUE
S1							
HR	Intercept	37.3254	0.245	1	210	152.239	< 0.0001
	Slope	-0.0110	0.005			-2.397	0.017
MR	Intercept	37.6897	0.112	1	210	335.885	< 0.0001
	Slope	-0.0016	< 0.001			-8.590	
MR/HR	Intercept	37.6799	0.125	1	210	302.553	<0.0001
	Slope	-0.0858	0.011			-7.643	
LCG	Intercept	36.5797	0.174	1	210	210.144	< 0.0001
	Slope	0.0093	0.010			0.929	0.354
Suit Outlet RH	Intercept	36.4892	0.097	1	210	377.635	< 0.0001
	Slope	0.0116	0.004			2.669	0.008
MR+MR/HR+RH	Intercept	37.4842	0.143	3	210	262.291	< 0.0001
	X1	-0.0013	< 0.001			-3.515	
	X2	-0.0223	0.021			-1.052	
	X3	0.0118	0.004			3.159	
S2							
HR	Intercept	36.7886	0.122	1	303	301.553	< 0.0001
	Slope	0.0042	0.001			4.715	
MR	Intercept	37.3873	0.062	1	303	600.442	< 0.0001
	Slope	-0.00003	<0.001			-0.472	0.637
MR/HR	Intercept	37.7094	0.085	1	303	445.873	<0.0001
	Slope	-0.0572	0.014			-4.221	
LCG	Intercept	2.6477	3.767	1	303	0.703	0.483
	Slope	2.3900	0.259			9.214	< 0.0001
Δ LCG	Intercept	34.9333	0.106	1	303	330.843	< 0.0001
	Slope	1.2986	0.056			23.074	
Suit Outlet RH	Intercept	36.1141	0.060	1	303	605.313	< 0.0001
	Slope	0.0489	0.002			21.192	
MR+MR/HR+ΔLCG	Intercept	34.8380	0.107	3	303	324.745	< 0.0001
	X1	0.0042	0.001			4.865	
	X2	-0.0004	< 0.001			-6.751	
	X3	1.2352	0.057			21.592	
MR+MR/HR+ +ΔLCG+RH	Intercept	35.1998	0.103	4	303	340.818	< 0.0001
	X1	0.0001	< 0.001			1.874	0.062
	X2	-0.0396	0.014			-2.840	< 0.0001
	X3	0.8563	0.056			15.163	< 0.0001
	X4	0.0272	0.002			12.095	< 0.0001

Table 6.5: Mean Skin Temperature Regression Model Predictors and Coefficients

PREDICTOR	TEST	COEFFICIENTS	SE	num Df	den Df	T-Stat	PVALUE
S1							
HR	Intercept	27.8335	0.577	1	151	48.219	< 0.0001
	Slope	0.0122	0.010			1.210	0.228
MR	Intercept	28.0063	0.345	1	151	81.281	< 0.0001
	Slope	0.0008	0.001			1.554	0.122
MR/HR	Intercept	27.7478	0.525	1	151	52.898	< 0.0001
	Slope	0.0698	0.047			1.501	0.136
LCG	Intercept	22.7698	0.506	1	151	44.987	< 0.0001
	Slope	0.3329	0.029			11.464	
Suit Outlet RH	Intercept	28.3995	0.398	1	151	71.406	< 0.0001
	Slope	0.0058	0.018			0.320	0.749
MR/HR+LCG	Intercept	20.6448	0.658	3	151	31.370	< 0.0001
	X1	0.1520	0.033			4.658	
	X2	0.3581	0.028			12.908	
S2							
HR	Intercept	26.9176	0.336	1	151	80.074	< 0.0001
	Slope	0.011	0.002			4.519	
MR	Intercept	28.1315	0.171	1	151	164.323	< 0.0001
	Slope	0.0003	< 0.001			1.773	0.078
MR/HR	Intercept	28.5896	0.240	1	151	119.305	< 0.0001
	Slope	-0.0273	0.039			-0.704	0.482
LCG	Intercept	-33.1389	10.169	1	151	-3.259	0.001
	Slope	4.2398	0.700			6.054	< 0.0001
Δ LCG	Intercept	23.2180	0.248	1	151	93.711	< 0.0001
	Slope	2.7874	0.132			21.105	
Suit Outlet RH	Intercept	26.5024	0.124	1	151	214.385	< 0.0001
	Slope	0.0685	0.004			15.964	
MR/HR+LCG+ ΔLCG	Intercept	25.1136	6.458	3	151	3.889	< 0.0001
	X1	-0.0552	0.019			-2.883	
	X2	-0.1134	0.456			-0.249	
	X3	2.8337	0.153			18.527	

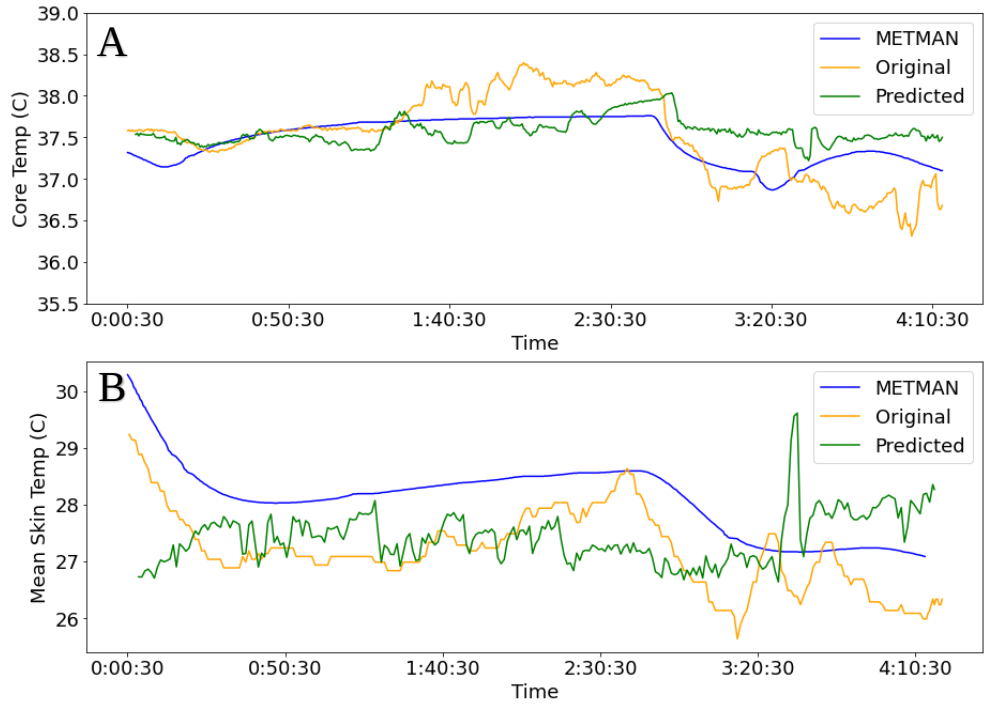

Figure 6.10: Core temperature and mean skin temperature predicted outputs compared to original measured values for S1 ARGOS EVA simulation R2. Core temperature predictions using the multiple regression model of physiologic inputs with suit thermal inputs showed prediction results similar to that of METMAN thermal outputs (A). Mean skin temperature prediction showed that the regression model performed at higher accuracy than METMAN simulated outputs (B).

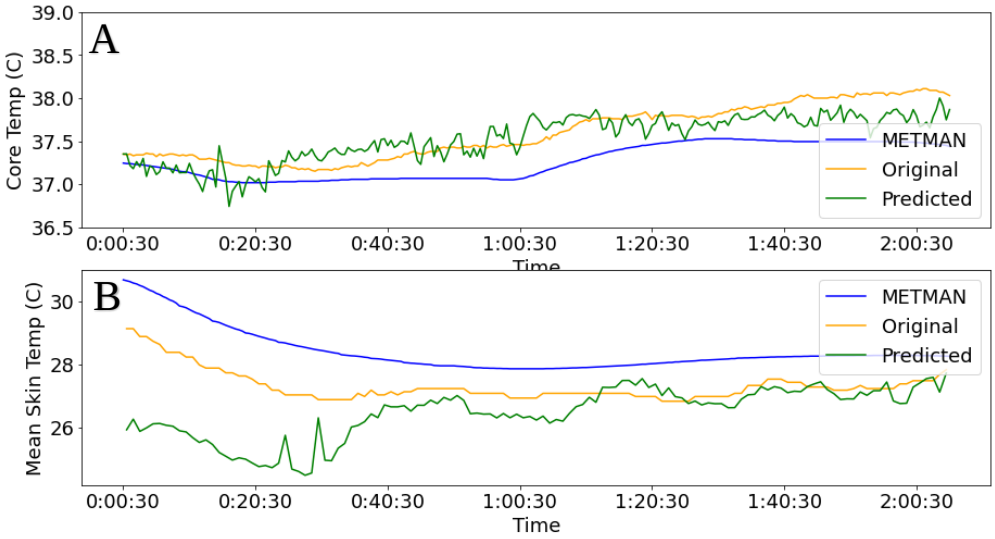

Figure 6. 11: Core temperature and mean skin temperature predicted outputs compared to original measured values for S2 ARGOS EVA simulation R2 first two hours. Core temperature predictions using the multiple regression model of physiologic inputs with suit thermal inputs showed to have better accuracy compared to results of METMAN thermal outputs (A). Mean skin temperature prediction showed that the regression model also performed at higher accuracy than METMAN simulated outputs (B).

Table 6.6: Thermal measured values compared to METMAN and cardiothermal regression predictions.

Operator	Core (°C)	METMAN Core (°C)	METMAN RMSE Core (C)	Regression Core (°C)	Core Temp RMSE (C)	Mean Skin Temp (°C)	METMAN Skin Temp (°C)	METMAN RMSE Skin (C)	Regression Skin Temp (°C)	Skin Temp RMSE (C)
S1 R2	37.5 ± 0.5	37.4 ± 0.3	0.29	37.6 ± 0.2	0.46	27.2 ± 0.7	28.4 ± 0.5	1.02	27.4 ± 0.4	0.67
S2 R2	37.6 ± 0.3	37.3 ± 0.2	0.23	37.5 ± 0.2	0.12	27.4 ± 0.5	29.3 ± 0.4	1.15	26.5 ± 0.7	0.74

HRV metrics were obtained utilizing the same techniques in Chapter 3. During increased metabolically demanding tasks LF values were shown to increase while HF values were shown to decrease for both S1 and S2 (Table 6.7 and Table 6.8). As a result, LF/HF values were shown to also increase due to metabolically demanding tasks. HF values showed more sensitivity during R2 tasks than LF values compared to R1 simulated EVAs.

Time-domain features of RMSSD and SDNN values were higher during tasks with higher metabolic rates and decreased with decreasing metabolic demand (Table 6.9, Table 6.10). This corresponds directly to increased maximum and minimum heart rates during increased metabolic loading. Non-linear metrics of SD1 showed to decrease with lowering metabolic demand while SD2 showed to increase with increased metabolic rates. The ratio of SD2/SD1 showed to increase with higher metabolic demanding tasks. DFA Alpha-2 had shown to increase with tasks requiring higher metabolic loads (Table 11, Table 12).

Table 6.7: Task-based metabolic rates and HRV frequency domain metrics of S1 and S2 R1 simulated EVA.

Task	Metabolic Rate (BTU/hr)		LF (n.u.)		HF (n.u.)		LF/HF	
	S1	S2	S1	S2	S1	S2	S1	S2
Suit Settings	478.54 ± 52.22	679.13 ± 159.36	42.13	56.90	57.86	43.04	0.73	1.32
Primus Movement	660.94 ± 79.55	752.84 ± 101.21	79.31	83.90	20.68	16.07	3.84	5.22
Object Relocation	904.33 ± 246.98	1093.22 ± 227.75	81.65	85.51	18.34	14.46	4.45	5.91
"Rest"	781.34 ± 244.10	539.69 ± 75.75	62.95	71.51	37.03	28.48	1.70	2.511

Table 6.8: Task-based metabolic rates and HRV frequency domain metrics of S1 and S2 R2 simulated EVA.

Task	Metabolic Rate (BTU/hr)		LF		HF		LF/HF	
	S1	S2	S1	S2	S1	S2	S1	S2
Up/Down Ladder	732.16 ± 64.92	601.83 ± 62.18	87.86	82.48	12.11	17.49	7.25	4.72
1.5 Km walk	1114.59 ± 130.70	931.72 ± 120.66	78.56	79.93	21.41	20.05	3.67	3.99
Geo 1	798.75 ± 120.93	872.31 ± 130.65	81.65	74.83	18.31	25.15	4.46	2.98
30% 500m	1328.01 ± 311.62	1413.37 ± 239.75	88.94	89.98	11.03	10.09	8.06	8.91
Geo 2	770.20 ± 126.23	879.53 ± 185.04	84.60	60.85	15.38	39.09	5.50	1.56
20% 500m	1203.18 ± 273.13	1201.40 ± 161.52	86.95	85.68	13.02	14.30	6.68	5.99
Obj Relocation	945.88 ± 176.45	1092.32 ± 216.04	71.71	80.47	28.22	19.50	2.54	4.13
10 % Grade 500m	1116.78 ± 183.01	1212.31 ± 183.95	77.28	78.70	22.70	21.24	3.40	3.71
“Rest”	629.63 ± 12.98	564.37 ± 48.09	70.18	72.18	29.76	27.80	2.36	2.60
2 Km walk back	1321.11 ± 271.57	1231.48 ± 242.08	89.92	82.75	10.06	17.19	8.94	4.81

Table 6.9: Task-based metabolic rates and HRV Time Domain metrics of S1 and S2 R1 simulated EVA.

Task	Metabolic Rate (BTU/hr)		Mean RR		Max HR		Min HR		RMSSD		SDNN	
	S1	S2	S1	S2	S1	S2	S1	S2	S1	S2	S1	S2
Suit Settings	478.54 ± 52.22	679.13 ± 159.36	1213.0	538.90	75	156	41	62	133.3	56.21	99.33	59.0
Primus Movement	660.94 ± 79.55	752.84 ± 101.21	1197.2	508.16	76	155	41	89	43.61	31.28	51.53	48.78
Object Relocation	904.33 ± 246.98	1093.22 ± 227.75	848.7	397.31	92	170	50	116	25.61	3.81	37.30	7.06
“Rest”	781.34 ± 244.10	539.69 ± 75.75	1085.7	430.82	67	169	48	83	31.06	14.39	30.09	20.22

Table 6.10: Task-based metabolic rates and HRV Time Domain metrics of S1 and S2 R2 simulated EVA.

Task	Metabolic Rate (BTU/hr)		Mean RR		Max HR		Min HR		RMSSD		SDNN	
	S1	S2	S1	S2	S1	S2	S1	S2	S1	S2	S1	S2
Up/Down Ladder	732.16 ± 64.92	601.83 ± 62.18	802.03	622.82	91	127	60	64	23.91	43.50	35.86	59.54
1.5 Km walk	1114.59 ± 130.70	931.72 ± 120.66	712.72	488.89	119	136	57	74	22.89	13.87	26.12	18.68
Geo 1	798.75 ± 120.93	872.31 ± 130.65	689.27	479.25	136	142	62	80	17.69	12.49	25.50	19.79
30% 500m	1328.01 ± 311.62	1413.37 ± 239.75	701.81	393.69	109	197	65	97	19.09	8.29	30.94	11.83
Geo 2	770.20 ± 126.23	879.53 ± 185.04	893.25	443.66	80	155	59	89	27.70	7.59	39.18	14.99
20% 500m	1203.18 ± 273.13	1201.40 ± 161.52	945.21	398.05	79	162	55	128	32.60	3.16	48.46	5.83
Object Relocation	945.88 ± 176.45	1092.32 ± 216.04	992.74	380.20	105	168	54	136	40.56	2.15	51.95	4.44
10 % Grade 500m	1116.78 ± 183.01	1212.31 ± 183.95	1002.95	391.66	78	172	52	95	30.66	7.93	38.86	12.03
“Rest”	629.63 ± 12.98	564.37 ± 48.09	778.91	534.92	115	130	50	74	32.76	29.59	31.22	47.31
2 Km walk back	1321.11 ± 271.57	1231.48 ± 242.08	682.66	394.99	113	171	62	82	15.27	6.60	26.13	11.00

Table 6.11: Task-based metabolic rates and HRV non-linear metrics of S1 and S2 R1 simulated EVA.

Task	Metabolic Rate (BTU/hr)		SD1		SD2		SD2/SD1		Alpha-1		Alpha-2	
	S1	S2	S1	S2	S1	S2	S1	S2	S1	S2	S1	S2
Suit Settings	478.54 ± 52.22	679.13 ± 159.36	94.85	40.02	140.8	138.80	1.48	3.47	0.91	1.12	0.96	0.86
Primus Movement	660.94 ± 79.55	752.84 ± 101.21	31.75	22.52	182.5	106.53	5.75	4.73	1.40	1.35	1.04	0.91
Object Relocation	904.33 ± 246.98	1093.22 ± 227.75	18.80	2.75	239.3	55.65	12.73	20.24	1.40	1.52	1.25	1.13
“Rest”	781.34 ± 244.10	539.69 ± 75.75	21.56	10.28	21.56	77.08	4.96	7.50	1.32	1.07	1.30	0.92

Table 6.12: Task-based metabolic rates and HRV non-linear metrics of S1 and S2 R2 simulated EVA.

Task	Metabolic Rate (BTU/hr)		SD1		SD2		SD2/SD1		Alpha-1		Alpha-2	
	S1	S2	S1	S2	S1	S2	S1	S2	S1	S2	S1	S2
Up/Down Ladder	732.16 ± 64.92	601.83 ± 62.18	17.31	31.14	115.77	131.95	6.69	4.24	1.47	1.34	1.11	0.89
1.5 Km walk	1114.59 ± 130.70	931.72 ± 120.66	16.44	8.97	217.38	52.23	13.22	5.82	1.41	1.43	1.24	0.88
Geo 1	798.75 ± 120.93	872.31 ± 130.65	12.85	9.91	140.46	47.22	10.93	4.76	1.62	1.49	1.27	1.04
30% 500m	1328.01 ± 311.62	1413.37 ± 239.75	13.76	5.99	155.24	54.67	11.28	9.13	1.57	1.51	1.13	0.98
Geo 2	770.20 ± 126.23	879.53 ± 185.04	19.93	5.47	79.21	49.28	3.97	9.00	1.45	1.68	0.92	1.07
20% 500m	1203.18 ± 273.13	1201.40 ± 161.52	23.49	2.28	90.85	28.24	3.87	12.34	1.51	1.63	0.76	1.31
Obj Relocation	945.88 ± 176.45	1092.32 ± 216.04	29.02	1.57	97.98	19.37	3.37	12.30	1.41	1.56	0.94	1.28
10 % Grade 500m	1116.78 ± 183.01	1212.31 ± 183.95	22.12	5.67	111.09	43.73	5.02	7.71	1.43	1.46	1.07	1.20
“Rest”	629.63 ± 12.98	564.37 ± 48.09	23.45	21.25	298.70	76.30	12.74	3.60	1.20	1.39	1.43	0.87
2 Km walk back	1321.11 ± 271.57	1231.48 ± 242.08	11.03	4.74	148.30	42.32	13.45	8.92	1.46	1.52	1.02	1.20

6.5 Discussion

The first objective of this chapter was to determine if the techniques developed in subsequent chapters could predict metabolic and workload rates. Metabolic rates and demand were predicted using a simple linear regression from heart rates for simulated Lunar EVA in the ARGOS. These simple linear regressions were comparable to RMSE error values determined during Apollo Lunar EVAs, the threshold being less than 200 BTU/hr. Utilizing the additional factors of thermal instrumentation on the MK III, the metabolic rate regression model accuracy was increased by adding more terms. These thermal suit parameters of inlet LCG temperature, outlet LCG temperature, suit inlet/outlet temperature as well as suit inlet/outlet humidity provided extra environmental factors that attribute to human thermal regulation and ultimately affect metabolic

energy expenditure. The final accuracy for suited operator predicted outputs decreased RMSE to < 180 BTU/hr while also capturing increased R^2 of greater than 0.72. During the S1 R1 simulated EVA the outlet LCG values were not captured due to technical error. As a result, the regression for S1 R2 did not include ΔLCG temperature which caused a slightly higher RMSE compared to the S1 R2 model.

As the general metabolic regression models increase in linearity with increased term inputs, there are still some pitfalls that occur with this technique. The model is only as good as the input values of metabolic rates and thermal parameters. Due to this fact, the regression model does lose resolution when attempting to predict high peak metabolic values greater than 1400 BTU/hr. In turn, the model also loses resolution when predicting absolute minimum values of < 400 BTU/hr (Figure 6.9A and B). However, the heart rate determinations of metabolic energy expenditure can provide an accurate prediction in a minute-by-minute real-time environment. This factor can be improved by incorporating individual crew responses of a range of metabolic activities with correlated cardiovascular function.

The second objective for this chapter was to build upon those techniques to determine thermal loading with the simulated lunar EVA environment. Simulations were completed using the METMAN model. The model provides a representation of the suited environment during EVA. Incorporated in this representation is the outer suit environment. In this situation, the outer suit environment consisted of the lab ambient metrics. Additionally, the added thermal sensor suite allowed for a higher accurate representation of the inner MK III suited environment during Lunar simulated EVA tasks. These higher accurate inputs allowed for better representation of suited operator thermal regulation and changes of metabolic activity. Corresponding outputs yielded simulated core temperature and mean skin temperature responses over time for various thermal

loading. The simulated predictions of core temperature had shown to have general correlations for accurate predictions, however, for S1 the METMAN outputs did not respond quickly to temperature inflections (Figure 6.10 A). However, simulated predictions of S2 provided a more stable response to core temperature (Figure 6.11 A). The variability in the core temperature inflections during the R2 simulated EVAs could be attributed to the physiologic efficiency of the cardiovascular response to activity loads. The mean heart rate for suited operator S1 was significantly lower than that of suited operator S2 during rest and high metabolic loading (Table 6.1). The responses of quick increases and decreases of core temperature could be due to the efficiency of S1 expelling heat to the periphery. In the METMAN simulations, the physiology of blood flow and cardiovascular changes is hard to set to a general orientation that may not capture the variation of subject variability and cardiovascular fitness.

As a comparison to METMAN and to provide a quicker minute-by-minute determination of thermal loading, a similar technique of linear regressions was built for core temperature regressions. These regressions were built using heart rates, metabolic rates, and suit thermal parameters. The predictions for S1 had shown to be comparable to the METMAN simulated core temperature and within 0.5 °C RMSE of original core temperature (Table 6.6). The thermal regression model for S1 had also shown a slight delay during quick decreases in core temperature (Figure 6.9 A). This factor for the regression model could be attributed to the use of only inlet LCG instead of the ΔLCG due to the S1 R1, attributed to a technical error, to which the regression was built. Additionally, it was noted that during the S1 R1 simulated EVA the suit operator turned off the flow to the LCG at various times. However, from this regression model, it was determined that the metric of MR/HR developed in Chapter 5 provided a good linear response incorporating both heart rate and metabolic rate components. This attributed to an added metric for multiple

regression terms and could provide a conversion factor if heart rate or metabolic rate instrumentation fails.

The thermal responses for S2 R2 were separated into two segments. This was due to a built-in break for the suited operator that had affected the core temperature values during this duration. For both segments, the METMAN model predicted the total core temperature accurately with an RMSE output of 0.23 °C. As mentioned earlier, the S2 suited operator had high heart rates that could be attributed to higher metabolic demand and less thermal efficiency. The core temperature in general for the S2 R2 run did not have drastic inflection points but rather stayed constant in subtle slope changes at high core temperature values. During the S2 R2 regression predictions the core temperature had outperformed the METMAN modeling outputs. The regression for core temperature had term inputs for ΔLCG which added to that accuracy leading to a 0.12 °C RMSE. It was also noted that during the S2 R1 simulated EVA the suited operator did not turn off the LCG allowing for more consistent cooling and fewer inflections in the built regression model.

In addition to core temperature outputs, the mean skin temperature was predicted using both the METMAN model and the regression techniques. The mean skin temperature regression model outperformed the METMAN model attributed to mean skin temperature. The METMAN model lagged the starting signal of mean skin temperature compared to both the original signal and the regression model. It could be attributed to heat transfer lags and heat storage thresholds within the model. The RMSE for both S1 and S2 predictions had shown to be relatively high with greater than 1 °C RMSE. The regression model showed slightly more accurate results during S1 predictions versus S2 predictions. This could be attributed to S1 turning off LCG flow at various times throughout the R1 simulated EVA whereas S2 did not turn off LCG flow. The temperature

values would result in a higher range of mean skin temperatures in the regression for S1, leading to more accurate predictions during the R2 simulated EVA.

A basis for heat generation within the body has a dependency on workload and energy expenditure. As workload was shown to increase for the EVA task metabolic rates, in turn, increased as a result for both suit operators during both ARGOS simulations. As a correlated response cardiovascular metrics shown through also shifted with increasing and decreasing metabolic demand. It was found through the same techniques used in Chapter 3, HRV metrics could be used to view cardiovascular responses to increased energy expenditure. The main metrics in a flight environment that determined stress responses were that of frequency-domain metrics LF, HF, and LF/HF. In this study as metabolic demand increased LF/HF values also increased, suggesting sympathetic dominance. As a corollary, it was also seen that LF values increased while HF values decreased, also solidifying the observation of sympathetic response to increased energy expenditure and resultant increased workload. Further, short-term metrics of RMSSD and SDNN had shown to decrease with increased metabolic activity corresponding to increases in maximum and minimum heart rates as well as mean RR intervals.

Additionally, non-linear metrics corresponding to Poincare plot designators SD1 and SD2 show to have inverse shifts depicting interrelation of short-term and long-term autonomic responses to changing workloads. SD1 decreased more drastically with increased metabolic demand suggesting that with higher metabolic costing tasks short-term stress responses of the sympathetic nervous system increase. This is further seen when SD2 increases at those high metabolic tasks. Continually, the Alpha-1 term for detrended fluctuation analysis shows decreased values of signal complexity at low metabolic loads while increasing complexity for high metabolic demand. This further points to the short-term stress responses of sympathetic dominance for an

increased workload. However, the Alpha-2 term also does show decreased values at low workloads with slightly higher values for high metabolic tasks suggesting a connection to long-term stress responses. These HRV values show similar stress responses in those seen in Chapter 3 with increased stress responses attributed to short-term HRV metrics. Pointing to the use of HRV to determine metabolic increased workload and increased stress responses on task.

6.6 Conclusions

In this chapter, techniques were validated and further utilized to predict energy expenditure and thermal loading during simulated Lunar EVA in the MK III space suit. A thermal sensor suite was developed to gather suit operator core temperature and mean skin temperature while also gathering suit thermal data of liquid cooling garment temperature, suit temperature, and suit humidity changes. The thermal data in tandem with cardiovascular metrics and metabolic rates were used to develop linear regression models to predict thermal loading. Techniques of metabolic prediction using heart rates were used from Chapter 5 to build upon improved prediction models for suited training. These same techniques were used to develop a cardiothermal regression model to predict the core temperature and mean skin temperature of the suit operator during training scenarios. The regression models were comparable to outputs from a popular human thermal regulation model METMAN and at times outperformed predictions of mean skin temperature. Additionally, HRV metrics identified from Chapter 3 were used to further define high metabolic demanding tasks corresponding to increased sympathetic dominance and short-term stress responses. Ultimately, these techniques can further space suit development by adding elements of predictive human performance for improved training scenarios during simulated gravity EVA.

PART IV: CONCLUSION

Chapter 7. RESEARCH SUMMARY, CONTRIBUTIONS, AND FUTURE RECOMMENDATIONS

7.1 Conclusions

Aerospace environments are physically and mentally demanding on in-flight crews. Commercial and high-altitude pilots, as well as astronauts during spaceflight, experience an increasing variety of task workloads. Pilots during these workloads can become fatigued, leading to human error, which is the main factor in airline accidents. Similarly, astronaut spacewalk, or extravehicular activity (EVA), workloads can cause fatigue but also overexertion, which could lead to overheating and other serious injuries. Post-flight analysis of early Gemini missions showed astronauts were overheated due to metabolic demand during EVA tasks. With increases in availability in space and the rise of space tourism, human factors has new domains that are relatively not researched in literature. In tandem with the increased commercial drive for increased travel and space-based flights, further space agencies such as NASA have plans to return Astronauts to the Lunar surface and eventually to Mars. These long-duration missions will require autonomy and developed methods to assess stress responses and task workloads objectively. Furthermore, the range of these aerospace environments can provide insight into physiology responses for workloads and heat strain on Earth. Heat is the leading cause of injury or death during weather-related events. As temperatures continue to climb in recent years and the potential for increasingly strong weather events, heat strain on the body remains dangerous for most vulnerable populations. This thesis has been structured to address the issues discussed above through a combined common technique of utilizing cardiovascular responses of heart rate and heart rate variability. The following sections outline the major conclusions of this thesis.

7.1.1 Pilot In-flight Workload Stress Responses

Pilot fatigue and workload stress have continually plagued commercial aviation. Developing objective measures to identify early warning signs of fatigue, workload stress, and drowsiness is a key factor in addressing this issue. However, within a flight environment, the ability to utilize instrumentation to measure psychophysiological responses to workload is limited by space. This thesis utilizes simple ECG-led placement to extract features of heart rate variability during in-flight tasks. Our studies suggest strong evidence of sympathetic nervous system dominance and classification stress responses to task demand identified through short-term HRV features in the frequency domain, time domain, and non-linear metrics. This type of analysis can be utilized in simple instrumentation capable of utility in-flight configurations.

7.1.2 Simulated microgravity cardiovascular

The human body is subjected to a plethora of deconditioning events attributed to spaceflight microgravity. Of those most affected is that of cardiovascular regulation. During spaceflight, the phenomenon of fluid shifts attributes to blood pressure and vascular remodeling. Availability of spaceflight is limited, leading to the development of microgravity simulations and analogs. Head down tilt bedrest at -6° head down tilt is the most accurate in simulating the effects of fluid shifts during prolonged bed rest. This thesis aimed at identifying cardiovascular vasoactivity due to fluid shift responses utilizing mechanical vibrations generated by the heart measured via seismocardiography. Further, it was found significantly deviated values of pulse transit times during prolonged bedrest suggesting vascular responses and dilatory effects similarly seen during spaceflight. Attributed mechanical peak morphology decreases due to fluid shifts and the presence of changing vascular mechanics of increased pulse transit time point to head down tilt bed rest as an accurate analog to spaceflight microgravity physiologic responses. Though, the attributed fluid

shifts could further change human thermal regulation. Our studies had also shown convincing evidence of seasonal effects on cardiovascular timing intervals suggesting thermal responses to vasoactivity. Continually, these thermal responses can further affect spaceflight human thermal regulation and energy expenditure as a result and warrant additional investigations.

7.1.3 EVA Task Energy Expenditure and Thermal Strain

During spaceflight missions, crew members will be required to perform extravehicular activities. These EVA operations are extensive, lasting in most cases greater than five hours within a spacesuit with limited consumables. Energy expenditure is a key element that provides objective measures of crew member physiologic state, aids in assessing workload, and provides a measurement of consumables (i.e., Oxygen) throughout the EVA. During early EVA operations, specifically during Gemini missions, it was determined that the astronauts were overexerting themselves and ultimately becoming overheated. Subsequent EVA operations allowed for real-time determination of metabolic rates as a factor in determining workloads. However, these metabolic rate determinations are only in a microgravity environment of low Earth orbit. Only 12 Astronauts have walked on the Lunar surface providing only a limited amount of data on workload and metabolic cost during Lunar EVA. This thesis aimed at providing objective measures for regression determinations of energy expenditure during simulated Lunar EVA in the MK III utilizing heart rates and suited thermal parameters. Additionally, our studies had found that metabolic rates could be predicted from simple linear regressions using heart rates from historic EVA data. Furthermore, this thesis found that core temperature, mean skin temperature, and metabolic rates could be predicted accurately using heart rates, liquid cooling garment temperature, and suit humidity. To further address the classification of developed techniques from subsequent chapters Lunar EVA tasks were investigated, showing increased stress responses

during increasingly metabolically demanding tasks identified by short-term cardiovascular measures of HRV metrics. This type of analysis suggests cardiovascular predictors for thermal loading within a spacesuit environment. Allowing also for the accurate predictions of metabolic loads of training scenarios within simulated EVA environments.

7.2 Future Directions

7.2.1 Extension of Pilot and EVA Stress Response Predictions Utilizing Short-term HRV Metrics

While this thesis identifies metrics of short-term HRV that are associated with increased stress responses corresponding to increasing task workload, there is continued work in improving a predictive model. Within Chapter 3 and the study of pilot stress responses, the population being studied was collegiate aviation students. The dataset could be improved by including more demographics of pilots, including sex, pilot flight hours, and age. Particularly having future studies that incorporate novice pilots to expert commercial pilots would give an accurate window to stress responses due to experience. Additionally, the thermal observations seen in Chapter 7, including an ability to measure localized skin temperature, could provide a metric for inflections of stress responses. Furthermore, within Chapter 7, the same HRV metrics identified for pilot task loads were utilized to identify high metabolically demanding tasks. The shifts in short-term HRV values corresponded to those inflections of metabolic rates providing a representation of cardiovascular and exergy expenditure in a suited environment. However, as this was study utilized simulated Lunar EVA in the ARGOS, incorporating more suited environments should be a focus in future studies (e.g., NBL, Habitat Analogs, and EVA). Additionally, the sample size for this included suit operators with experience in the MK III suit it would prove beneficial to also study novice and expert suit operators. The thermal sensor suite developed in Chapter 7 provides a plate form for

improving these correlations in simulated EVA and could continue to be improved through increasing the number of suited simulations of EVA tasks.

Continually, the HRV and cardiovascular observations were seen as part of instrumentation that could fit within a pilot headset. The next course of studies needs to focus on incorporating these applications in compact and modular instrumentation for a flight environment. Utilizing the categorization of stress-inducing tasks tied to frequency-domain, time-domain, and non-linear metrics would enable further development of the predictive model through machine learning techniques. The levels of HRV metrics shift in response to threshold values that are in comparison to expert determined task workloads. Using those thresholds, a model should be investigated to allow for real-time determinations of stress indicators that could incorporate into the instrumentation during flight.

7.2.2 Evaluating Thermal Regulation Models to Simulated Microgravity and Fluid Shifts Associated to Head-Down Tilt Bedrest

In Chapter 4 it was observed that variations of cardiovascular timing intervals occurred, particularly pulse transit time, between head-down tilt bed rest campaigns. Through further investigations of blood plasma volume and small subject variability, there was little variation between subjects of these metrics. It then was hypothesized that these observed variations of cardiovascular timing intervals could potentially occur due to seasonal effects. The first campaign occurred during January, while the second campaign was conducted during September. The study that was conducted was not designed to investigate seasonal effects and it is recommended that future head-down tilt bedrest studies take seasonal effects and thermal regulation into account. Further, a follow-up study to the prolonged head-down tilt bed rest should be investigated to incorporate investigations of blood flow, core temperature, and skin temperatures. A great effort

has been conducted from previous research groups to accurately represent human thermal regulation through mathematical simulations. However, these mathematical representations of human thermal models were built using terrestrial 1G Earth environments. By including blood flow measurements and thermal metrics of core temperature with corresponding skin temperatures during head-down tilt bed rest, a higher accurate representation of vascular mechanics during fluid shifts. These fluid shift responses could be used to improve blood flow weights within thermal models aiding in human thermal convection. Higher accurate models from this type of study would provide increased quality to provide spaceflight human thermal design requirements.

7.2.3 Expanding Regression Models to Further Increase Accuracy of Energy Expenditure and Human Thermal Predictions Within a Suited Environment

This thesis found as an objective to determine energy expenditure and human thermal metrics from relations with cardiovascular responses to workload, particularly utilizing heart rates in regression models to predict metabolic rate outputs. The outcome of the study in Chapter 5 developed techniques to predict metabolic rates in a suited environment during historic EVA operations using measured heart rates. This model could be further improved by incorporating suit thermal metrics such as liquid cooing temperature and suit temperature/humidity as regression terms. These were identified to improve the model during simulated EVA in Chapter 7. Additionally, the data collection sampling rate for suited EVA operations is relatively low (e.g., heart rate every 20 seconds and metabolic rates every 2 minutes). By including more regression terms, it can improve the accuracy of predictions for future uses during microgravity and Lunar EVA. During simulated EVA training environments, the collection sampling rate is higher and allows for more instrumentation to be incorporated with the suit. However, creating relations such as these regression models can allow for simplified instrumentation to be closer to flight

environments. In future correlations, the regression models should be tested on suit testing that investigates more suited operators of different sex, age, and experience in the suit. Also, the regression models should be tested in different suited environments such as, during NBL training and Habitat Analogs.

REFERENCES

[1] H. Kharoufah, J. Murray, G. Baxter, and G. Wild, "A review of human factors causations in commercial air transport accidents and incidents: From to 2000–2016," *Progress in Aerospace Sciences*, vol. 99, pp. 1–13, May 2018, doi: 10.1016/j.paerosci.2018.03.002.

[2] D. A. Wiegmann and S. A. Shappell, "A human error analysis of commercial aviation accidents using the Human Factors Analysis and Classification System (HFACS)." American Psychological Association, 2001. doi: 10.1037/e420582004-001.

[3] R. M. Petrilli, G. D. Roach, D. Dawson, and N. Lamond, "The Sleep, Subjective Fatigue, and Sustained Attention of Commercial Airline Pilots during an International Pattern," *Chronobiology International*, vol. 23, no. 6, pp. 1357–1362, Jan. 2006, doi: 10.1080/07420520601085925.

[4] H. Paul, "Energy Expenditure During Extravehicular Activity Through Apollo," in *42nd International Conference on Environmental Systems*, American Institute of Aeronautics and Astronautics. doi: 10.2514/6.2012-3504.

[5] G. F. Kelly and D. O. Coons, "Medical Aspects of Gemini Extravehicular Activities," *Aerospace Medicine*, vol. 39, no. 6, pp. 611–615, 1968.

[6] R. S. Johnston and L. F. Dietlein, *Biomedical Results from Skylab*. Scientific and Technical Information Office, National Aeronautics and Space Administration, 1977.

[7] A. Vaidyanathan, J. Malilay, P. Schramm, and S. Saha, "Heat-Related Deaths — United States, 2004–2018," *MMWR Morb Mortal Wkly Rep*, vol. 69, no. 24, pp. 729–734, Jun. 2020, doi: 10.15585/mmwr.mm6924a1.

[8] H. T. Hammel and J. B. Pierce, "Regulation of Internal Body Temperature," *Annual Review of Physiology*, vol. 30, no. 1, pp. 641–710, 1968, doi: 10.1146/annurev.ph.30.030168.003233.

[9] K. R. Diller, "Heat Transfer in Health and Healing1," *J Heat Transfer*, vol. 137, no. 10, pp. 1030011–10300112, Oct. 2015, doi: 10.1115/1.4030424.

[10] N. Charkoudian, "Skin Blood Flow in Adult Human Thermoregulation: How It Works, When It Does Not, and Why," *Mayo Clinic Proceedings*, vol. 78, no. 5, pp. 603–612, May 2003, doi: 10.4065/78.5.603.

[11] J. González-Alonso, "Human thermoregulation and the cardiovascular system," *Experimental Physiology*, vol. 97, no. 3, pp. 340–346, 2012, doi: 10.1113/expphysiol.2011.058701.

[12] F. Shaffer and J. P. Ginsberg, "An Overview of Heart Rate Variability Metrics and Norms," *Front. Public Health*, vol. 5, 2017, doi: 10.3389/fpubh.2017.00258.

[13] A. K. Verma *et al.*, "Comparison of Autonomic Control of Blood Pressure During Standing and Artificial Gravity Induced via Short-Arm Human Centrifuge," *Front. Physiol.*, vol. 9, 2018, doi: 10.3389/fphys.2018.00712.

[14] A. P. Blaber, H. Hinghofer-Szalkay, and N. Goswami, "Blood Volume Redistribution During Hypovolemia," *Aviation, Space, and Environmental Medicine*, vol. 84, no. 1, pp. 59–64, Jan. 2013, doi: 10.3357/ASEM.3424.2013.

[15] R. M. Baevsky *et al.*, "Autonomic cardiovascular and respiratory control during prolonged spaceflights aboard the International Space Station," *Journal of Applied Physiology*, vol. 103, no. 1, pp. 156–161, Jul. 2007, doi: 10.1152/japplphysiol.00137.2007.

[16] R. L. Hughson *et al.*, "Increased postflight carotid artery stiffness and inflight insulin resistance resulting from 6-mo spaceflight in male and female astronauts," *American Journal of Physiology-Heart and Circulatory Physiology*, vol. 310, no. 5, pp. H628–H638, Jan. 2016, doi: 10.1152/ajpheart.00802.2015.
[17] A. R. Hargens and S. Richardson, "Cardiovascular adaptations, fluid shifts, and countermeasures related to space flight," *Respiratory Physiology & Neurobiology*, vol. 169, pp. S30–S33, Oct. 2009, doi: 10.1016/j.resp.2009.07.005.
[18] P. Norsk, "Adaptation of the cardiovascular system to weightlessness: Surprises, paradoxes and implications for deep space missions," *Acta Physiologica*, vol. 228, no. 3, p. e13434, 2020, doi: 10.1111/apha.13434.
[19] G. Antonutto and P. E. di Prampero, "Cardiovascular deconditioning in microgravity: some possible countermeasures," *Eur J Appl Physiol*, vol. 90, no. 3, pp. 283–291, Oct. 2003, doi: 10.1007/s00421-003-0884-5.
[20] L. H. Loerch, "Exercise Countermeasures on ISS: Summary and Future Directions," Dec. 2015. https://www.ingentaconnect.com/contentone/asma/amhp/2015/00000086/A00112s1/art00014# (accessed Oct. 19, 2018).
[21] S. P. Chappell, J. R. Norcross, A. F. Abercromby, and M. L. Gernhardt, "Risk of Injury and Comprised Performance Due to EVA Operations: Evidence Report." NASA Human Research Program, 2015.
[22] C. M. Westby, D. S. Martin, S. M. C. Lee, M. B. Stenger, and S. H. Platts, "Left ventricular remodeling during and after 60 days of sedentary head-down bed rest," *Journal of Applied Physiology*, vol. 120, no. 8, pp. 956–964, Oct. 2015, doi: 10.1152/japplphysiol.00676.2015.
[23] S. M. Fortney, "Exercise Thermoregulation: Possible Effects of Spaceflight," *SAE Transactions*, vol. 100, pp. 1396–1406, 1991.
[24] P. A. Souvestre, A. P. Blaber, and C. K. Landrock, "Space motion sickness: The sensory motor controls and cardiovascular correlation," *Acta Astronautica*, vol. 63, no. 7, pp. 745–757, Oct. 2008, doi: 10.1016/j.actaastro.2008.05.003.
[25] A. R. Hargens and S. Richardson, "Cardiovascular adaptations, fluid shifts, and countermeasures related to space flight," *Respiratory Physiology & Neurobiology*, vol. 169, pp. S30–S33, Oct. 2009, doi: 10.1016/j.resp.2009.07.005.
[26] A. K. Verma *et al.*, "Comparison of Autonomic Control of Blood Pressure During Standing and Artificial Gravity Induced via Short-Arm Human Centrifuge," *Front Physiol*, vol. 9, Jun. 2018, doi: 10.3389/fphys.2018.00712.
[27] A. R. Hargens, R. Bhattacharya, and S. M. Schneider, "Space physiology VI: exercise, artificial gravity, and countermeasure development for prolonged space flight," *Eur J Appl Physiol*, vol. 113, no. 9, pp. 2183–2192, Sep. 2013, doi: 10.1007/s00421-012-2523-5.
[28] L.-F. Zhang, "Vascular adaptation to microgravity: what have we learned?," *Journal of Applied Physiology*, vol. 91, no. 6, pp. 2415–2430, Dec. 2001, doi: 10.1152/jappl.2001.91.6.2415.
[29] K. S. Fraser, D. K. Greaves, J. K. Shoemaker, A. P. Blaber, and R. L. Hughson, "Heart Rate and Daily Physical Activity with Long-Duration Habitation of the International Space Station," Jun. 2012. https://www.ingentaconnect.com/content/asma/asem/2012/00000083/00000006/art00006# (accessed Oct. 08, 2018).

[30] A. P. Blaber, C. K. Landrock, and P. A. Souvestre, “Cardio-postural deconditioning: A model for post-flight orthostatic intolerance,” *Respiratory Physiology & Neurobiology*, vol. 169, pp. S21–S25, Oct. 2009, doi: 10.1016/j.resp.2009.04.007.
[31] F. A. Gaffney, J. V. Nixon, E. S. Karlsson, W. Campbell, A. B. C. Dowdey, and C. G. Blomqvist, “Cardiovascular deconditioning produced by 20 hours of bedrest with head-down tilt (−5°) in middle-aged healthy men,” *The American Journal of Cardiology*, vol. 56, no. 10, pp. 634–638, Oct. 1985, doi: 10.1016/0002-9149(85)91025-2.
[32] K.-I. Iwasaki, R. Zhang, J. H. Zuckerman, J. A. Pawelczyk, and B. D. Levine, “Effect of head-down-tilt bed rest and hypovolemia on dynamic regulation of heart rate and blood pressure.,” *American journal of physiology. Regulatory, integrative and comparative physiology*, vol. 279, no. 6, p. NaN-NaN, 2000, doi: 10.1152/ajpregu.2000.279.6.R2189.
[33] V. A. Convertino, D. F. Doerr, D. L. Eckberg, J. M. Fritsch, and J. Vernikos-Danellis, “Head-down bed rest impairs vagal baroreflex responses and provokes orthostatic hypotension,” *Journal of Applied Physiology*, vol. 68, no. 4, pp. 1458–1464, Apr. 1990, doi: 10.1152/jappl.1990.68.4.1458.
[34] A. Pavy-Le Traon, M. Heer, M. V. Narici, J. Rittweger, and J. Vernikos, “From space to Earth: advances in human physiology from 20 years of bed rest studies (1986–2006),” *Eur J Appl Physiol*, vol. 101, no. 2, pp. 143–194, Sep. 2007, doi: 10.1007/s00421-007-0474-z.
[35] Norsk Peter *et al.*, “Vasorelaxation in Space,” *Hypertension*, vol. 47, no. 1, pp. 69–73, Jan. 2006, doi: 10.1161/01.HYP.0000194332.98674.57.
[36] R. L. Hughson *et al.*, “Cardiovascular regulation during long-duration spaceflights to the International Space Station,” *Journal of Applied Physiology*, vol. 112, no. 5, pp. 719–727, Mar. 2012, doi: 10.1152/japplphysiol.01196.2011.
[37] L.-F. Zhang, “Region-specific vascular remodeling and its prevention by artificial gravity in weightless environment,” *Eur J Appl Physiol*, vol. 113, no. 12, pp. 2873–2895, Dec. 2013, doi: 10.1007/s00421-013-2597-8.
[38] O. Henriksen, “Local sympathetic reflex mechanism in regulation of blood flow in human subcutaneous adipose tissue,” *Acta Physiol Scand Suppl*, vol. 450, pp. 1–48, 1977.
[39] B. E. Shykoff *et al.*, “Cardiovascular response to submaximal exercise in sustained microgravity,” *Journal of Applied Physiology*, vol. 81, no. 1, pp. 26–32, Jul. 1996, doi: 10.1152/jappl.1996.81.1.26.
[40] P. Norsk *et al.*, “Volume-homeostatic mechanisms in humans during a 12-h posture change,” *Journal of Applied Physiology*, vol. 75, no. 1, pp. 349–356, Jul. 1993, doi: 10.1152/jappl.1993.75.1.349.
[41] D. Grahn and C. Heller, “The Physiology of Mammalian Temperature Homeostasis,” *ITACCS Critical Care Monograph*, pp. 1–21, Jan. 2004.
[42] D. D. Heistad, F. M. Abboud, A. L. Mark, and P. G. Schmid, “Interaction of thermal and baroreceptor reflexes in man,” *J Appl Physiol*, vol. 35, no. 5, pp. 581–586, Nov. 1973, doi: 10.1152/jappl.1973.35.5.581.
[43] K. L. Nyberg, K. R. Diller, and E. H. Wissler, “Model of Human/Liquid Cooling Garment Interaction for Space Suit Automatic Thermal Control,” *J Biomech Eng*, vol. 123, no. 1, pp. 114–120, Feb. 2001, doi: 10.1115/1.1336147.
[44] K. L. Nyberg, K. R. Diller, and E. H. Wissler, “Automatic control of thermal neutrality for space suit applications using a liquid cooling garment,” *Aviat Space Environ Med*, vol. 71, no. 9, pp. 904–913, Sep. 2000.

[45] D. W. Hensley, A. E. Mark, J. R. Abella, G. M. Netscher, E. H. Wissler, and K. R. Diller, "50 Years of Computer Simulation of the Human Thermoregulatory System," *J Biomech Eng*, vol. 135, no. 2, Feb. 2013, doi: 10.1115/1.4023383.
[46] E. H. Wissler, "Steady-state temperature distribution in man," *Journal of Applied Physiology*, vol. 16, no. 4, pp. 734–740, Jul. 1961, doi: 10.1152/jappl.1961.16.4.734.
[47] S. M. Fortney, E. R. Nadel, C. B. Wenger, and J. R. Bove, "Effect of blood volume on sweating rate and body fluids in exercising humans," *Journal of Applied Physiology*, vol. 51, no. 6, pp. 1594–1600, Dec. 1981, doi: 10.1152/jappl.1981.51.6.1594.
[48] D. S. F. Portree, *Walking to Olympus: An EVA Chronology*. NASA History Office, Office of Policy and Plans, NASA Headquarters, 1997.
[49] "Significant Incidents and Close Calls in Human Spaceflight: EVA Operaitons.," National Aeronautics and Space Administration, Houston, TX, US, 2017.
[50] M. Miller, A. Claybrook, S. Greenlund, J. Marquez, and K. Feigh, *Operational Assessment of Apollo Lunar Surface Extravehicular Activity*. NASA Technical Publication, 2017. doi: 10.13140/RG.2.2.28009.80487.
[51] J. M. Waligora and D. J. Horrigan, "Metabolism and Heat Dissipation During Apollo EVA Periods," Washington, DC, US, 1975.
[52] J. Steele, G. Quinn, C. Watts, J. Makinen, C. Campbell, and D. Westheimer, "Advanced Space Suit PLSS 2.0 Cooling Loop EValuation and PLSS 2.5 Recommendations," Jul. 2016, Accessed: Sep. 23, 2020. [Online]. Available: https://ttu-ir.tdl.org/handle/2346/67619
[53] M. I. Board, "International Space Station (ISS) EVA Suit Water Intrusion, High Visibility Close Call," National Aeronautics and Space Administration, Washington, DC, US.
[54] A. Steptoe and M. Kivimäki, "Stress and cardiovascular disease," *Nat Rev Cardiol*, vol. 9, no. 6, pp. 360–370, Jun. 2012, doi: 10.1038/nrcardio.2012.45.
[55] B. Myers, "Corticolimbic regulation of cardiovascular responses to stress," *Physiol Behav*, vol. 172, pp. 49–59, Apr. 2017, doi: 10.1016/j.physbeh.2016.10.015.
[56] K. A. Matthews, K. L. Woodall, and M. T. Allen, "Cardiovascular reactivity to stress predicts future blood pressure status.," *Hypertension*, vol. 22, no. 4, pp. 479–485, Oct. 1993, doi: 10.1161/01.HYP.22.4.479.
[57] J. F. Thayer, S. S. Yamamoto, and J. F. Brosschot, "The relationship of autonomic imbalance, heart rate variability and cardiovascular disease risk factors," *International Journal of Cardiology*, vol. 141, no. 2, pp. 122–131, May 2010, doi: 10.1016/j.ijcard.2009.09.543.
[58] B. H. Friedman and J. F. Thayer, "Autonomic balance revisited: Panic anxiety and heart rate variability," *Journal of Psychosomatic Research*, vol. 44, no. 1, pp. 133–151, Jan. 1998, doi: 10.1016/S0022-3999(97)00202-X.
[59] S. Delliaux, A. Delaforge, J.-C. Deharo, and G. Chaumet, "Mental Workload Alters Heart Rate Variability, Lowering Non-linear Dynamics," *Front. Physiol.*, vol. 0, 2019, doi: 10.3389/fphys.2019.00565.
[60] A. Matuz, D. van der Linden, Z. Kisander, I. Hernádi, K. Kázmér, and Á. Csathó, "Enhanced cardiac vagal tone in mental fatigue: Analysis of heart rate variability in Time-on-Task, recovery, and reactivity," *PLOS ONE*, vol. 16, no. 3, p. e0238670, Mar. 2021, doi: 10.1371/journal.pone.0238670.
[61] A. Zeki Al Hazzouri, T. Elfassy, M. R. Carnethon, D. M. Lloyd-Jones, and K. Yaffe, "Heart Rate Variability and Cognitive Function In Middle-Age Adults: The Coronary

Artery Risk Development in Young Adults," *American Journal of Hypertension*, vol. 31, no. 1, pp. 27–34, Jan. 2018, doi: 10.1093/ajh/hpx125.
[62] R. Orsila *et al.*, "Perceived Mental Stress and Reactions in Heart Rate Variability—A Pilot Study Among Employees of an Electronics Company," *International Journal of Occupational Safety and Ergonomics*, vol. 14, no. 3, pp. 275–283, Jan. 2008, doi: 10.1080/10803548.2008.11076767.
[63] "Reduce Fatigue-Related Accidents," National Transportation Safety Board, Washington, DC, US, 2016.
[64] S. J. Vine, L. Uiga, A. Lavric, L. J. Moore, K. Tsaneva-Atanasova, and M. R. Wilson, "Individual reactions to stress predict performance during a critical aviation incident," *Anxiety, Stress, & Coping*, vol. 28, no. 4, pp. 467–477, Jul. 2015, doi: 10.1080/10615806.2014.986722.
[65] M.-P. Fornette, M.-H. Bardel, C. Lefrançois, J. Fradin, F. E. Massioui, and R. Amalberti, "Cognitive-Adaptation Training for Improving Performance and Stress Management of Air Force Pilots," *The International Journal of Aviation Psychology*, vol. 22, no. 3, pp. 203–223, Jul. 2012, doi: 10.1080/10508414.2012.689208.
[66] S. Shappell, C. Detwiler, K. Holcomb, C. Hackworth, A. Boquet, and D. A. Wiegmann, "Human Error and Commercial Aviation Accidents: An Analysis Using the Human Factors Analysis and Classification System," *Hum Factors*, vol. 49, no. 2, pp. 227–242, Apr. 2007, doi: 10.1518/001872007X312469.
[67] "Loss of Control on Approach, Colgan Air, Inc., Operating as Continental Connection Flight 3407, Bombardier DHC 8 400, N200WQ," National Transportation Safety Board, Accident report AAR-10-01, Feb. 2010. Accessed: Sep. 22, 2021. [Online]. Available: https://www.ntsb.gov/investigations/AccidentReports/Pages/AAR1001.aspx
[68] "Crash During a Nighttime Nonprecision Instrument Approach to Landing, UPS Flight 1354," National Transportation Safety Board, Accident report AAR1402, Sep. 2014. Accessed: Sep. 23, 2021. [Online]. Available: https://www.ntsb.gov/investigations/accidentreports/pages/AAR1402.aspx
[69] J. J. Caldwell, "Fatigue in the aviation environment: an overview of the causes and effects as well as recommended countermeasures," *Aviat Space Environ Med*, vol. 68, no. 10, pp. 932–938, Oct. 1997.
[70] F. H. Previc *et al.*, "The Effects of Sleep Deprivation on Flight Performance, Instrument Scanning, and Physiological Arousal in Pilots," *The International Journal of Aviation Psychology*, vol. 19, no. 4, pp. 326–346, Oct. 2009, doi: 10.1080/10508410903187562.
[71] G. P. Krueger, "Sustained work, fatigue, sleep loss and performance: A review of the issues," *Work & Stress*, vol. 3, no. 2, pp. 129–141, Apr. 1989, doi: 10.1080/02678378908256939.
[72] "Runway Overrun During Landing, American Airlines Flight 1420, McDonnell Douglas MD-82," National Transportation Safety Board, Accident report AAR-01-02, Oct. 2001. Accessed: Sep. 23, 2021. [Online]. Available: https://www.ntsb.gov/investigations/AccidentReports/Pages/AAR0102.aspx
[73] "A Review of Flightcrew-Involved Major Accidents of U.S. Air Carriers, 1978 Through 1990," National Transportation Safety Board, Washington, DC, US, NTSB/SS-94-01, 1994.
[74] "Manual for the Oversight of Fatigue Management Approaches," International Civil Aviation Organization, Montréal, Quebec, Canada, 2016.

[75] Y. Q. Wingelaar-Jagt, T. T. Wingelaar, W. J. Riedel, and J. G. Ramaekers, “Fatigue in Aviation: Safety Risks, Preventive Strategies and Pharmacological Interventions,” *Frontiers in Physiology*, vol. 12, p. 1399, 2021, doi: 10.3389/fphys.2021.712628.
[76] X. Hu and G. Lodewijks, “Detecting fatigue in car drivers and aircraft pilots by using non-invasive measures: The value of differentiation of sleepiness and mental fatigue,” *Journal of Safety Research*, vol. 72, pp. 173–187, Feb. 2020, doi: 10.1016/j.jsr.2019.12.015.
[77] L. C. Thomas, C. Gast, R. Grube, and K. Craig, “Fatigue Detection in Commercial Flight Operations: Results Using Physiological Measures,” *Procedia Manufacturing*, vol. 3, pp. 2357–2364, Jan. 2015, doi: 10.1016/j.promfg.2015.07.383.
[78] S. G. Hart, “Nasa-Task Load Index (NASA-TLX); 20 Years Later,” *Proceedings of the Human Factors and Ergonomics Society Annual Meeting*, vol. 50, no. 9, pp. 904–908, Oct. 2006, doi: 10.1177/154193120605000909.
[79] S. G. Hart and L. E. Staveland, “Development of NASA-TLX (Task Load Index): Results of Empirical and Theoretical Research,” in *Advances in Psychology*, vol. 52, P. A. Hancock and N. Meshkati, Eds. North-Holland, 1988, pp. 139–183. doi: 10.1016/S0166-4115(08)62386-9.
[80] H. P. A. Van Dongen, G. Maislin, J. M. Mullington, and D. F. Dinges, “The Cumulative Cost of Additional Wakefulness: Dose-Response Effects on Neurobehavioral Functions and Sleep Physiology From Chronic Sleep Restriction and Total Sleep Deprivation,” *Sleep*, vol. 26, no. 2, pp. 117–126, Mar. 2003, doi: 10.1093/sleep/26.2.117.
[81] N. Wilson, B. Guragain, A. Verma, L. Archer, and K. Tavakolian, “Blending Human and Machine: Feasibility of Measuring Fatigue Through the Aviation Headset,” *Hum Factors*, vol. 62, no. 4, pp. 553–564, Jun. 2020, doi: 10.1177/0018720819849783.
[82] T. J. Balkin *et al.*, “Comparative utility of instruments for monitoring sleepiness-related performance decrements in the operational environment,” *Journal of Sleep Research*, vol. 13, no. 3, pp. 219–227, 2004, doi: 10.1111/j.1365-2869.2004.00407.x.
[83] M. Basner and D. F. Dinges, “Maximizing Sensitivity of the Psychomotor Vigilance Test (PVT) to Sleep Loss,” *Sleep*, vol. 34, no. 5, pp. 581–591, May 2011, doi: 10.1093/sleep/34.5.581.
[84] E. E. Flynn-Evans *et al.*, “Changes in performance and bio-mathematical model performance predictions during 45 days of sleep restriction in a simulated space mission,” *Sci Rep*, vol. 10, no. 1, p. 15594, Sep. 2020, doi: 10.1038/s41598-020-71929-4.
[85] J. B. West, “A strategy for in-flight measurements of physiology of pilots of high-performance fighter aircraft,” *Journal of Applied Physiology*, vol. 115, no. 1, pp. 145–149, Jul. 2013, doi: 10.1152/japplphysiol.00094.2013.
[86] A. Popov, W. Fink, and A. Hess, “PHM for Astronauts – A New Application,” *Annual Conference of the PHM Society*, vol. 5, no. 1, Art. no. 1, 2013, doi: 10.36001/phmconf.2013.v5i1.2333.
[87] J. R. Braden and D. L. Akin, “Development and Testing of a Space Suit Analogue for Neutral Buoyancy EVA Research,” Jul. 2002, pp. 2002-01–2364. doi: 10.4271/2002-01-2364.
[88] I. L. Schlacht *et al.*, “Space Analog Survey: Review of Existing and New Proposal of Space Habitats with Earth Applications,” Jul. 2016, Accessed: Aug. 02, 2019. [Online]. Available: https://ttu-ir.tdl.org/handle/2346/67692

[89] X. Cao *et al.*, "Heart Rate Variability and Performance of Commercial Airline Pilots during Flight Simulations," *International Journal of Environmental Research and Public Health*, vol. 16, no. 2, Art. no. 2, Jan. 2019, doi: 10.3390/ijerph16020237.
[90] G. Ernst, *Heart Rate Variability*, vol. 1. Hoboken, NJ: Springer, 2014.
[91] A. Alaimo, A. Esposito, C. Orlando, and A. Simoncini, "Aircraft Pilots Workload Analysis: Heart Rate Variability Objective Measures and NASA-Task Load Index Subjective Evaluation," *Aerospace*, vol. 7, no. 9, Art. no. 9, Sep. 2020, doi: 10.3390/aerospace7090137.
[92] F. Sauvet, J. C. Jouanin, C. Langrume, P. Van Beers, Y. Papelier, and C. Dussault, "Heart Rate Variability in Novice Pilots During and After a Multi-Leg Cross-Country Flight," *Aviation, Space, and Environmental Medicine*, vol. 80, no. 10, pp. 862–869, Oct. 2009, doi: 10.3357/ASEM.2531.2009.
[93] S. Majumder *et al.*, "Using Photoplethysmography Based Features As Indicators of Drowsiness: Preliminary Results," presented at the 2019 Design of Medical Devices Conference, Jul. 2019. doi: 10.1115/DMD2019-3236.
[94] C.-P. Chua, G. McDarby, and C. Heneghan, "Combined electrocardiogram and photoplethysmogram measurements as an indicator of objective sleepiness," *Physiol. Meas.*, vol. 29, no. 8, pp. 857–868, Jul. 2008, doi: 10.1088/0967-3334/29/8/001.
[95] D. R. Jenkins, *Dressing for Altitude: U.S. Aviation Pressure Suits, Wiley Post to Space Shuttle*. Government Printing Office, 2012.
[96] D. P. Gradwell and D. J. Rainford, "Ernsting's Aviation and space medicine," *Journal of The Royal Naval Medical Service*, vol. 103, no. 2, Jun. 2017, doi: 10.1136/jrnms-103-147.
[97] S. A. Nunneley, "Water cooled garments: A review," *Space Life Sciences*, vol. 2, no. 3, pp. 335–360, Dec. 1970, doi: 10.1007/BF00929293.
[98] K. B. Pandolf, L. A. Stroschein, R. R. Gonzalez, and M. N. Sawka, "Predicting human heat strain and performance with application to space operations," *Aviat Space Environ Med*, vol. 66, no. 4, pp. 364–368, Apr. 1995.
[99] V. L. Pisacane, L. H. Kuznetz, J. S. Logan, J. B. Clark, and E. H. Wissler, "Thermoregulatory Models of Space Shuttle and Space Station Activities," *Aviation, Space, and Environmental Medicine*, vol. 78, no. 4, pp. A48–A55, Apr. 2007.
[100] D. R. Levin, "A Systematic Review of the Psychological Effects of Heat Stress on Subjects in Uncooled, Sealed, Environment Suits," Thesis, 2017. Accessed: Sep. 24, 2021. [Online]. Available: https://utmb-ir.tdl.org/handle/2152.3/11177
[101] P. S. Auerbach, T. A. Cushing, and N. S. Harris, *Auerbach's Wilderness Medicine*. Elsevier Health Sciences, 2016.
[102] M. J. Barwood, P. S. Newton, and M. J. Tipton, "Ventilated Vest and Tolerance for Intermittent Exercise in Hot, Dry Conditions With Military Clothing," *Aviation, Space, and Environmental Medicine*, vol. 80, no. 4, pp. 353–359, Apr. 2009, doi: 10.3357/ASEM.2411.2009.
[103] P. A. Hancock and I. Vasmatzidis, "Effects of heat stress on cognitive performance: the current state of knowledge," *International Journal of Hyperthermia*, vol. 19, no. 3, pp. 355–372, Jan. 2003, doi: 10.1080/0265673021000054630.
[104] N. I. for O. S. and Health, *Occupational Exposure to Hot Environments: Revised Criteria 1986*. U.S. Department of Health and Human Services, Public Health Service, Centers for Disease Control, National Institute for Occupational Safety and Health, Division of Standards Development and Technology Transfer, 1986.

[105] M. J. Buller, A. P. Welles, and K. E. Friedl, “Wearable physiological monitoring for human thermal-work strain optimization,” *Journal of Applied Physiology*, vol. 124, no. 2, pp. 432–441, Feb. 2018, doi: 10.1152/japplphysiol.00353.2017.
[106] D. Amos, R. Hansen, W.-M. Lau, and J. T. Michalski, “Physiological and Cognitive Performance of Soldiers Conducting Routine Patrol and Reconnaissance Operations in the Tropics,” *Military Medicine*, vol. 165, no. 12, pp. 961–966, Dec. 2000, doi: 10.1093/milmed/165.12.961.
[107] B. R. Ely, M. R. Ely, S. N. Cheuvront, R. W. Kenefick, D. W. DeGroot, and S. J. Montain, “Evidence against a 40°C core temperature threshold for fatigue in humans,” *Journal of Applied Physiology*, vol. 107, no. 5, pp. 1519–1525, Nov. 2009, doi: 10.1152/japplphysiol.00577.2009.
[108] M. N. Sawka and A. J. Young, “Physiological Systems and Their Responses to Conditions of Heat and Cold,” ARMY RESEARCH INST OF ENVIRONMENTAL MEDICINE NATICK MA THERMAL AND MOUNTAIN MEDICINE DIVISION, Jan. 2006.
[109] M. A. S. Boksem, T. F. Meijman, and M. M. Lorist, “Effects of mental fatigue on attention: An ERP study,” *Cognitive Brain Research*, vol. 25, no. 1, pp. 107–116, Sep. 2005, doi: 10.1016/j.cogbrainres.2005.04.011.
[110] L. G. Faber, N. M. Maurits, and M. M. Lorist, “Mental Fatigue Affects Visual Selective Attention,” *PLOS ONE*, vol. 7, no. 10, p. e48073, Oct. 2012, doi: 10.1371/journal.pone.0048073.
[111] I. D. Brown, “Driver Fatigue,” *Hum Factors*, vol. 36, no. 2, pp. 298–314, Jun. 1994, doi: 10.1177/001872089403600210.
[112] C. Reis, C. Mestre, H. Canhão, D. Gradwell, and T. Paiva, “Sleep complaints and fatigue of airline pilots,” *Sleep Science*, vol. 9, no. 2, pp. 73–77, Apr. 2016, doi: 10.1016/j.slsci.2016.05.003.
[113] S. Lee and J. K. Kim, “Factors contributing to the risk of airline pilot fatigue,” *Journal of Air Transport Management*, vol. 67, pp. 197–207, Mar. 2018, doi: 10.1016/j.jairtraman.2017.12.009.
[114] A. van Drongelen, C. R. L. Boot, H. Hlobil, T. Smid, and A. J. van der Beek, “Risk factors for fatigue among airline pilots,” *Int Arch Occup Environ Health*, vol. 90, no. 1, pp. 39–47, Jan. 2017, doi: 10.1007/s00420-016-1170-2.
[115] J. A. Caldwell, “Fatigue in aviation,” *Travel Medicine and Infectious Disease*, vol. 3, no. 2, pp. 85–96, May 2005, doi: 10.1016/j.tmaid.2004.07.008.
[116] M. R. Rosekind, E. L. Co, K. B. Gregory, and D. L. Miller, “Crew Factors in Flight Operations,” NAS 1.15:209610, Sep. 2000. Accessed: Jul. 19, 2021. [Online]. Available: https://ntrs.nasa.gov/citations/20010039028
[117] G. F. Wilson, “An Analysis of Mental Workload in Pilots During Flight Using Multiple Psychophysiological Measures,” *The International Journal of Aviation Psychology*, vol. 12, no. 1, pp. 3–18, Jan. 2002, doi: 10.1207/S15327108IJAP1201_2.
[118] M. S. Young, K. A. Brookhuis, C. D. Wickens, and P. A. Hancock, “State of science: mental workload in ergonomics,” *Ergonomics*, vol. 58, no. 1, pp. 1–17, Jan. 2015, doi: 10.1080/00140139.2014.956151.
[119] S. Laborde, E. Mosley, and J. F. Thayer, “Heart Rate Variability and Cardiac Vagal Tone in Psychophysiological Research – Recommendations for Experiment Planning, Data Analysis, and Data Reporting,” *Front. Psychol.*, vol. 0, 2017, doi: 10.3389/fpsyg.2017.00213.

[120] B. H. Friedman and J. F. Thayer, “Anxiety and autonomic flexibility: a cardiovascular approach,” *Biological Psychology*, vol. 47, no. 3, pp. 243–263, Mar. 1998, doi: 10.1016/S0301-0511(97)00027-6.
[121] M. G. Ziegler, “Chapter 61 - Psychological Stress and the Autonomic Nervous System,” in *Primer on the Autonomic Nervous System (Third Edition)*, D. Robertson, I. Biaggioni, G. Burnstock, P. A. Low, and J. F. R. Paton, Eds. San Diego: Academic Press, 2012, pp. 291–293. doi: 10.1016/B978-0-12-386525-0.00061-5.
[122] A. H. ROSCOE, “Heart rate as a psychophysiological measure for in-flight workload assessment,” *Ergonomics*, vol. 36, no. 9, pp. 1055–1062, Sep. 1993, doi: 10.1080/00140139308967977.
[123] A. H. Roscoe, “Heart rate monitoring of pilots during steep-gradient approaches,” *Aviat Space Environ Med*, vol. 46, no. 11, pp. 1410–1413, Nov. 1975.
[124] F.-T. Sun, C. Kuo, H.-T. Cheng, S. Buthpitiya, P. Collins, and M. Griss, “Activity-Aware Mental Stress Detection Using Physiological Sensors,” in *Mobile Computing, Applications, and Services*, Berlin, Heidelberg, 2012, pp. 282–301. doi: 10.1007/978-3-642-29336-8_16.
[125] R. Mccraty and F. Shaffer, “Heart Rate Variability: New Perspectives on Physiological Mechanisms, Assessment of Self-regulatory Capacity, and Health Risk,” *Glob Adv Health Med*, vol. 4, no. 1, pp. 46–61, Jan. 2015, doi: 10.7453/gahmj.2014.073.
[126] F. Shaffer, R. McCraty, and C. L. Zerr, “A healthy heart is not a metronome: an integrative review of the heart’s anatomy and heart rate variability,” *Front. Psychol.*, vol. 0, 2014, doi: 10.3389/fpsyg.2014.01040.
[127] Z. Li *et al.*, “A longitudinal study in youth of heart rate variability at rest and in response to stress,” *International Journal of Psychophysiology*, vol. 73, no. 3, pp. 212–217, Sep. 2009, doi: 10.1016/j.ijpsycho.2009.03.002.
[128] T. F. of the E. S. of C. the N. A. S. of P. Electrophysiology, “Heart Rate Variability,” *Circulation*, vol. 93, no. 5, pp. 1043–1065, Mar. 1996, doi: 10.1161/01.CIR.93.5.1043.
[129] H.-G. Kim, E.-J. Cheon, D.-S. Bai, Y. H. Lee, and B.-H. Koo, “Stress and Heart Rate Variability: A Meta-Analysis and Review of the Literature,” *Psychiatry Investigation*, vol. 15, no. 3, p. 235, Mar. 2018, doi: 10.30773/pi.2017.08.17.
[130] G. Ernst, “Heart-Rate Variability—More than Heart Beats?,” *Front. Public Health*, vol. 0, 2017, doi: 10.3389/fpubh.2017.00240.
[131] A. B. Ciccone, J. A. Siedlik, J. M. Wecht, J. A. Deckert, N. D. Nguyen, and J. P. Weir, “Reminder: RMSSD and SD1 are identical heart rate variability metrics,” *Muscle & Nerve*, vol. 56, no. 4, pp. 674–678, 2017, doi: 10.1002/mus.25573.
[132] M. Brennan, M. Palaniswami, and P. Kamen, “Poincaré plot interpretation using a physiological model of HRV based on a network of oscillators,” *American Journal of Physiology-Heart and Circulatory Physiology*, vol. 283, no. 5, pp. H1873–H1886, Nov. 2002, doi: 10.1152/ajpheart.00405.2000.
[133] P. Guzik *et al.*, “Correlations between Poincaré Plot and Conventional Heart Rate Variability Parameters Assessed during Paced Breathing,” *The Journal of Physiological Sciences*, vol. advpub, pp. 0702020009–0702020009, 2007, doi: 10.2170/physiolsci.RP005506.
[134] M. Brennan, M. Palaniswami, and P. Kamen, “Do existing measures of Poincare plot geometry reflect nonlinear features of heart rate variability?,” *IEEE Transactions on*

Biomedical Engineering, vol. 48, no. 11, pp. 1342–1347, Nov. 2001, doi: 10.1109/10.959330.
[135] A. Mizobuchi, K. Osawa, M. Tanaka, A. Yumoto, H. Saito, and S. Fuke, "Detrended fluctuation analysis can detect the impairment of heart rate regulation in patients with heart failure with preserved ejection fraction," *Journal of Cardiology*, vol. 77, no. 1, pp. 72–78, Jan. 2021, doi: 10.1016/j.jjcc.2020.07.027.
[136] P. Lehrer, M. Karavidas, S.-E. Lu, E. Vaschillo, B. Vaschillo, and A. Cheng, "Cardiac data increase association between self-report and both expert ratings of task load and task performance in flight simulator tasks: An exploratory study," *International Journal of Psychophysiology*, vol. 76, no. 2, pp. 80–87, May 2010, doi: 10.1016/j.ijpsycho.2010.02.006.
[137] W. Boucsein, A. Haarmann, and F. Schaefer, "Combining Skin Conductance and Heart Rate Variability for Adaptive Automation During Simulated IFR Flight," in *Engineering Psychology and Cognitive Ergonomics*, Berlin, Heidelberg, 2007, pp. 639–647. doi: 10.1007/978-3-540-73331-7_70.
[138] Y.-H. Lee and B.-S. Liu, "Inflight Workload Assessment: Comparison of Subjective and Physiological Measurements," *Aviation, Space, and Environmental Medicine*, vol. 74, no. 10, pp. 1078–1084, Oct. 2003.
[139] H. Mansikka, K. Virtanen, D. Harris, and P. Simola, "Fighter pilots' heart rate, heart rate variation and performance during an instrument flight rules proficiency test," *Applied Ergonomics*, vol. 56, pp. 213–219, Sep. 2016, doi: 10.1016/j.apergo.2016.04.006.
[140] M. Regula *et al.*, "Study of heart rate as the main stress indicator in aircraft pilots," in *Proceedings of the 16th International Conference on Mechatronics - Mechatronika 2014*, Dec. 2014, pp. 639–643. doi: 10.1109/MECHATRONIKA.2014.7018334.
[141] A. J. Tattersall and G. R. J. Hockey, "Level of Operator Control and Changes in Heart Rate Variability during Simulated Flight Maintenance," *Hum Factors*, vol. 37, no. 4, pp. 682–698, Dec. 1995, doi: 10.1518/001872095778995517.
[142] A. Lindqvist, E. Keskinen, K. Antila, L. Halkola, T. Peltonen, and I. Välimäki, "Heart rate variability, cardiac mechanics, and subjectively evaluated stress during simulator flight," *Aviation, Space, and Environmental Medicine*, vol. 54, no. 8, pp. 685–690, 1983.
[143] A. J. Hormeño-Holgado and V. J. Clemente-Suárez, "Effect of different combat jet manoeuvres in the psychophysiological response of professional pilots," *Physiology & Behavior*, vol. 208, p. 112559, Sep. 2019, doi: 10.1016/j.physbeh.2019.112559.
[144] F. W. Skibniewski *et al.*, "Preliminary Results of the LF/HF Ratio as an Indicator for Estimating Difficulty Level of Flight Tasks," *Aerospace Medicine and Human Performance*, vol. 86, no. 6, pp. 518–523, Jun. 2015, doi: 10.3357/AMHP.4087.2015.
[145] J. P. Fuentes-García, V. J. Clemente-Suárez, M. Á. Marazuela-Martínez, J. F. Tornero-Aguilera, and S. Villafaina, "Impact of Real and Simulated Flights on Psychophysiological Response of Military Pilots," *International Journal of Environmental Research and Public Health*, vol. 18, no. 2, Art. no. 2, Jan. 2021, doi: 10.3390/ijerph18020787.
[146] M. P. Tarvainen, J.-P. Niskanen, J. A. Lipponen, P. O. Ranta-aho, and P. A. Karjalainen, "Kubios HRV – Heart rate variability analysis software," *Computer Methods and Programs in Biomedicine*, vol. 113, no. 1, pp. 210–220, Jan. 2014, doi: 10.1016/j.cmpb.2013.07.024.

[147] A. H. Roscoe, “Assessing pilot workload. Why measure heart rate, HRV and respiration?,” *Biological Psychology*, vol. 34, no. 2, pp. 259–287, Nov. 1992, doi: 10.1016/0301-0511(92)90018-P.
[148] P. Norsk, A. Asmar, M. Damgaard, and N. J. Christensen, “Fluid shifts, vasodilatation and ambulatory blood pressure reduction during long duration spaceflight,” *The Journal of Physiology*, vol. 593, no. 3, pp. 573–584, 2015, doi: 10.1113/jphysiol.2014.284869.
[149] J. J. Smith, C. M. Porth, and M. Erickson, “Hemodynamic Response to the Upright Posture,” *The Journal of Clinical Pharmacology*, vol. 34, no. 5, pp. 375–386, 1994, doi: 10.1002/j.1552-4604.1994.tb04977.x.
[150] A. R. Hargens, R. Bhattacharya, and S. M. Schneider, “Space physiology VI: exercise, artificial gravity, and countermeasure development for prolonged space flight,” *Eur J Appl Physiol*, vol. 113, no. 9, pp. 2183–2192, Sep. 2013, doi: 10.1007/s00421-012-2523-5.
[151] J. M. Fritsch-Yelle, J. B. Charles, M. M. Jones, L. A. Beightol, and D. L. Eckberg, “Spaceflight alters autonomic regulation of arterial pressure in humans,” *Journal of Applied Physiology*, vol. 77, no. 4, pp. 1776–1783, Oct. 1994, doi: 10.1152/jappl.1994.77.4.1776.
[152] Blaber Andrew P., Goswami Nandu, Bondar Roberta L., and Kassam Mahmood S., “Impairment of Cerebral Blood Flow Regulation in Astronauts With Orthostatic Intolerance After Flight,” *Stroke*, vol. 42, no. 7, pp. 1844–1850, Jul. 2011, doi: 10.1161/STROKEAHA.110.610576.
[153] J. M. Fritsch, J. B. Charles, B. S. Bennett, M. M. Jones, and D. L. Eckberg, “Short-duration spaceflight impairs human carotid baroreceptor-cardiac reflex responses,” *Journal of Applied Physiology*, vol. 73, no. 2, pp. 664–671, Aug. 1992, doi: 10.1152/jappl.1992.73.2.664.
[154] J. Gisolf, R. V. Immink, J. J. van Lieshout, W. J. Stok, and J. M. Karemaker, “Orthostatic blood pressure control before and after spaceflight, determined by time-domain baroreflex method,” *Journal of Applied Physiology*, vol. 98, no. 5, pp. 1682–1690, May 2005, doi: 10.1152/japplphysiol.01219.2004.
[155] A. R. Hargens and D. E. Watenpaugh, “Cardiovascular adaptation to spaceflight.,” *Med Sci Sports Exerc*, vol. 28, no. 8, pp. 977–982, Aug. 1996, doi: 10.1097/00005768-199608000-00007.
[156] N. Goswami *et al.*, “Short-arm human centrifugation with 0.4g at eye and 0.75g at heart level provides similar cerebrovascular and cardiovascular responses to standing,” *Eur J Appl Physiol*, vol. 115, no. 7, pp. 1569–1575, Jul. 2015, doi: 10.1007/s00421-015-3142-8.
[157] A. K. Verma *et al.*, “Comparison of Autonomic Control of Blood Pressure During Standing and Artificial Gravity Induced via Short-Arm Human Centrifuge,” *Front Physiol*, vol. 9, Jun. 2018, doi: 10.3389/fphys.2018.00712.
[158] N. Goswami, A. P. Blaber, H. Hinghofer-Szalkay, and V. A. Convertino, “Lower Body Negative Pressure: Physiological Effects, Applications, and Implementation,” *Physiological Reviews*, vol. 99, no. 1, pp. 807–851, Dec. 2018, doi: 10.1152/physrev.00006.2018.
[159] D. E. Watenpaugh *et al.*, “Lower body negative pressure exercise plus brief postexercise lower body negative pressure improve post-bed rest orthostatic tolerance,” *Journal of Applied Physiology*, vol. 103, no. 6, pp. 1964–1972, Dec. 2007, doi: 10.1152/japplphysiol.00132.2007.

[160] A. K. Verma *et al.*, “Non-linear Heart Rate and Blood Pressure Interaction in Response to Lower-Body Negative Pressure,” *Front. Physiol.*, vol. 8, 2017, doi: 10.3389/fphys.2017.00767.
[161] S. H. Platts *et al.*, “Cardiovascular Adaptations to Long-Duration Head-Down Bed Rest,” *Aviation, Space, and Environmental Medicine*, vol. 80, no. 5, pp. A29–A36, May 2009, doi: 10.3357/ASEM.BR03.2009.
[162] R. L. CROMWELL, J. M. SCOTT, M. DOWNS, P. O. YARBOUGH, S. B. ZANELLO, and L. PLOUTZ-SNYDER, “Overview of the NASA 70-day Bed Rest Study,” *Med Sci Sports Exerc*, vol. 50, no. 9, pp. 1909–1919, Sep. 2018, doi: 10.1249/MSS.0000000000001617.
[163] A. Pavy-Le Traon, M. Heer, M. V. Narici, J. Rittweger, and J. Vernikos, “From space to Earth: advances in human physiology from 20 years of bed rest studies (1986–2006),” *Eur J Appl Physiol*, vol. 101, no. 2, pp. 143–194, Sep. 2007, doi: 10.1007/s00421-007-0474-z.
[164] T. A. Dorfman *et al.*, “Cardiac atrophy in women following bed rest,” *Journal of Applied Physiology*, vol. 103, no. 1, pp. 8–16, Jul. 2007, doi: 10.1152/japplphysiol.01162.2006.
[165] M. A. Perhonen *et al.*, “Cardiac atrophy after bed rest and spaceflight,” *Journal of Applied Physiology*, vol. 91, no. 2, pp. 645–653, Aug. 2001, doi: 10.1152/jappl.2001.91.2.645.
[166] R. L. Summers, D. S. Martin, J. V. Meck, and T. G. Coleman, “Computer systems analysis of spaceflight induced changes in left ventricular mass,” *Computers in Biology and Medicine*, vol. 37, no. 3, pp. 358–363, Mar. 2007, doi: 10.1016/j.compbiomed.2006.04.003.
[167] J. L. Hastings *et al.*, “Effect of rowing ergometry and oral volume loading on cardiovascular structure and function during bed rest,” *Journal of Applied Physiology*, vol. 112, no. 10, pp. 1735–1743, Feb. 2012, doi: 10.1152/japplphysiol.00019.2012.
[168] E. G. Caiani, P. Massabuau, L. Weinert, P. Vaïda, and R. M. Lang, “Effects of 5 days of head-down bed rest, with and without short-arm centrifugation as countermeasure, on cardiac function in males (BR-AG1 study),” *Journal of Applied Physiology*, vol. 117, no. 6, pp. 624–632, Sep. 2014, doi: 10.1152/japplphysiol.00122.2014.
[169] M. Kozàkovà *et al.*, “Impact of prolonged cardiac unloading on left ventricular mass and longitudinal myocardial performance: an experimental bed rest study in humans,” *Journal of Hypertension*, vol. 29, no. 1, pp. 137–143, Jan. 2011, doi: 10.1097/HJH.0b013e32833f5e01.
[170] F. Hoffmann *et al.*, “Cardiac adaptations to 60 day head-down-tilt bed rest deconditioning. Findings from the AGBRESA study,” *ESC Heart Failure*, vol. 8, no. 1, pp. 729–744, 2021, doi: 10.1002/ehf2.13103.
[171] D. E. Watenpaugh, “Analogs of microgravity: head-down tilt and water immersion,” *Journal of Applied Physiology*, vol. 120, no. 8, pp. 904–914, Feb. 2016, doi: 10.1152/japplphysiol.00986.2015.
[172] D. Xu, M. F. Tremblay, A. K. Verma, K. Tavakolian, N. Goswami, and A. P. Blaber, “Cardio-postural interactions and muscle-pump baroreflex are severely impacted by 60-day bedrest immobilization,” *Scientific Reports*, vol. 10, no. 1, Art. no. 1, Jul. 2020, doi: 10.1038/s41598-020-68962-8.
[173] N. Goswami, “Falls and Fall-Prevention in Older Persons: Geriatrics Meets Spaceflight!,” *Front. Physiol.*, vol. 8, 2017, doi: 10.3389/fphys.2017.00603.

[174] O. T. Inan *et al.*, “Ballistocardiography and Seismocardiography: A Review of Recent Advances,” *IEEE Journal of Biomedical and Health Informatics*, vol. 19, no. 4, pp. 1414–1427, Jul. 2015, doi: 10.1109/JBHI.2014.2361732.
[175] W. C. Hixson and D. E. Beischer, “BIOTELEMETRY OF THE TRIAXIAL BALLISTOCARDIOGRAM AND ELECTROCARDIOGRAM IN A WEIGHTLESS ENVIRONMENT. MONOGR NO. 10,” *Res Rep U S Nav Sch Aviat Med*, pp. 1–112, Sep. 1964.
[176] M. Di Rienzo *et al.*, “Wearable seismocardiography: Towards a beat-by-beat assessment of cardiac mechanics in ambulant subjects,” *Autonomic Neuroscience*, vol. 178, no. 1, pp. 50–59, Nov. 2013, doi: 10.1016/j.autneu.2013.04.005.
[177] K. Tavakolian, G. A. Dumont, G. Houlton, and A. P. Blaber, “Precordial Vibrations Provide Noninvasive Detection of Early-Stage Hemorrhage,” *Shock*, vol. 41, no. 2, pp. 91–96, Feb. 2014, doi: 10.1097/SHK.0000000000000077.
[178] K. Tavakolian, G. A. Dumont, and A. P. Blaber, “Analysis of seismocardiogram capability for prediction of mild to moderate haemorrhage; Preliminary results,” in *Computing in Cardiology 2013*, Sep. 2013, pp. 1107–1110.
[179] M. Di Rienzo, E. Vaini, P. Castiglioni, P. Meriggi, and F. Rizzo, “Beat-to-beat estimation of LVET and QS2 indices of cardiac mechanics from wearable seismocardiography in ambulant subjects,” in *2013 35th Annual International Conference of the IEEE Engineering in Medicine and Biology Society (EMBC)*, Osaka, Jul. 2013, pp. 7017–7020. doi: 10.1109/EMBC.2013.6611173.
[180] M. Di Rienzo, E. Vaini, and P. Lombardi, “Development of a smart garment for the assessment of cardiac mechanical performance and other vital signs during sleep in microgravity,” *Sensors and Actuators A: Physical*, vol. 274, pp. 19–27, May 2018, doi: 10.1016/j.sna.2018.02.034.
[181] A. K. Verma, R. Fazel-Rezai, A. Blaber, and K. Tavakolian, “Pulse transit time extraction from Seismocardiogram and its relationship with pulse pressure,” in *2015 Computing in Cardiology Conference (CinC)*, Sep. 2015, pp. 37–40. doi: 10.1109/CIC.2015.7408580.
[182] A. K. Verma, R. Fazel-Rezai, J. M. Zanetti, and K. Tavakolian, “Preliminary Results for Estimating Pulse Transit Time Using Seismocardiogram,” *J. Med. Devices*, vol. 9, no. 2, Jun. 2015, doi: 10.1115/1.4030124.
[183] P. Dehkordi *et al.*, “Comparison of Different Methods for Estimating Cardiac Timings: A Comprehensive Multimodal Echocardiography Investigation,” *Front. Physiol.*, vol. 10, 2019, doi: 10.3389/fphys.2019.01057.
[184] F. Khosrow-khavar, K. Tavakolian, A. P. Blaber, J. M. Zanetti, R. Fazel-Rezai, and C. Menon, “Automatic Annotation of Seismocardiogram With High-Frequency Precordial Accelerations,” *IEEE Journal of Biomedical and Health Informatics*, vol. 19, no. 4, pp. 1428–1434, Jul. 2015, doi: 10.1109/JBHI.2014.2360156.
[185] F. Khosrow-Khavar, K. Tavakolian, A. Blaber, and C. Menon, “Automatic and Robust Delineation of the Fiducial Points of the Seismocardiogram Signal for Non-invasive Estimation of Cardiac Time Intervals,” *IEEE Trans Biomed Eng*, vol. 64, no. 8, pp. 1701–1710, 2017, doi: 10.1109/TBME.2016.2616382.
[186] J. O. Ramsay, G. Hooker, and S. Graves, *Functional Data Analysis with R and Matlab*. Springer, 2009.

[187] F. Landreani *et al.*, "Heartbeat Detection Using Three-Axial Seismocardiogram Acquired by Mobile Phone," in *2018 Computing in Cardiology Conference (CinC)*, Sep. 2018, vol. 45, pp. 1–4. doi: 10.22489/CinC.2018.215.
[188] K. Sørensen, S. E. Schmidt, A. S. Jensen, P. Søgaard, and J. J. Struijk, "Definition of Fiducial Points in the Normal Seismocardiogram," *Scientific Reports*, vol. 8, no. 1, Art. no. 1, Oct. 2018, doi: 10.1038/s41598-018-33675-6.
[189] J. Ramos-Castro *et al.*, "Heart rate variability analysis using a seismocardiogram signal," in *2012 Annual International Conference of the IEEE Engineering in Medicine and Biology Society*, Aug. 2012, pp. 5642–5645. doi: 10.1109/EMBC.2012.6347274.
[190] L. Giovangrandi, O. T. Inan, R. M. Wiard, M. Etemadi, and G. T. A. Kovacs, "Ballistocardiography – A Method Worth Revisiting," *Conf Proc IEEE Eng Med Biol Soc*, vol. 2011, pp. 4279–4282, 2011, doi: 10.1109/IEMBS.2011.6091062.
[191] J. Rabineau *et al.*, "Cardiovascular adaptation to simulated microgravity and countermeasure efficacy assessed by ballistocardiography and seismocardiography," *Scientific Reports*, vol. 10, no. 1, Art. no. 1, Oct. 2020, doi: 10.1038/s41598-020-74150-5.
[192] R. Fadil *et al.*, "Temporal Changes of Fiducial Seismocardiogram Points Due to Different Sensor Placement on the Chest," Sep. 2020.
[193] D. E. Watenpaugh and A. R. Hargens, "The Cardiovascular System in Microgravity," in *Comprehensive Physiology*, American Cancer Society, 2011, pp. 631–674. doi: 10.1002/cphy.cp040129.
[194] M. Ds, S. Da, W. Ml, B. Mw, and M. Jv, "Comparison of echocardiographic changes after short- and long-duration spaceflight.," *Aviat Space Environ Med*, vol. 73, no. 6, pp. 532–536, Jun. 2002.
[195] A. G. Barnett, S. Sans, V. Salomaa, K. Kuulasmaa, A. J. Dobson, and for the W. M. Project, "The effect of temperature on systolic blood pressure," *Blood Pressure Monitoring*, vol. 12, no. 3, pp. 195–203, Jun. 2007, doi: 10.1097/MBP.0b013e3280b083f4.
[196] Q. Wang *et al.*, "Environmental ambient temperature and blood pressure in adults: A systematic review and meta-analysis," *Science of The Total Environment*, vol. 575, pp. 276–286, Jan. 2017, doi: 10.1016/j.scitotenv.2016.10.019.
[197] P. A. Modesti, S. Rapi, A. Rogolino, B. Tosi, and G. Galanti, "Seasonal blood pressure variation: implications for cardiovascular risk stratification," *Hypertension Research*, vol. 41, no. 7, Art. no. 7, Jul. 2018, doi: 10.1038/s41440-018-0048-y.
[198] A. Iwabu *et al.*, "Inverse Correlation Between Seasonal Changes in Home Blood Pressure and Atmospheric Temperature in Treated-Hypertensive Patients," *Clinical & Experimental Hypertension*, vol. 32, no. 4, pp. 221–226, Jul. 2010, doi: 10.3109/10641963.2010.491886.
[199] A. C. Stahn *et al.*, "Increased core body temperature in astronauts during long-duration space missions," *Scientific Reports*, vol. 7, no. 1, Art. no. 1, Nov. 2017, doi: 10.1038/s41598-017-15560-w.
[200] J. M. Evans, C. F. Knapp, and N. Goswami, "Artificial Gravity as a Countermeasure to the Cardiovascular Deconditioning of Spaceflight: Gender Perspectives," *Front. Physiol.*, vol. 9, 2018, doi: 10.3389/fphys.2018.00716.
[201] O. White, M. Barbiero, and N. Goswami, "The effects of varying gravito-inertial stressors on grip strength and hemodynamic responses in men and women," *Eur J Appl Physiol*, vol. 119, no. 4, pp. 951–960, Apr. 2019, doi: 10.1007/s00421-019-04084-y.

[202] N. Goswami, A. P. Blaber, H. Hinghofer-Szalkay, and J.-P. Montani, “Orthostatic Intolerance in Older Persons: Etiology and Countermeasures,” *Front. Physiol.*, vol. 8, 2017, doi: 10.3389/fphys.2017.00803.
[203] S. J. Strath, D. R. Bassett, A. M. Swartz, and D. L. Thompson, “Simultaneous heart rate-motion sensor technique to estimate energy expenditure,” *Med Sci Sports Exerc*, vol. 33, no. 12, pp. 2118–2123, Dec. 2001, doi: 10.1097/00005768-200112000-00022.
[204] J. M. Serrador, H. C. Finlayson, and R. L. Hughson, “Physical activity is a major contributor to the ultra low frequency components of heart rate variability,” *Heart*, vol. 82, no. 6, pp. e9–e9, Dec. 1999, doi: 10.1136/hrt.82.6.e9.
[205] K. S. Fraser, D. K. Greaves, J. K. Shoemaker, A. P. Blaber, and R. L. Hughson, “Heart Rate and Daily Physical Activity with Long-Duration Habitation of the International Space Station,” *Aviation, Space, and Environmental Medicine*, vol. 83, no. 6, pp. 577–584, Jun. 2012, doi: 10.3357/ASEM.3206.2012.
[206] S. N. Blair and L. W. Gibbons, “Guidelines for Exercise Testing and Prescription, Third Edition,” *Journal of Cardiopulmonary Rehabilitation and Prevention*, vol. 6, no. 8, pp. 315–316, Aug. 1986.
[207] M. Wuligoru, R. Huwkins, G. F. Humbert, and L. H. KEcznetz, “APOLLO EXPERIENCE REPORT - ASSESSMENT OF METABOLIC EXPENDITURES,” *Tech Rep NASA TN D-7883*, 1975.
[208] C. Campbell, “Advanced EMU Portable Life Support System (PLSS) and Shuttle/ISS EMU Schematics, a Comparison,” in *42nd International Conference on Environmental Systems*, American Institute of Aeronautics and Astronautics. doi: 10.2514/6.2012-3411.
[209] R. Buresh, K. Berg, and J. Noble, “Heat Production and Storage Are Positively Correlated With Measures of Body Size/Composition and Heart Rate Drift During Vigorous Running,” *Research Quarterly for Exercise and Sport*, vol. 76, no. 3, pp. 267–274, Sep. 2005, doi: 10.1080/02701367.2005.10599298.
[210] A. P. Welles *et al.*, “Estimation of core body temperature from skin temperature, heat flux, and heart rate using a Kalman filter,” *Computers in Biology and Medicine*, vol. 99, pp. 1–6, Aug. 2018, doi: 10.1016/j.compbiomed.2018.05.021.
[211] J. Malchaire and B. I. Palella, “Evaluation of the metabolic rate based on the recording of the heart rate,” *Industrial Health*, p. 14, 2017.
[212] J. D. Périard, T. M. H. Eijsvogels, and H. A. M. Daanen, “Exercise under heat stress: thermoregulation, hydration, performance implications, and mitigation strategies,” *Physiological Reviews*, vol. 101, no. 4, pp. 1873–1979, Oct. 2021, doi: 10.1152/physrev.00038.2020.
[213] R. L. Hughson, S. D. Peterson, N. J. Yee, and D. K. Greaves, “Cardiac output by pulse contour analysis does not match the increase measured by rebreathing during human spaceflight,” *Journal of Applied Physiology*, vol. 123, no. 5, pp. 1145–1149, Nov. 2017, doi: 10.1152/japplphysiol.00651.2017.
[214] M. Reagan, B. Janoiko, J. Johnson, S. Chappell, Ph.D., and A. Abercromby, “NASA’s Analog Missions: Driving Exploration Through Innovative Testing,” presented at the AIAA SPACE 2012 Conference & Exposition, Pasadena, California, Sep. 2012. doi: 10.2514/6.2012-5238.
[215] D. Eppler, “Desert Research and Technology Studies (DRATS) 2010 Science Operations: Operational Approaches and Lessons Learned for Managing Science during Human Planetary Surface Missions,” *Acta Astronautica*, pp. 224–241, Mar. 2012.

[216] O. S. Bekdash *et al.*, “Development and Evaluation of the Active Response Gravity Offload System as a Lunar and Martian EVA Simulation Environment,” p. 12.
[217] A. F. J. Abercromby *et al.*, “Crew Health and Performance Extravehicular Activity Roadmap: 2020,” p. 74, 2020.
[218] D. C. E. Larsen, “NASA Experience with Pogo in Human Spaceflight Vehicles,” p. 23.
[219] J. Norcross *et al.*, “Characterization of Partial-Gravity Analog Environments for Extravehicular Activity Suit Testing,” *NASA/TM-2010-216139*, Dec. 2010.
[220] J. Norcross, S. Chappell, and M. Gernhardt, “Lessons Learned from Performance Testing of Humans in Spacesuits in Simulated Reduced Gravity,” NASA Technical Report, NASA/TP-2010-00005154, 2010.
[221] J. Norcross, S. Jarvis, O. Bekdash, S. Cupples, and A. Andrew, “EVA Human Health and Performance Benchmarking Study Overview and Development of a Microgravity Protocol,” NASA Technical Report, NASA/TP-2017-0000796, 2017.
[222] P. Valle, “Reduced Gravity Testing of Robots (and Humans) Using the Active Response Gravity Offload System,” NASA technical Report, NASA/TP-2017-0008856, 2017.
[223] C. R. Cullinane, R. A. Rhodes, and L. A. Stirling, “Mobility and Agility During Locomotion in the Mark III Space Suit,” *Aerospace Medicine and Human Performance*, vol. 88, no. 6, pp. 589–596, Jun. 2017, doi: 10.3357/AMHP.4650.2017.
[224] F. A. Korona, J. Norcross, B. Conger, and M. Navarro, *Carbon Dioxide Washout Testing Using Various Inlet Vent Configurations in the Mark-III Space Suit*. 44th International Conference on Environmental Systems, 2014. Accessed: Oct. 24, 2021. [Online]. Available: https://ttu-ir.tdl.org/handle/2346/59676
[225] A. Abercromby, S. S. Thaxton, E. A. Onady, and S. L. Rajulu, “Reach Envelope and Field of Vision Quantification in Mark III Space Suit using Delaunay Triangulation,” *NASA/TP-2006-213729*, Jan. 2006.
[226] D. Mitchell and C. H. Wyndham, “Comparison of weighting formulas for calculating mean skin temperature,” *Journal of Applied Physiology*, vol. 26, no. 5, pp. 616–622, May 1969, doi: 10.1152/jappl.1969.26.5.616.
[227] Z. J. Schlader, B. D. Johnson, R. R. Pryor, J. Stooks, B. M. Clemency, and D. Hostler, “Human thermoregulation during prolonged exposure to warm and extremely humid environments expected to occur in disabled submarine scenarios,” *American Journal of Physiology-Regulatory, Integrative and Comparative Physiology*, vol. 318, no. 5, pp. R950–R960, May 2020, doi: 10.1152/ajpregu.00018.2020.
[228] J. A. Stolwijk, “A Mathematical Model of Physiological Temperature Regulation in Man,” NASA Technical Report, NASA/CR-1855, 1971.
[229] A. Karimi, “Reexamination of METMAN, Recommendations on Enhancement of LCVG, and Development of New Concepts for EMU Heat Sink,” Dec. 1990.
[230] G. C. Bue, A. H. Cook, and G. C. Franklin, “Computer program documentation-41-Node Transient Metabolic Man Program,” Lockheed Engineering and Sciences Co., LESC-27578, 1989.
[231] H. H. Pennes, “Analysis of tissue and arterial blood temperatures in the resting human forearm. 1948,” *J Appl Physiol (1985)*, vol. 85, no. 1, pp. 5–34, Jul. 1998, doi: 10.1152/jappl.1998.85.1.5.
[232] H. J. Song, “Overview of Human Thermal Modeling, Thermoregulation, and Thermal Comfort at NASA,” NASA, 2017.